Novel Catalysts for Hydrogenolysis of Biomass-Derived Feedstocks and Hydrogenation of α,β-Unsaturated Carbonyl Compounds

Thesis Submitted to AcSIR
for the Award of the Degree of
Doctor of Philosophy
in
Chemical Sciences

AcSIR

By
Atul Sopan Nagpure
(AcSIR Roll No.: 10CC11J26071)

Under the Guidance of
Dr. C. V. V. Satyanarayana

CSIR-National Chemical Laboratory
Pune-411008, India

March 2016

Certificate

This is to certify that the work incorporated in this *Ph.D. thesis* entitled *"Novel Catalysts for Hydrogenolysis of Biomass-Derived Feedstocks and Hydrogenation of α,β-Unsaturated Carbonyl Compounds"* submitted by *Mr. Atul Sopan Nagpure* to the Academy of Scientific and Innovative Research (AcSIR), in fulfillment of the requirements for the award of the Degree of *Doctor of Philosophy*, embodies original research work under my supervision.

I further certify that this work has not been submitted to any other University or Institution in part or full for the award of any degree or diploma. Research materials obtained from other sources has been duly acknowledged in the thesis. Any text, illustrations, tables *etc* used in this thesis from other sources have been duly cited and acknowledged.

Mr. Atul Sopan Nagpure

(Research Student)

Dr. C. V. V. Satyanarayana

(Research Guide)

Date: 22nd March 2016

Place: Pune

DECLARATION

I hereby declare that the work described in the thesis entitled *"Novel Catalysts for Hydrogenolysis of Biomass-Derived Feedstocks and Hydrogenation of α,β-Unsaturated Carbonyl Compounds"* submitted for the degree of *Doctor of Philosophy* in *Chemical Sciences* to the Academy of Scientific and Innovative Research (AcSIR), New Delhi, has been carried out by me at the *Catalysis and Inorganic Chemistry Division*, *CSIR-National Chemical Laboratory, Pune–411008, India*, under the supervision of **Dr. C. V. V. Satyanarayana**. I further declare that the material obtained from other sources has been duly acknowledged in this thesis. The work is original and has not been submitted in part or full by me for any other degree or diploma to this or any other university.

Date: 22nd March 2016

Place: Pune

Mr. Atul Sopan Nagpure

(Research Student)

**Dedicated to my parents
& friends**

Acknowledgements…..

Table of Contents

Chapter 2 : Catalyst synthesis and characterization

Chapter 3 : Reductive upgradation of biomass-derived furanic compounds over supported metal catalysts using H_2

Chapter 4 : Catalytic transfer hydrogenolysis of biomass-derived furanic compounds over nitrogen-doped mesoporous carbon supported metal catalysts

Chapter 5 : Chemoselective hydrogenation of cinnamaldehyde over Pd and Au supported on nitrogen-doped mesoporous carbon

Chapter 6 : Summary and conclusions

List of Figures

List of Schemes

List of Tables

List of Abbreviations

HMF	5-Hydroxymethylfurfural
BHMF	2,5-Bis(hydroxymethyl)furan
MFU	5-Methyl furfural
MFA	5-Methyl furfuryl alcohol
FA	Furfuryl alcohol
BHMTHF	2,5-Bis(hydroxymethyl)tetrahydrofuran
MTHFA	5-Methyl tetrahydrofurfuryl alcohol
DMF	2,5-Dimethylfuran
DMTHF	2,5-Dimethyltetrahydrofuran
MF	2-Methylfuran
MTHF	2-Methyl tetrahydrofuran
THF	Tetrahydrofuran
THFA	Tetrahydrofurfuryl alcohol
CA	Cinnamaldehyde
HCA	Hydrocinnamaldehyde
CAL	Cinnamyl alcohol
PPL	3-Phenyl propanol
CNTs	Carbon nanotubes
SWCNTs	Single-walled carbon nanotubes
MWCNTs	Multi-walled carbon nanotubes
CNFs	Carbon nanofibers
HT	Hydrotalcite
NMC	Nitrogen-doped mesoporous carbon
MC	Mesoporous carbon
AC	Activated carbon
IW	Incipient-wetness
DP	Deposition-precipitation
SI	Sol-immobilization
XRD	X-ray diffraction

SEM	Scanning electron microscopy
TEM	Transmission electron microscopy
XPS	X-ray photoelectron spectroscopy
ICP-OES	Inductively coupled plasma-optical emission spectrometry
TPD	Temperature programmed desorption
TPR	Temperature programmed reduction
RON	Research octane number
CTH	Catalytic transfer hydrogenation
GC	Gas chromatography
FID	Flame ionization detector
MS	Mass spectrometry
BET	Brunauer-Emmett-Teller

Chapter 1
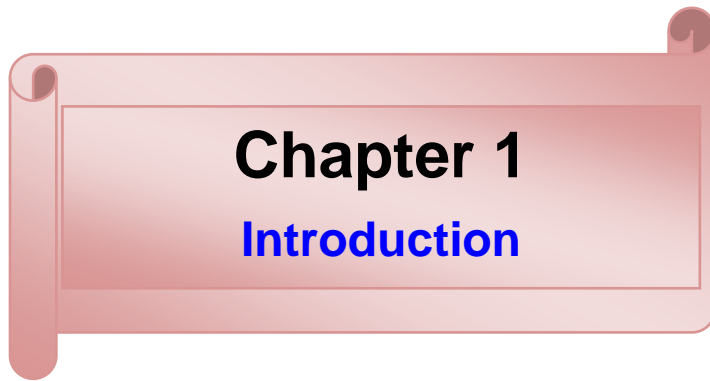
Introduction

1.1. Introduction

Catalysis plays vital role in everyday life and contributes significantly to societal welfare. The research in the field of catalysis leads to development of novel catalytic industrial processes for manufacturing of various chemicals. Thus, it is not surprising that several important chemical processes which require catalysts for hydrogenation, hydrogenolysis, oxidation, polymerization, *etc*. are of great interest to both industries and academia. This in turn leads to increasing demand for development of novel catalytic processes and catalysts with an in-depth understanding of their function. The continuous discovery of novel catalysts led to major innovations in chemical processing. Heterogeneous catalysis is the pillar of modern chemical technology.

Swedish chemist Berzelius coined the term *'catalysis'* in 1836, which implied *'loosen'* and *'down'*.[1] He observed that the chemical reactions occurred by catalytic contact and according to him; besides 'affinity' a new force must be operative that is *'catalytic force'*.[1] In 1895, Ostwald proposed a definition which stated that *"a catalyst accelerates a chemical reaction without affecting the position of the equilibrium"*.[2] By the end of the 19th century various catalytic processes were developed for selective hydrogenation, hydrogenolysis, dehydrogenation, oxidation, isomerization, polymerization, *etc*. All these catalyst processes accelerated the industrial revolution.[3] Ammonia synthesis (Haber-Bosch process), HCN synthesis (Andrussow oxidation), Fischer-Tropsch synthesis, sulfuric acid preparation (Contact process), nitric acid preparation (Ostwald process), olefin polymerization (Ziegler Natta polymerization), desulfurization of petroleum fractions (hydro-desulfurization), methanol synthesis and its conversion to hydrocarbons, olefin metathesis, Sharpless epoxidation, *etc*., are some of the important industrial processes.[2,4] Therefore, the catalysis became backbone to the chemical industry contributing significantly to our societal prosperity.

Principal focus was on the discovery of new processes during the industrial revolution; however, no efforts were made towards waste minimization and sustainability. As a result, plenty of waste was generated during several chemical and pharmaceutical processes. This led to environment damage, which triggered the transition from traditional methodology to greener processes which focused on eliminating the use of toxic materials, elimination of waste and complete utilization of raw materials.

1.2. Sustainability and Green chemistry

Transforming of the conventional reaction concepts into an environmentally benign industrial process provides the way for '*sustainable chemistry*'. The Brundtland report[5] came with the ideas of sustainable development which was defined as: *Meeting the needs of the present generation without compromising the ability of future generations to meet their own needs.* The ideology of sustainability is drawing more attention, in which *'Green chemistry'* has become an important part. If sustainability is the final goal, then the key tool to achieve it is '*Green chemistry*'. The term *'Green Chemistry'* was coined in the early 1990's by Anastas *et al.*[6] as:

"Green chemistry efficiently uses (preferably renewable) raw materials, eliminates waste and avoids the use of toxic and/or hazardous reagents and solvents in the synthesis and application of chemical products".

All the criteria of '*green chemistry*' are assembled in the set of 12 principles (Fig. 1.1).

Fig. 1.1 Principles of green chemistry.[6]

The principles of green chemistry demands the development of new catalytic systems and chemical reactivity that would help the chemical synthesis in terms of increased environment safety, saved resources, energy efficiency, enhanced selectivity of desired product and simplicity of operation. The academia and industry have widely recognized the green chemistry principles such as atom efficiency and waste reduction. A replacement of outdated processes which involves stoichiometric reagents with greener catalytic alternatives has led to considerable decreased in waste generation. The next approach to reach sustainable chemical industry will be the one in order to utilize the renewable resources for production of fine chemicals and fuels, which is in accordance with the seventh principle of green chemistry.

1.3. Renewable raw materials

Prior to the use of fossil fuels, the plant biomass was an important source to meet the energy requirements of the society. Discovery of crude oil in 19th century has led to the rapid industrialization which improved the standard of living. Since then, fossil fuels became the main source of materials, energy and chemicals for the modern society.

Presently, fossil fuels such as natural gas, coal and petroleum meets nearly 90% of the world energy demand.[7] It is hypothesized that by 2030, nearly 600×10^{15} Btu of fossil resources would be required to fulfill the world energy demand (Fig. 1.2).[8] However, the fossil fuel reserves are limited, becoming increasingly expensive and is less attractive as carbon source.[9] Furthermore, the utilization of fossil fuels and their derivatives for the manufacture of power and heat is associated with a net increment to CO_2 levels in atmosphere, which has a detrimental effect on environment due to global warming and climatic change.[10] These concerns have forced the society to look for alternative sources of energy and chemicals. In this perspective, the ambitious aim of synthesizing 25% of chemicals and 20% of fuels from renewable feedstocks by 2030 appears to be a proper approach for a steady transformation from fossil based economy to a renewable one.
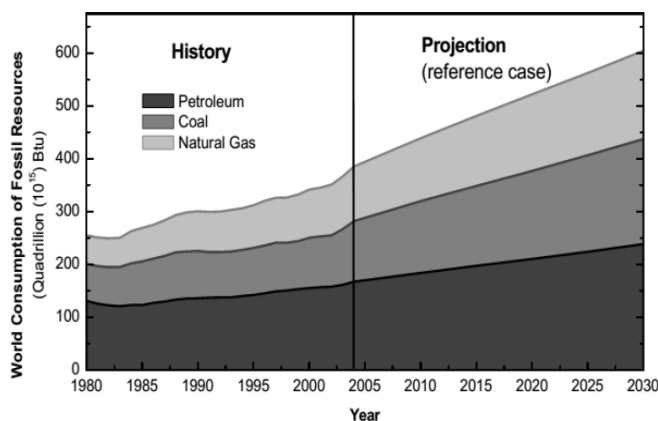
Fig. 1.2 World consumption of fossil fuels from 1980-2030.[8]

1.4. Biomass valorization

1.4.1. Superiority, motivations and scope

A modern economy demands effective utilization of renewable resources using novel technologies. Renewable resources comprise water, wind, solar and biomass. The kinetic energy of water and potential energy of wind is used for the generation of electricity; solar flux gives

heat and thermal energy. On the other hand biomass offers chemical energy stored as chemical bonds. Among the renewable resources, biomass is superior as it is the only source that possesses the energy in the form of chemical bonds. The biomass feedstocks can be exploited for the production of numerous chemicals and fuels in addition to heat and electricity generation.

"The term biomass refers to non-fossilized and biodegradable organic materials obtained from plants and animals on a renewable basis, that includes waste and residues of wood, agricultural crop, aquatic animals and plants, municipal and other waste materials" (Fig. 1.3).[11] Thus, the availability of biomass is widespread, abundant and also economical.[12] These excellent features make biomass a better and sustainable source for future requirement of chemicals and energy.
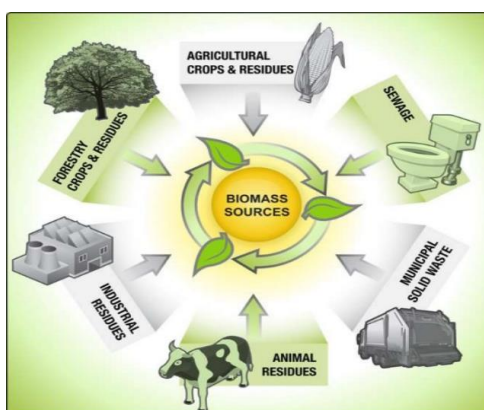
Fig. 1.3 Different sources of biomass.[11]

According to American national renewable energy laboratory, *"biorefinery is a facility that integrates biomass conversion processes and equipment to synthesize chemicals, fuels and power from biomass"*.[13] In a biorefinery the biomass can be processed either biologically or chemically. The CO_2 released during the upgradation of renewable compounds is utilized for the photosynthesis process to generate biomass (Fig. 1.4). This process is cyclic which make biomass a very attractive renewable feedstock. To achieve the goals of sustainable progress, biorefinery should play a vital role in near future.

1.4.2. Composition of lignocellulosic biomass

Biomass is a result of life on earth, in which simple molecules such as CO_2, H_2O, N_2, O_2 and several others are activated due to numerous bio-chemical processes. The most abundant class of biomass is the lignocellulosic biomass since it contributes to structural integrity of the plants and is always present in them. Lignocellulosic biomass is the most promising renewable

source of carbon, as it is widely available around the world at relatively low cost. Therefore, this plant biomass is the most viable resource for the synthesis of a variety of fine chemicals and fuels in a sustainable way.[14,15] Lignocellulosic biomass consists of three different fractions: cellulose, hemicellulose and lignin (Fig. 1.5).
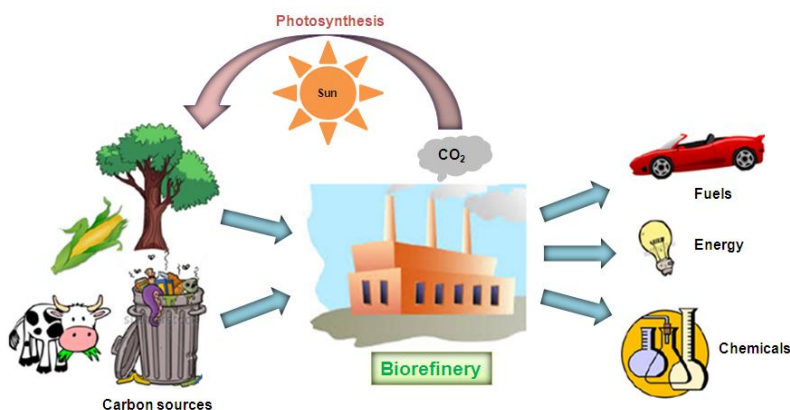
Fig. 1.4 Biorefinery concept for sustainable production of the chemicals and fuels from biomass.[13]
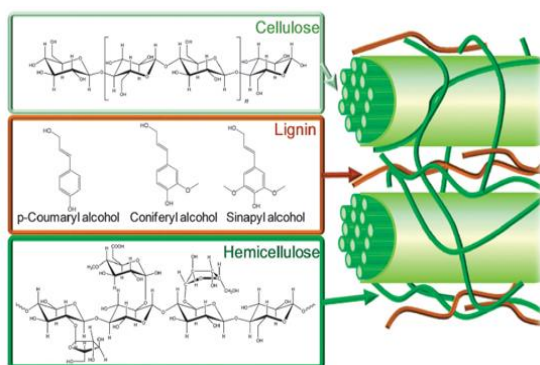
Fig. 1.5 Composition of lignocellulosic biomass.[15c]

1.4.2.1. Cellulose

Cellulose is a polymer of glucose units linked *via* β-glycosidic bonds, imparting the structure with rigid crystallinity that hinders hydrolysis (Fig. 1.5).[16] It comprises 40-50% of total lignocellulosic biomass feedstock. Cellulose is entrapped within the complex lignin/hemicellulose matrix and it is largely inaccessible to hydrolysis in untreated biomass. The hydrogen bonds in the cellulose help to maintain and reinforce the linear, flat conformation of the chain. The degree of polymerization of cellulose varies from source to source; it is approximately 10,000 to 15,000 glucopyranose monomer units for wood and cotton, respectively.[17] The biomass pre-treatment *via* physical/chemical processes helps to pervade

lignin and extract hemicelluloses, so that subsequent hydrolysis of cellulose is more effective offering glucose monomers. Partial acid hydrolysis of cellulose gives cellobiose (glucose dimer), cellotriose (glucose trimer) and cello-tetrose (glucose tetramer), while complete acid hydrolysis breaks it into glucose.[18] High yields of glucose (>90%) can be achieved through enzymatic hydrolysis of cellulose following biomass pretreatment.

1.4.2.2. Hemicellulose

Hemicellulose is an amorphous polymer of the lignocelluloses, which is generally comprised of five different sugar monomers, L-arabinose, D-xylose, D-glucose, D-galactose and D-mannose.[19] The most copious building block of hemicellulose is xylan (a polymer of xylose). Hemicellulose constitutes 20-40% of the plant biomass. It is bound to lignin and cellulose strands are interwoven with it (Fig. 1.5). Its extraction can be achieved through various chemical and physical methods. It is relatively easy to carry out acid hydrolysis of hemicelluloses, compared to cellulose, to give its monomer sugars. After extraction and hydrolysis, xylose monomers are appropriate feedstocks for synthesis of furfural *via* dehydration or for ethanol production through fermentation.

1.4.2.3. Lignin

Lignin portion of biomass is a highly cross linked, amorphous polymer comprised of methoxylated phenylpropane structures, like sinapyl alcohol, coumaryl alcohol and coniferyl alcohol.[20] High degree of cross linking makes the plant structurally rigid and provides a hydrophobic vascular system for the transportation of solutes and water. It constitutes 15-30% of the total lignocellulosic biomass. The structure and composition of lignins depends on the part of the plant and on the type of wood. Lignin encompasses the cellulose, hemicellulose fractions and it acts like an adhesive holding these fibers together (Fig. 1.5). This irregular polymer is formed by an enzyme-initiated free-radical polymerization of the alcohol precursors.[21] Effective biomass pretreatment processes are necessary to split the lignin seal making the carbohydrate portions easily accessible. Being rich in oxygenated aromatic species, lignin is an ideal feedstock for the production of phenolic resins. Several research groups have demonstrated the strategies for the production of aromatic compounds and bio-oils from lignin.[22]

The technologies for the transformation of abundant lignocellulosic biomass to generate fuels and chemicals are not so effective and still remain a major challenge worldwide. Because

of the structural and chemical complexity of biomass, it hinders its conversion to desired products with high yields. There are numerous methods employed for the conversion of lignocellulosic biomass to chemicals and fuels, while the major ones are pyrolysis, gasification and hydrolysis (Fig. 1.6). The first two approaches convert the biomass to fuels while the last one converts it to chemicals. Varieties of chemicals can be obtained *via* hydrolysis reaction, which can be further upgraded by adopting interesting transformations revealing the potential of this technology. All these technologies are discussed in detail in the following sections.
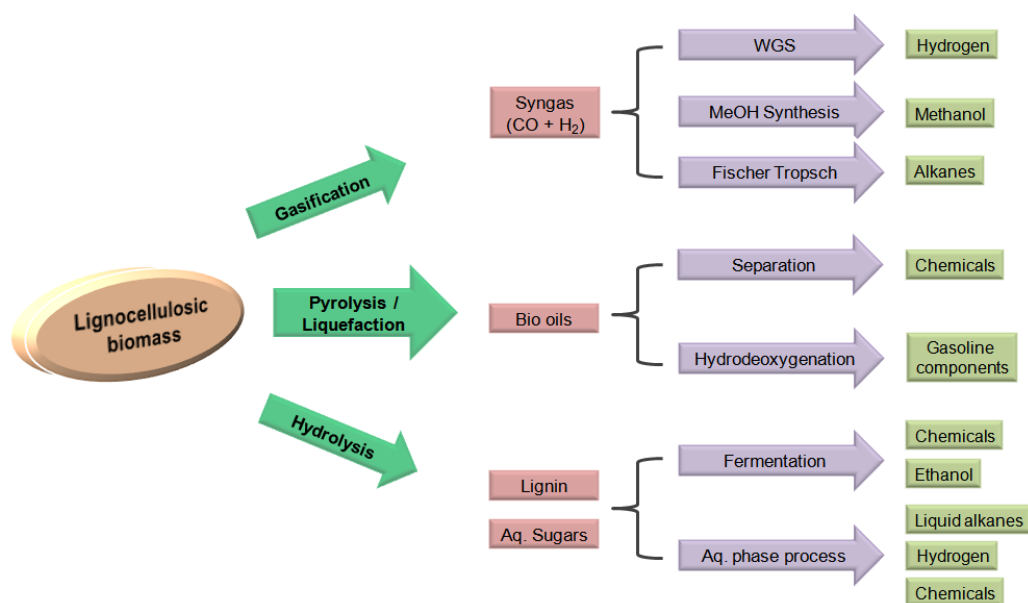
Fig. 1.6 Conversion routes of lignocellulosic biomass to chemicals and fuels.[10]

1.4.3. Processes for conversion of biomass to chemicals and fuels

1.4.3.1. Gasification

Biomass gasification is carried out through partial combustion of biomass to produce syngas (CO and H_2). It is normally conducted at very high temperature (800 °C) as the reaction process is highly endothermic.[23] The obtained syngas can be upgraded to liquid fuels like gasoline and diesel *via* Fischer-Tropsch process[24] or methanol synthesis.[25] Streams rich in H_2 can be produced by tuning the ratio of reactants in the syngas, by carrying out water gas shift (WGS) reaction[26] or by insitu CO_2 absorption pathways[27]. All three components of lignocellulosic biomass can be used for gasification process but there are drawbacks associated with it. There are some issues in gasification route, such as poor quality or highly diluted stream of syngas, consumption of large amount of biomass feedstocks and the moisture content of

biomass which in turn affects the thermal efficiency of the process. These shortcomings increase the overall economy of the process.[28] The detailed process of biomass gasification is illustrated in Fig. 1.7.
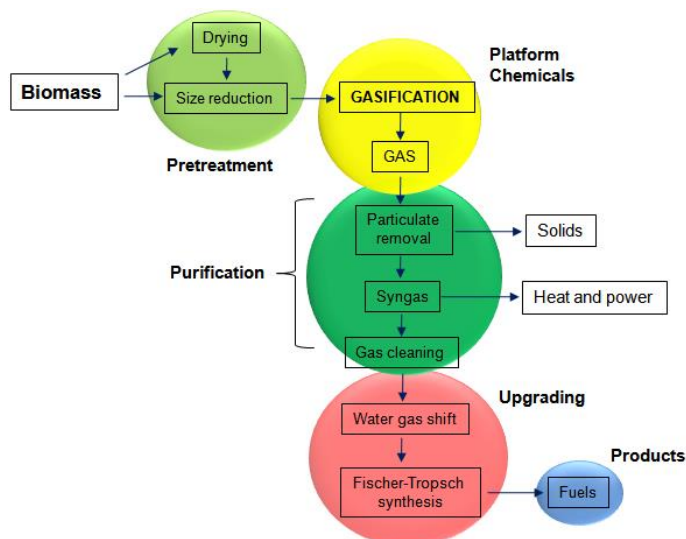
Fig. 1.7 Process schematic of biomass gasification and upgradation.[15a]
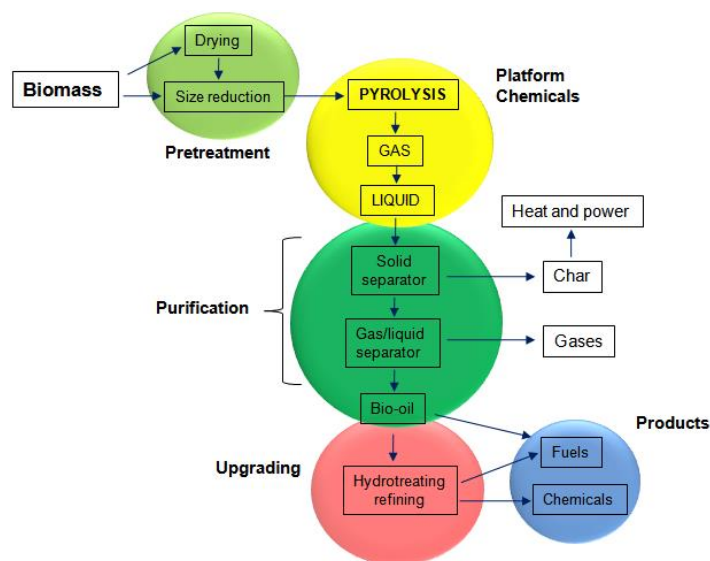
Fig. 1.8 Process schematic of biomass pyrolysis and upgradation.[15a]

1.4.3.2. Pyrolysis/Liquefaction

Another process for valorization of biomass is pyrolysis or liquefaction. In this method, biomass is heated in an inert atmosphere at lower temperatures (300 –700 °C) to give bio-oil, a dark organic liquid.[29] It yields liquid mixture of more than 350 compounds like aldehydes,

ketones, acids, alcohols, esters, sugars and aromatics, which are collectively referred to as 'bio-oil'. Due to diverse constituents of bio-oil, it is an excellent source of chemicals. But, the energy efficiency is low due to high oxygen content of it and thus further processing is required to enhance its fuel properties. This can be achieved by deoxygenation in presence of external H_2 [30] or its conversion to aromatic compounds using zeolites based catalysts.[31] The operational simplicity of the process is neutralized by costly isolation and upgradation techniques and lack of product selectivity. The detailed process of biomass pyrolysis is demonstrated in Fig. 1.8.

1.4.3.3. Hydrolysis

Hydrolysis pathways are most appropriate for obtaining desired products with high selectivity from biomass. This methodology is superior to gasification and pyrolysis since the operational temperatures are low. Lignocellulose biomass is a highly complex and having rigid structure resulting in low surface area and high crystallinity. This makes its depolymerization to sugars a really tough task.[32] In order to break such complex feedstock into monomers very efficient pretreatment method is required. The outermost and rigid lignin seal can be ruptured by pretreatment process, which exposed the cellulose and hemicellulose fraction. These fractions then become more accessible for the acids or enzymes for hydrolysis and could be converted to sugars (hexose or pentose). By visualizing the significance of such pretreatment methods they are of various origins ranging from physical, chemical or biological.[33] On hydrolysis, the morphology and network of lignin may gets changed under the reaction conditions with simultaneous hydrolysis of hemicellulose fraction with acids. Since cellulose is linear and crystalline, more severe conditions are required for its depolymerization. Thus, through hydrolysis, sugars could be derived from biomass feedstock. These obtained sugars can be further upgraded to many fine chemicals and fuels *via* various chemical transformations.

1.5. Value added chemicals and fuels from carbohydrate biomass

Photosynthesis process produces around 170 billion metric tons of biomass per year, 75% of which can be assigned to carbohydrates, 20% lignin and 5% other natural products like fats, alkaloids, oils, nucleic acid, proteins and terpenes.[34] Therefore, it is very important to look for efficient techniques for utilization of this abundant biomass. These carbohydrates have many applications in various sectors such as fermentation, food, paper, petroleum production and pharmaceutical industries.[35] Thus, it can be concluded that carbohydrates are ample, varied and

reusable source of carbon. Carbohydrates are macromolecules of carbon, hydrogen and oxygen with the general formula $C_m(H_2O)_n$ (m is not equal to n). They are usually divided into mono-, di-, oligo- and polysaccharides, where mono- and disaccharides are commonly referred to as sugars. Natural saccharides are composed of this monomer with the general formula $(CH_2O)_n$, where n is three or more. Hexoses (C_6) and pentoses (C_5) are the major building block of polysaccharides.

Table 1.1 List of biomass-derived platform chemicals.	
C_2	Acids (acetic, glycolic, oxalic), ethanol, ethylene
C_3	Acids (3-hydroxypropionic, lactic, propionic, acrylic), acetone, glycerol, propane diols
C_4	Acids (fumaric, succinic, asperic, malic, butyric), 1,2,4-butane triol, 1-butanol, acetoin, 2,3-butane diol
C_5	Acids (levulinic, itaconic, glutamic), furfural, sugars (xylose, arabinose)
C_6	Acids (adipic, citric, gluconic), sorbitol, 5-hydroxymethylfurfural, lysine

Petrochemical feedstocks offer many fine chemicals like aromatics (benzene, toluene, xylene), alkanes (ethane and butane), propylene, 1,3-butadiene, *etc.*, which can serve as platform chemicals.[36] Recently, many researchers adopted diverse approaches for obtaining various fine chemicals and fuels from carbohydrates and lignin. They have recognized some molecules which have the potential to act as platform compounds (Table 1.1). These chemicals can be obtained from biomass primary products (starch, cellulose, hemicellulose, lignin, proteins and oils) *via* chemical transformations.[37] Among those listed chemicals, many can be obtained from carbohydrates. For processing of biomass, usually liquid-phase technologies are preferred because of high functionality, high reactivity and low volatility of biomass feedstocks.[38] In general, numerous chemical intermediates and fuels can be produced from carbohydrates using chemical/biological pathways (Fig. 1.9).[39] They can be further transformed in to furanics[40], alcohols[41] and acids[42] which have been identified as the top 12 value added chemicals by U.S. department of energy.[43] Efficient conversion of these compounds into chemicals and fuels are the measure of successful biomass utilization strategy.
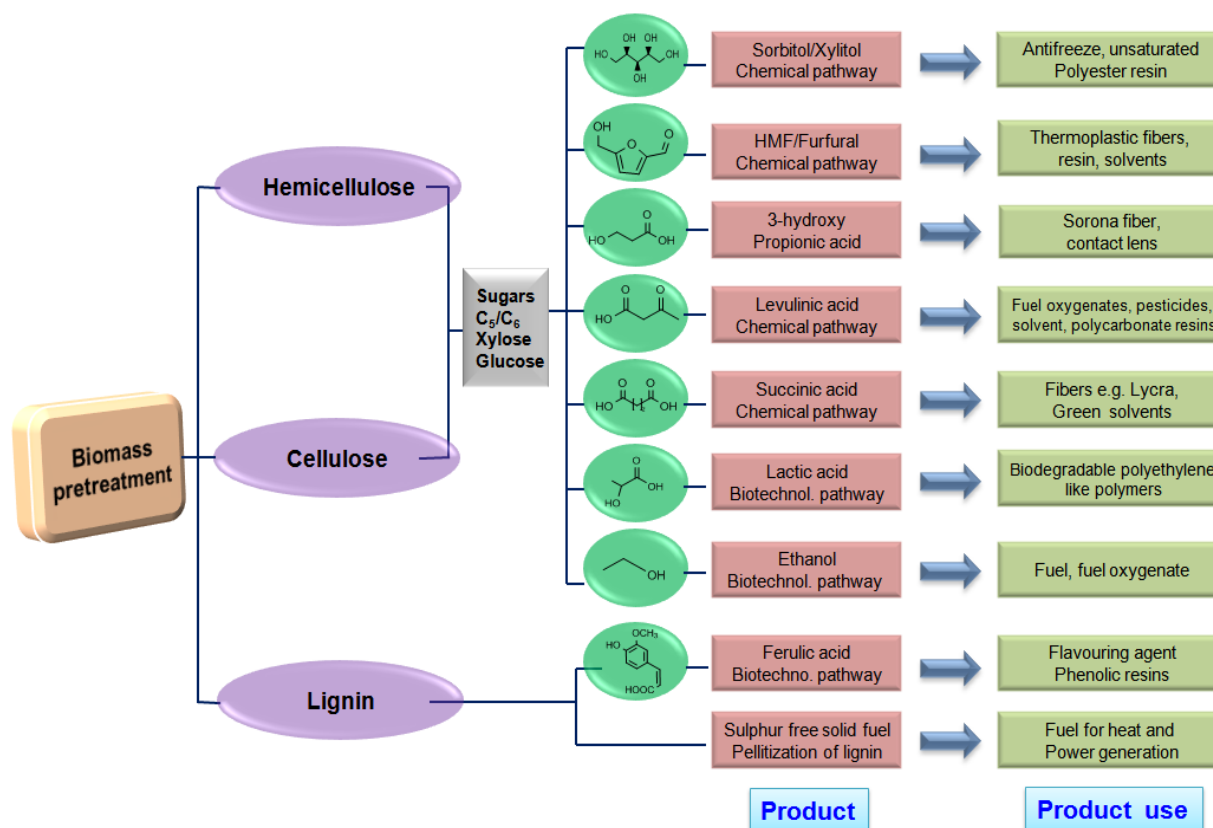
Fig. 1.9 Value added chemicals and fuels from biomass feedstock.[43]

For production of fine chemicals and renewable fuels from biomass feedstocks, a range of chemical transformations are employed that include hydrolysis, dehydration, isomerization, aldol condensation, hydrogenation, hydrogenolysis, aqueous phase reforming, oxidation, *etc*.[44] Huge dependence on fossil fuels for chemicals and fuels is alarming, as it is not sustainable in the long run. Thus, the preparation of renewable fuels and valuable chemicals from biomass feedstocks has become an important area of research to replace petroleum based fossil fuels.[38,44] Hydrogenation and hydrogenolysis of biomass-derived components provide an excellent prospect for future biorefinery concept, as biomass-derived substrates have high oxygen content.[45] With this outlook, three important chemicals, *viz*., furfuryl alcohol (FA) through hydrogenation of furfural, 2-methylfuran (MF) by hydrogenolysis of furfural and 2,5-dimethylfuran (DMF) by hydrogenolysis of 5-hydroxymethylfurfural (HMF) were taken up. Hence, a major part of the present thesis focuses on the selective hydrogenation and hydrogenolysis of biomass-derived compounds to FA, MF and DMF. Therefore, various aspects of these important chemicals are elaborated below.

1.5.1. Furfural and 5-hydroxymethylfurfural as "platform chemicals"

The term "platform chemical" is used to describe a molecule that can undergo multiple transformations to give several useful products. Biomass-derived compounds can be converted to furanics by different chemical pathways, which are heterocyclic compounds with an aromatic ring comprised of four carbon atoms and an oxygen atom. Furanics that are increasingly becoming important are furfural and HMF. Furfural consists of a furan ring with an aldehyde group at the 2 position whereas HMF has furan ring, aldehyde and a hydroxymethyl group at the 2 and 5 positions, respectively. Furfural and HMF can be prepared from pentose and hexose sugars, respectively *via* dehydration on heating under acidic conditions (Scheme 1.1).[46] Additionally, HMF has been detected in foods such as cereals, dried fruits, coffee and baking products.[47] HMF can be toxic to humans when ingested at concentrations of 75 mg per kg of body weight or greater. An excellent review by Rosatella *et al.* summarizes the biological properties and applications of furfural and HMF.[48]
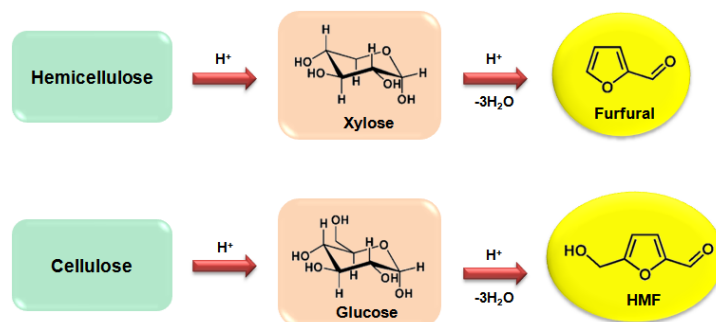
Scheme 1.1 Formation of furfural and HMF from biomass-derived compounds.

The real value of furfural and HMF is in the truth that they can be converted to various useful compounds *via* different chemical transformations. The synthetic routes from furfural and HMF are depicted in Scheme 1.2 and 1.3, respectively. Oxidation of furfural renders 2-furoic acid, which is used as preservative because of its bactericide and fungicide properties.[49] 2-Furoic acid is also considered as an acceptable flavoring agent and used as starting material for the production of furoate ester. Hydrogenation of furfural gives FA, tetrahydrofurfuryl alcohol (THFA), 2-methyltetrahydrofuran (MTHF) and tetrahydrofuran (THF). All these are highly essential chemicals in chemical industries. Furfural hydrogenolysis gives MF and 1,5-pentane diol. MF is an important chemical used in chemical industries and it is also a fuel candidate.[50] 1,5-Pentane diol is used as a monomer for polyester synthesis. On decarbonylation, furfural

offers furan; a bulk chemical. Furfural on rearrangement provides cyclopentanone; a useful intermediate in organic synthesis.[51]
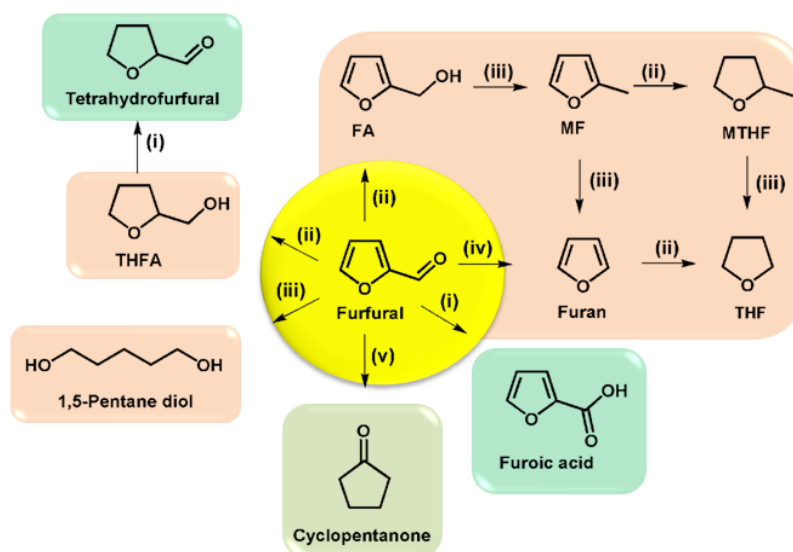
Scheme 1.2 Synthetic routes from furfural by (i) oxidation, (ii) hydrogenation, (iii) hydrogenolysis, (iv) decarbonylation and (v) rearrangement reaction.

Oxidation of HMF gives 2,5-furandicarboxylic acid (FDCA) and 2,5-biformylfuran (BFF). The former is of vital interest since it can be used as a replacement for isophthalic and terephthalic acids, which are used for the preparation of polyesters, polyurethanes and polyamides.[52] Hydrogenation of HMF transforms it to 2,5-bis(hydroxymethyl)tetrahydrofuran (BHMTHF) and 2,5-bis(formyl)tetrahydrofuran (BFTHF). These compounds on condensation generate polymers which have the potential to become liquid alkanes.[53] On hydrogenolysis, HMF gives DMF, 2,5-dimethyltetrahydrofuran (DMTHF), 5-methyl furfural (MFU) and MTHF. Among them, DMF has great significance as a biofuel.[54] Hydrogenolysis of HMF can give 1,6-hexane diol, a precursor for adipic acid synthesis.[55] HMF rehydration decomposes it into levulinic acid (LA) and formic acid, both being important chemicals.[56] Additionally, LA can be converted into γ-valerolactone (GVL); a liquid fuel additive.[57] Moreover, HMF can also undergo undesirable condensation to form insoluble polymers known as humins by reaction with itself or with reactant molecules.
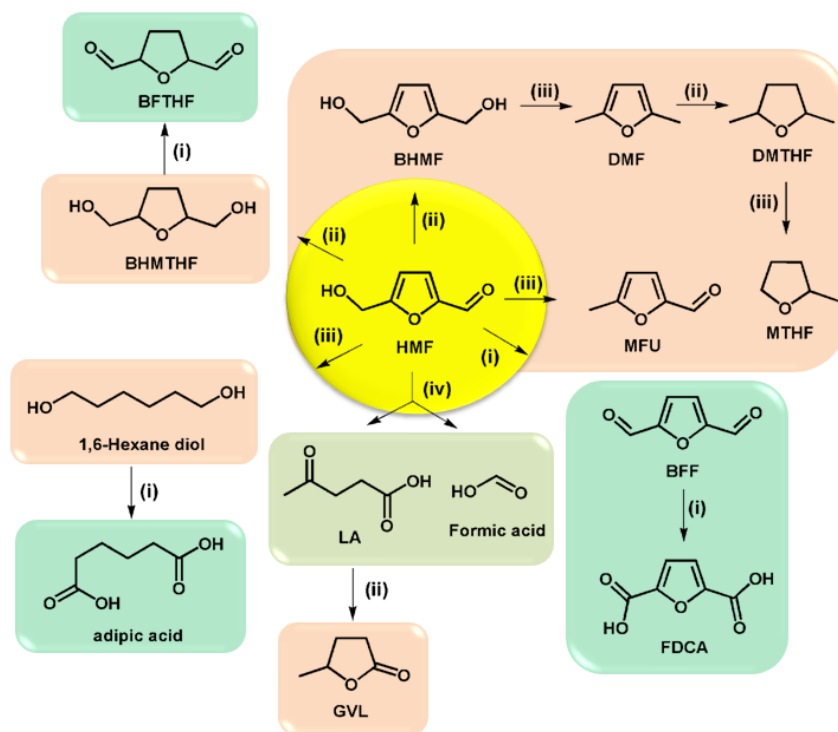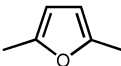
Scheme 1.3 Synthetic routes from HMF by (i) oxidation, (ii) hydrogenation, (iii) hydrogenolysis and (iv) rehydration.

1.5.2. Furfuryl alcohol and 2-methylfuran

FA and MF are very important furfural derived compounds. FA is prepared by the selective hydrogenation of furfural and is widely used in the chemical manufacture. The main applications of FA are synthesis of corrosion resistant fiber glass, acid proof bricks, thermostatic resins, corrosion resistant polymer concrete and liquid resins for galvanic bath tub.[58a] It is also used as important chemical intermediate in the manufacture of vitamin C, dispersing agents, lysine, lubricants, THFA and plasticizer.[58a] Additionally, it can serve as a solvent for pigments of low solubility and also as a component in rocket fuel.[58b] MF is obtained *via* selective hydrogenolysis of furfural. It is a versatile chemical intermediate used in the production of antimalarial drugs, perfumes, crysanthemate pesticides and chloroquine lateral chains in medical polymers.[58b] Various properties of gasoline and biomass-derived fuels are summarized in Table 1.2.[59,60] The energy density of MF is higher compared to bio-ethanol and is similar to DMF (Table 1.2).[59,60] But, the flash point (-22 °C) and boiling point (64.7 °C) of MF are inferior to DMF (-1 and 92-94 °C), which would also resolves the cold engine start problems generally associated with the bio-ethanol.[60] Wang *et al.* successfully tested MF as a biofuel in a single cylinder spray guided direct-injection spark-ignition (DISI) engine.[60] The performance of MF

was satisfactory against gasoline in terms of ignition, emission and combustion properties. Thus, MF can be used as an alternative liquid fuel for transportation.

Table 1.2 Properties of gasoline and biomass-derived fuels.				
Properties	Gasoline	Bioethanol	MF	DMF
Molecular formula	C_5 - C_{10}	OH		
Boiling point (°C)	35-150	78.4	64.7	92-94
Water solubility at 25 °C (mg/mL)	insoluble	highly soluble	partially soluble	insoluble
H/C ratio	1.86	3.0	1.2	1.33
Stoichiometric air/fuel ratio	14.56	8.95	10.05	10.72
Gravimetric calorific value (MJ/kg)	43.2	26.9	31.2	33.7
Research octane number (RON)	95.8	110	103	119

1.5.3. 2,5-Dimethylfuran

Hydrogenolysis of biomass-derived HMF to DMF is an important reaction in the upgradation of biomass-derived platform compounds for obtaining biofuels. DMF is known as one of the potential transportation liquid fuel. Compared to the bio-ethanol, DMF possesses a high research octane number (RON=119), superior energy density (33.7 MJ/kg) and ideal boiling point (92-94 °C).[54] DMF consumes only one-third of the energy for the separation by distillation, compared to that required for the separation of ethanol from fermented broth.[54] Furthermore, it is immiscible with water and also easier to blend with gasoline compared to ethanol.[54] The DMF has been successfully tested as a biofuel in a single cylinder spray guided DISI engine.[60] The performance of DMF was satisfactory against gasoline. These excellent characteristics make DMF a more ideal and promising biomass-derived liquid biofuel. Moreover, DMF is also a renewable source for the synthesis of p-xylene *via* Diels-Alder reaction.[61]

1.6. Catalytic hydrogenation in chemical industries

Catalytic hydrogenation is an important reaction in the manufacture of a variety of products in chemical industries. For example aniline, cyclohexane, toluene diamine, hexamethylene diamine and 1,4-butanediol which are used in the production of plastics and polymers are synthesized *via* hydrogenation process. Sorbitol utilized in the making of personal care items is produced through hydrogenation of glucose.[62] The indirect synthesis of H_2O_2

involves the hydrogenation step of substituted anthraquinone to the corresponding hydroquinone. In petroleum industry, hydrogenation is a crucial step in the production of commodities like gasoline. Hydrogenation is also a key process for synthesizing fine chemicals and active pharmaceutical ingredients. Partial or complete hydrogenation of unsaturated fatty acid in vegetable oils is significant reaction in food industry. It is also a decisive step in the biomass upgradation to biofuels. Some industrial important hydrogenation processes have been listed in Table 1.3.

Entry	Reactant	Product	Catalyst
Table 1.3 Some industrial important hydrogenation processes.			
Entry	Reactant	Product	Catalyst
1	N_2	NH_3	Fe(111)
2	CO	CH_3OH	Cu/Zn/Al oxides
3	Unsaturated esters	Unsaturated alcohols	Cr/Cu oxides
4	Benzene	Cyclohexane	Ni
5	Olefins/CO	Aldehydes	Rh complex
6	Nitrobenzene	Aniline	Pd/C
7	Benzene	Cyclohexene	Rh(Zn)
8	Adiponitrile	Hexamethylene diamine	Ni
9	Aldehydes	Alcohols	Cu/Cr oxides
10	Maleic anhydride	Butyrolactone	Cu/Cr oxides
11	Oils	Unsaturated alcohols	Cu/Cr oxides
12	Dinitrotoluene	Diaminotoluene	Ni
13	Glucose	Sorbitol	Ni

1.7. Selectivity in catalytic hydrogenation

Selectivity is an important aspect in catalytic hydrogenation. It is defined as the ratio of the amount of desired product formed to the sum of the total amounts of all the products obtained in a particular reaction. Generally hydrogenation reactions are classified into three categories.

➢ Regioselective hydrogenation

➢ Chemoselective hydrogenation

➢ Stereoselective hydrogenation

Regioselective hydrogenation refers to the hydrogenation of one functional group in the presence of the same functional group present at a different location in an organic molecule (Scheme 1.4).[63]
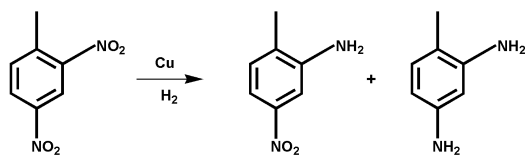
Scheme 1.4 Regioselective hydrogenation of 1-methyl-2,4-dinitrobenzene.

Chemoselective hydrogenation of the reducible functionalities has been key issue in the field of heterogeneous catalysis. It is important when one functional group has to be selectively hydrogenated in a molecule which contains more than one functional group (Scheme 1.5).[64]
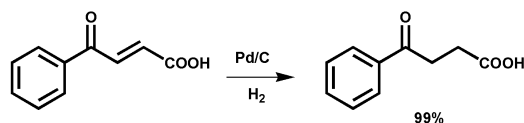
Scheme 1.5 Chemoselective hydrogenation of 4-oxo-4-phenylbut-2-enoic acid.

Stereoselective hydrogenation is related to the formation of selectively one stereoisomer. If the stereoisomers are enantiomers then such transformation is known as enantioselective hydrogenation (Scheme 1.6).[65]
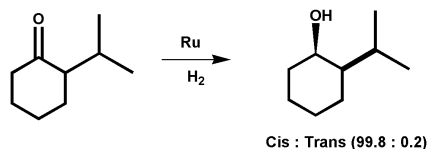
Scheme 1.6 Stereoselective hydrogenation of 2-isopropyl cyclohexanone.

1.8. Chemoselective hydrogenation of α,β-unsaturated carbonyl compounds

Chemoselective hydrogenation of α,β-unsaturated carbonyl compounds is a vital step in the field of fine chemicals, flavors and fragrance chemistry.[66] In this study cinnamaldehyde (CA) is selected as a representative α,β-unsaturated aldehyde. CA is a major constituent of cassia (≈90%) and Ceylon cinnamon bark oils (~75%). It is also present in minute amounts in many other essential oils. Selective hydrogenation of C=C group is easier than C=O group because thermodynamics favor C=C hydrogenation. CA can be selectively hydrogenated to hydrocinnamaldehyde (HCA) and cinnamyl alcohol (CAL), depending on whether C=C bond is hydrogenated or the C=O bond (Scheme 1.7). HCA and CAL are key intermediate for the synthesis of many fine chemicals, perfumes and pharmaceuticals.[67] For example CAL is an intermediate in the manufacture of antibiotic chloromycetin, in the preparation of inks used in multicolor printing, in the production of animal repellent, in the preparation of photosensitive

polymers, *etc*. HCA is used in pharmaceuticals for the synthesis of protease inhibitors, which are used in HIV treatment,[67] in the preparation of herbicidal compositions, in the sunscreen formulations for inhibiting light penetration, *etc*.
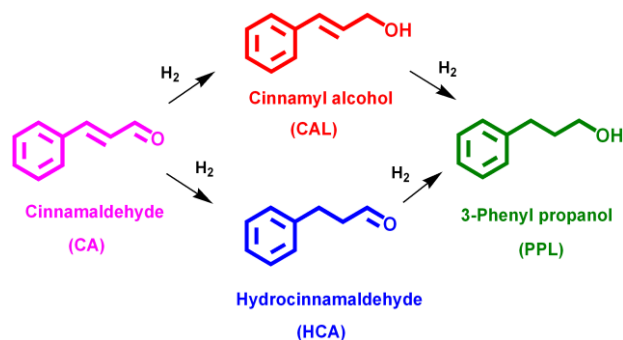
Scheme 1.7 Reaction pathways for hydrogenation of cinnamaldehyde.

CA can be selectively hydrogenated to HCA and CAL by using homogeneous catalysts, but the heterogeneous catalysts are more environmental friendly, easier to separate and can be reused compared to homogeneous catalysts. However, design of active and selective heterogeneous supported metal catalysts is not an easy task. The activity and selectivity of catalysts is highly dependent on metal and support type, metal precursor, additive, catalyst preparation and activation method, operation mode (eg. liquid or gas phase system) and selection of reaction conditions. Therefore, it is important to understand the structure of the catalyst and correlate its properties to its catalytic performance. This task is quite demanding as the hydrogenation over heterogeneous catalysts proceeds through various surface reaction steps, such as adsorption of reactant molecules, reaction and desorption of products. Moreover, the reaction mechanism is rather complicated involving dissociative/non-dissociative and competitive/non-competitive adsorption in addition to formation of coke, adsorption of solvents, side reactions, *etc*.[67a,68] Thus, it is very essential to get a complete picture of all these phenomena on the catalyst surface for achieving higher selectivities of the desired products at high substrate conversion. A part of the present thesis focuses on the selective hydrogenation of CA to HCA and CAL over supported metal catalysts.
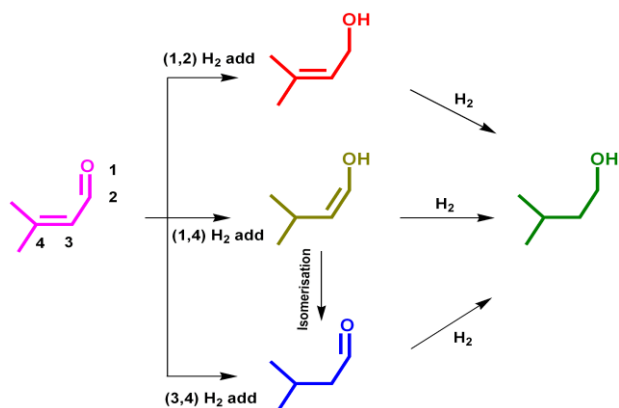
Scheme 1.8 Hydrogenation products of α,β-unsaturated aldehyde.

Gallezot *et al.* published a detailed review explaining the factors influencing the activity and selectivity of supported metal catalysts in hydrogenation of α,β-unsaturated aldehydes.[69] Hydrogenation of these compounds gives various products (Scheme 1.8). 1,2 Addition of hydrogen provides unsaturated alcohols; 3,4-addition offers the saturated aldehyde; 1,4-addition yields enolic form which then isomerizes into a saturated aldehyde. A consequent hydrogenation of C=C and C=O furnishes saturated alcohols. Over supported metal catalysts, hydrogenation of α,β-unsaturated carbonyl compounds occurs *via* Horiuti-Polanyi mechanism, which is based on Langmuir-Hinshelwood model. The mechanism involves on-top η_1, di-$\sigma_{C=C}$ η_2, di-$\sigma_{C=O}$ η_2, $\pi_{C=C}$ η_2, $\pi_{C=O}$ η_2 or di-π η_2 (η_4) and these are shown in Scheme 1.9.
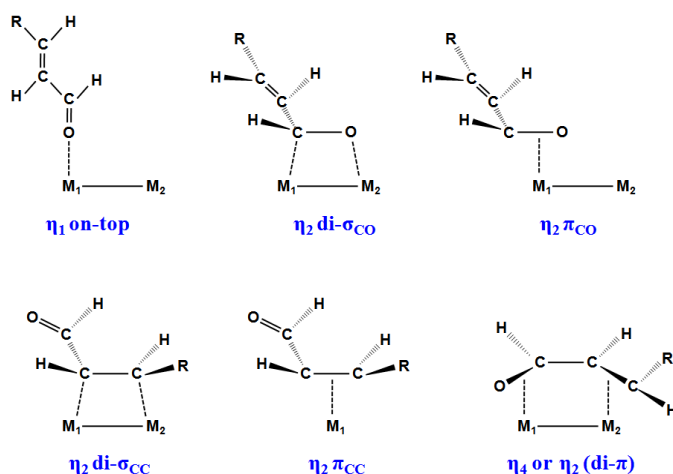
Scheme 1.9 Schematic illustrations of adsorption states involved in hydrogenation of α,β-unsaturated carbonyl compounds over supported metal catalysts.[70]

Based on the theoretical studies of semiempirical extended Huckel calculations, Delbecq *et al.* explained the adsorption of several α,β-unsaturated aldehydes (CA, acrolein and

crotonaldehyde) on Pd and Pt surfaces.[70] The results revealed that the mode of molecule adsorption depends upon the nature of the active metal and the type of exposed plane. For instance, di-σ form is preferred on Pt(111), a planar η_4 one on Pd(111) and Pt(100) and a $\pi_{C=C}$ one on Pt(110).

1.9. Hydrotalcites

Hydrotalcites (HTs)-like materials, also known as layered double hydroxides (LDHs) are a class of nanostructured anionic clays. Its structure can be described as containing brucite [$Mg(OH)_2$] like layers in which part of the divalent cations (Mg^{2+}) coordinated octahedrally by hydroxyl groups are replaced isomorphously by trivalent cations such that the layers acquire positive charge and the charge-balancing anions exist in the interlayer region along with some water molecules (Fig. 1.10).[71] HTs are formed in nature by the weathering of basalts or from precipitation in saline water sources. They may be represented by the general formula:

$$[M^{2+}_{1-x} M^{3+}_x (OH)_2]^{x+}(A^{n-})_{x/n} \cdot m H_2O$$
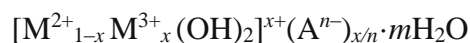
where M^{2+} (M = Mg, Fe, Co, Cu, Ni or Zn) and M^{3+} (M = Al, Cr, Ga, Mn or Fe) are di- and tri-valent cations, respectively; the value of x is equal to the molar ratio of $M^{2+}/(M^{2+} + M^{3+})$ and is normally in the range of 0.2 to 0.33 and A^{n-} is an anion (A = CO_3^{2-}, NO_3^-, Br^-, Cl^-, F^-, OH^-, SO_4^{2-}, CrO_4^{2-}, $HAsO_4^{2-}$ or HPO_4^{2-}). Many HTs involving the mixtures of different M^{2+} and/or M^{3+} cations can be prepared. In addition, M^+ and M^{4+} cations can also be used to partially substitute M^{2+} and M^{3+}. Therefore, a large class of iso-structural materials with a broad range of physico-chemical features can be prepared by changing the molar ratios of M^{2+}/M^{3+}, the nature of the metal cations and the type of interlayer anions.
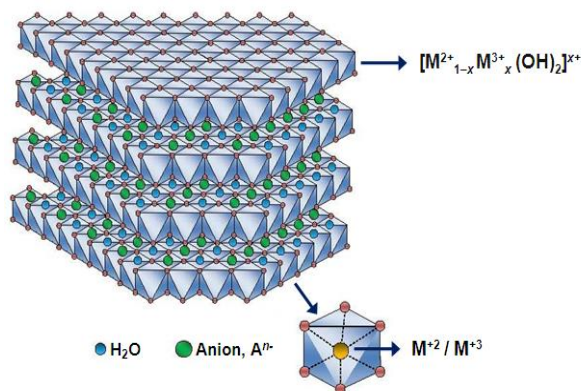
Fig. 1.10 Schematic illustration of the hydrotalcites.

As prepared HTs as well as the oxides obtained upon its thermal treatment are promising materials for a large number of practical applications in pharmaceuticals, electrochemistry, photochemistry, catalysis, adsorption and in other areas.[71-73] This is due to their easily tailored properties, high versatility and low preparation cost, which allowed the designing of materials in order to fulfill the specific requirements. In recent years, growing interest has been devoted to the use of HTs as host materials for developing inorganic-organic host-guest hybrid structures with desirable chemical and physical properties. In these types of structures, the brucite layers may impose a restricted geometry on the interlayer guests leading to improved control of stereochemistry, product distributions and rates of reaction. The opportunity in the development of three-dimensional pillared layered structure by suitable intercalation methods offers new perceptions for functional materials with novel properties.

1.10. Zeolites

Zeolites are crystalline microporous aluminosilicates with highly ordered structures either of natural or synthetic origin.[74] They consist of interlinked tetrahedra of alumina (AlO_4^-) and silica (SiO_4) through shared oxygen atoms resulting into a three dimensional network of channels with some cavities. The presence of trivalent Al atoms in the framework gives excess negative charge which is compensated by the cations which are mostly alkali or alkaline-earth metal ions (Na^+, K^+, Ca^{2+} and Mg^{2+}) present in the intrazeolitic channels along with H_2O molecules. These metal ions are loosely held and can be easily exchanged for other ions. Hence, the interior of the pores becomes the active surface of zeolites. If metal ions are exchanged by protons, Brønsted acidity is imparted in zeolite pores and cavities. Thus, number of acid sites is related to Si/Al molar ratio in these materials. The inner porosity depends on zeolite structure and its composition. The crystallographic unit cell of a zeolite may be represented as:

$$M_{y/n} [(SiO_2)_x(AlO_2)_y].zH_2O$$
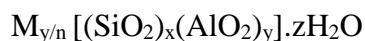
where, M is a charge compensating metal ion with valency 'n'. The value of ratio x/y may be from 1 to ∞. The 'z' represents the number of H_2O molecules in the zeolite pores, which can be reversibly adsorbed or desorbed. The structure of zeolites provides them with excellent features like high BET surface area, active acidic sites, adsorption properties, good thermal/hydrothermal stability, shape selectivity because of uniform channels and pores, ease of regeneration, *etc*. These admirable properties of zeolites makes them strong candidates for ion exchange, gas

separation, as detergent builders and adsorbents, as catalysts especially in petrochemical sector, oil refinery and in the production of fine chemicals.[75]

1.10.1. Nomenclature

Even though, there is no systematic nomenclature for molecular sieve materials, the International zeolite association (IZA) and IUPAC have allocated three capital alphabets as structural codes to natural and synthetic zeolites.[76] These three capital letters have been used to categorize the structure types (Table 1.4). These codes for zeolite identification are usually derived from the names of the type of materials and do not contain numbers and characters other than roman letters. The structure type codes are not dependent on chemical composition, crystal symmetry, cell dimensions or distribution of various T atoms (e.g. Si^{4+}, Ti^{4+}, Al^{3+}, *etc*).

Table 1.4 Some common structural codes of zeolites.	
Structural code	*Zeolite*
FAU	Faujasite: X and Y
MFI	Mobil Five: ZSM-5
MEL	Mobil Eleven: ZSM-11
MOR	Mordenite
FER	Ferrierite
BEA	Beta

1.10.2. Classification

Various efforts have been made to categorize the zeolites on the basis of their chemical composition, natural occurrence, pore diameter and crystal structure which are discussed in the following sections.

1.10.2.1. Nature of secondary building units

Zeolites have been classified on the basis of variations in the secondary building units (SBU).[77] The SBU's are aluminosilicates oligomers having chain, ring and cage like structures, which are the basic building blocks of zeolites framework. The various SBU's are pictorially presented in Fig. 1.11. These SBU's come together in different combinations to form zeolite structures. All known structures of zeolites can be produced using the SBU's mentioned here.
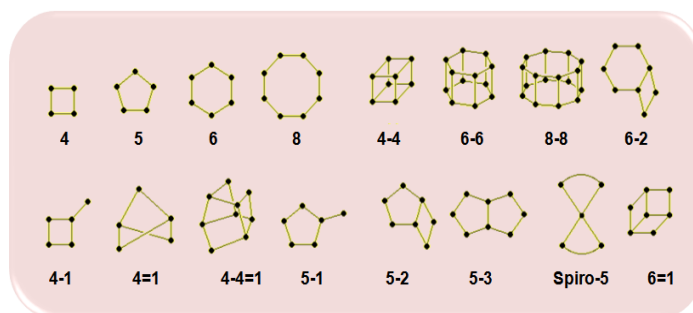
Fig. 1.11 Secondary building units in zeolites.[77]

1.10.2.2. Chemical composition

Zeolites can be categorized according to their chemical composition.[78] Depending on Si/Al ratio, zeolites are classified as low silica, intermediate silica, high silica and pure silica zeolites (silicalites) (Table 1.5).

Table 1.5 Classification of zeolites on the basis of chemical composition.		
Type	*Si/Al ratios*	*Examples*
Low silica	1.0 to 1.5	Sodalite, X, Y
Intermediate silica	2 to 5	L, Mordenite, Omega, FAU
High silica	5 to thousands	ZSM-5, EU-1
Silicate (all silica)	Infinity	Silicalite-1, Silicalite-2

Table 1.6 Classification of zeolites on the basis of pore size.		
Small pore (8 member ring)	*Medium pore (10 member ring)*	*Large pore (12 member ring)*
MTN	Ferrierite (FER)	Cancrinite
NU-1	ZSM-5 (MFI)	Linde X, Y, L
Chabazite	ZSM-11 (MEL)	Mazzite
Erionite	ZSM-50 (EU-1)	Mordenite
Clinoptillolite	Stilbite	Offretite
ZK-5	ZSM-23	ZSM-12 (MTW)
Linde A	ZSM-22 (Theta-1)	Omega
Rho	ZSM-48 (EU-2)	Beta (BEA)

1.10.2.3. Pore size

Zeolites have also been categorized on the basis of their pore diameter. The pore diameter of zeolite depends upon the number of tetrahedra present in the ring aperture. Depending on the

pore openings, zeolites are generally classified into small pore (6 or 8-member ring), medium pore (10-member ring) and large pore (12-member ring).[79] Table 1.6 demonstrates the examples depending on the pore size classification.

1.10.3. Faujasite zeolite

The faujasite zeolite framework consists of sodalite cages which are connected *via* hexagonal prisms. The pores formed by a 12 membered ring has a large diameter of 7.4 Å. The inner cavity (Supercage) has a diameter of 12 Å and is surrounded by 10 sodalite cages.[80a] The pores are organized perpendicular to each other. The faujasite zeolite possesses cubic crystal system. This group consists of faujasite-Na, faujasite-Mg and faujasite-Ca and they all share the same basic formula: $(Na_2,Ca,Mg)_{3.5}[Al_7Si_{17}O_{48}] \cdot 32(H_2O)$. The framework structure of faujasite zeolite is shown in Fig. 1.12. Faujasite zeolite was named after the French geologist and volcanologist Barthélemy Faujas de Saint-Fond (1741-1819). Zeolite Y exhibits the faujasite (FAU) structure. It has a 3-dimensional pore structure and pores are perpendicular to each other in the x, y and z planes.[80b] It is consist of SBU 4, 6 and 6-6. The unit cell is cubic (a= 24.7 Å) with Fd-3m symmetry.
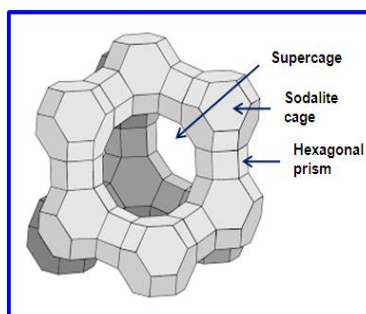
Fig. 1.12 Framework structure of faujasite zeolite.

1.11. Carbon materials and nitrogen-doped carbon

1.11.1. Different structures of carbon

Carbon is one of the most abundant elements in nature. There are several allotropes of carbon depending on its specific hybridization and bonding arrangement to surrounding atoms. Carbon with sp^3 hybridization gives diamond with a tetrahedral lattice. Carbon with sp^2 hybridization will form fullerene (60 carbon atoms forming a sphere), graphite (arranged in hexagonal sheets) or carbon nanotubes (long hollow tubes of carbon) depending on the synthesis conditions. Some allotropes of carbon like diamond and graphite occurred naturally and were

known from ancient times. On the other hand nanotubes and buckyballs were discovered recently and are being prepared and characterized.[81] Carbon materials have revolutionized the material science field in recent years. Carbon nanomaterials and its allotropes provide a wide range of useful properties pertaining to high tensile strength, high BET surface area, chemical and thermal stability, *etc*., making them very fascinating materials to a broad range of industries. Graphite and amorphous carbon are the two most common allotropes and they make up the majority of natural carbon compounds for example soot and coal. In the following sections various types of carbon allotrope are discussed.

1.11.1.1. Amorphous carbon

Amorphous carbon does not have any crystalline structure (Fig. 1.13).[82a] This carbon form is highly disordered with no structural integrity. The disorder permits it to have many available bonds and because of that more complex carbon based structures can be constructed. As with all amorphous materials, some-short range order may be observe with amorphous carbon. The true amorphous carbon has localized π electrons and bonds formed in it are inconsistent in lengths compared to any other allotrope of carbon.[82a] It also possesses dangling bonds with high concentration, which causes deviations in interatomic spacing as well as significant change in bond angle.
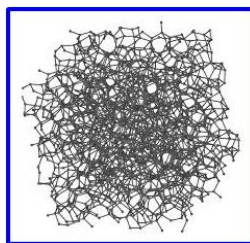
Fig. 1.13 Structure of amorphous carbon.

1.11.1.2. Graphite

Graphite is a crystalline form of carbon. It has layered and planar structure. Graphite is the most stable form of carbon in standard conditions. Carbon atoms are arranged in a honeycomb lattice in each layer with carbon-carbon sp^2 bond length of 0.142 nm and the spacing between these carbon layers is 0.335 nm (Fig. 1.14).[82b] Atoms in plane are covalently bonded with only three of the four possible bonding sites satisfied. The fourth electron is free to migrate in the plane and is no longer local to a single carbon atom (i.e. delocalized electron) and thus making graphite electrically conductive. But, it does not conduct electricity in a direction at right

angle to the plane. The layers are bonded through weak van der Waals forces, allowing layers of graphite to be easily separated or to slide past each other. There are two forms of graphite namely alpha and beta.[82b] They have very similar physical properties, except the graphene layers stack slightly differently. The alpha form of graphite possess hexagonal lattice with ABAB stacking sequence of the layers whereas beta form has rhombohedral lattice with ABCABC stacking sequence of the layers. The beta form is unstable and converts into alpha when it is heated above 1300 °C. Also, the alpha form can be converted to the beta form *via* mechanical treatment. Natural graphite has been found to contain up to 30% of the beta form. A pure alpha form of graphite can be produced synthetically.
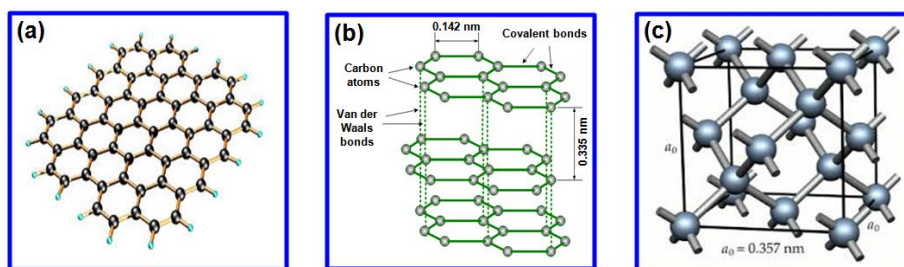
Fig. 1.14 Structure of (a) graphene, (b) graphite and (c) diamond.

1.11.1.3. Diamond

Diamond is another allotrope of carbon and is less stable than graphite. In diamond, the carbon atoms are arranged in a face-centered cubic crystal structure called a diamond lattice (Fig. 1.14c).[82c] Diamond is famous as a material with superior physical properties, most of which comes from the strong covalent bonding between its atoms. For example, it has the highest hardness and thermal conductivity of any bulk material. Naturally occurring diamonds are formed at high temperature and pressure at depths of 140-190 kilometers in the Earth's mantle. Diamond has been successfully grown synthetically in a HPHT method which nearly stimulates the conditions in the Earth's mantle.

1.11.1.4. Activated carbon

Activated carbon is crude form of graphite. It differs from graphite by having an imperfect random structure and highly porous with over broad range of pore sizes.[82d] Hence, it has large surface area, often more than 1000 m^2/g, thus having stronger physical adsorption forces. Further, chemical treatment can amplify the adsorption properties. Activated carbon is a carbon synthesized from carbonaceous materials like wood, peat, nutshells, coconut husk, coir,

coal and petroleum pitch. It can be produced *via* physical (steam) activation or chemical activation.

1.11.1.5. Fullerene

The first fullerene molecule was discovered in 1985 by Richard Smalley, Robert Curl, James Heath, Harold Kroto and Sean O'Brien at Rice University.[82e] This novel form of carbon was named as Buckminsterfullerene or C_{60}. This name was given to honor Buckminster Fuller, who popularized geodesic domes. It is a molecule with 60 carbon atoms dispersed on the summits of a regular polyhedron constituted of hexagonal and pentagonal facets (Fig. 1.15). Latter other fullerenes such as C_{70}, C_{80}, *etc* were also discovered.
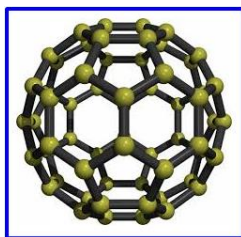
Fig. 1.15 Structure of fullerene.
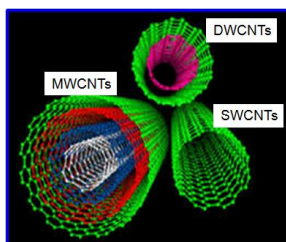
Fig. 1.16 Schematic illustration of different types of carbon nanotubes.

1.11.1.6. Carbon nanotubes

Carbon nanotubes (CNTs) are the members of fullerene structural family and can be considered as elongated fullerenes. CNTs name is derived from their long, hollow structure with the walls formed by one-atom-thick sheets of carbon, called graphene, which rolled up into a cylinder (Fig. 1.16).[82f] These graphene sheets are wrapped at specific and distinct angles. The combination of the rolling angle and radius decide the CNTs properties. CNTs can be categorized into two types: single-walled carbon nanotubes (SWCNTs) and multi-walled carbon nanotubes (MWCNTs). The structure of SWCNTs can be hypothesized by rolling a graphene sheet into a seamless cylinder. On the other hand MWCNTs consist of multiple rolled layers (concentric tubes) of graphene.

1.11.2. Nitrogen-doped carbon

In carbon materials it is the long- and short-range coordination and sequencing of carbon atoms that necessarily decides the electrical properties and hence its potential for different chemical processes.[83] Graphitic carbon materials have been extensively employed as catalyst supports for anchoring metal nanoparticles in various industrial applications. However, metal nanoparticles supported on carbon materials easily leach out during catalytic processes because of weak interaction between metal nanoparticles and carbon surface. Therefore, there is a need to modify the carbon materials in majority of cases in order to meet increasing demands of catalysis.[84] Without defects SWCNTs cannot effectively anchor Pd nanoparticles.[85] For strengthening the interaction between metal nanoparticles and the support, carbon materials are usually oxidized with HNO_3 before used as host materials to generate more defects.[86] In case of heterogeneous catalysts, support and metal are not independent systems. Here, the support plays an important role, which is similar to that of ligands in homogeneous catalysis.

The properties of carbon materials can be significantly modulated by size confinement effect as well as by doping with hetero atoms. Phosphorus and nitrogen as electron donors or boron as an electron acceptor, have been incorporated into carbon matrix in order to alter the position of conduction band and valence band of the doped carbon material, resulting in modified work function and often a slightly opened band gap.[87] The most common dopant in carbon materials is the nitrogen, which can considerably reduce the work function of nitrogen-doped carbon. This will transform the material significantly to more noble. Once the band gap of the nitrogen-doped carbon is opened, a space charged layer may form between N-doped carbon and metal nanoparticles (Fig. 1.17). This is very important for activating the metal nanoparticles by increasing their electron density. Additionally, N-doping improves the carbon-metal nanoparticles binding interaction and also amplifies the number of chemically active sites. This can be witnessed by increased metal dispersion, much higher resistance to metal sintering and coarsening and enhanced catalytic performance. X-ray photoelectron spectroscopy (XPS) showed that N-doped carbon compounds contain mostly three types of nitrogen atoms including pyridinic-N, pyrrolic-N and graphitic-N (Fig. 1.18), with their respective fractions highly dependent on the method of preparation. DFT studies further showed that the carbon materials containing reasonable to high N-doping levels in the form of N interstitials and carbon-N defect, can act as local heterogeneous anchoring sites for metal nanoparticles.[87] These theoretical

predictions could be confirmed by the large number of experimental studies. For instance, Lei *et al.* observed strong interaction between Pt nanoparticles and nitrogen atoms, which is crucial for good dispersion of Pt on N-doped carbon.[88] Therefore, N-doped carbon materials are considered as good supports to stabilize and activate metal nanoparticles.
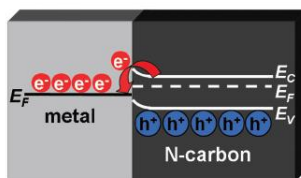
Fig. 1.17 Schematic view of the typical metal-N-carbon contact.
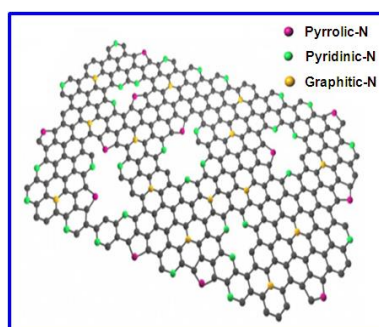
Fig. 1.18 Schematic view of the N-doped carbon showing different types of N atoms.

N-doped carbon supported metal catalysts have been extensively used for fuel cell catalysis. For example, a large number of studies demonstrate that N-doped carbon supported Pt catalysts exhibited admirable catalytic activity and durability for both oxygen electro-reduction and methanol electro-oxidation as compared to N-free carbon supported metal catalysts.[87-88] Furthermore, the results also suggest that the metal-free N-doped mesoporous carbon, N-doped CNTs and N-doped graphene displayed very good activity and durability for both oxygen electro-reduction and methanol electro-oxidation, which is well beyond the activity of N-free carbon materials.[89] In principle, N-doped carbon supported metal catalysts can also provide superior catalytic activity in various useful organic transformations. Motoyama *et al.* reported Pd nanoparticles supported on carbon nanofibers (CNFs) as highly efficient recyclable catalysts for the selective hydrogenation of nitro-groups of functionalized nitroarenes.[90] A similar promotional effect of the N-doped carbon has been observed by the same research group over Pt nanoparticle based catalyst in the partial hydrogenation of internal alkynes to the corresponding *(Z)*-alkenes.[91] As compared to other efficient reported catalysts (e.g., Lindlar quinoline catalyst

and Pd/SiO$_2$-DMSO), the N-doped CNFs supported Pd catalyst gave better selectivity and higher turnover numbers.[91] Thus, it can be visualized that more efforts will be focused in the near future on the utilization of N-doped carbon supported metal catalysts as highly efficient and stable catalysts for the chemical industries.

1.12. Objectives of the thesis

The overall objective of this thesis is to unravel factors influencing the catalytic activity of supported metal catalysts in hydrogenation/hydrogenolysis reactions. One of the objectives is to prepare supported metal catalysts for selective hydrogenolysis of biomass-derived furfural and HMF to achieve high space time yields of MF and DMF, using molecular H$_2$ and transfer hydrogenating agents. The other aim is to develop catalysts that are highly active under benign reaction conditions to get HCA and CAL on hydrogenation of CA.

1.13. Organization of the thesis

The thesis is divided into six chapters. A brief description of the contents of each chapter is given below.

Chapter 1: Introduction

Chapter 1 gives an introduction to the potential of biomass-derived compounds for the production of fine chemicals and fuels. Prime importance is given to the hydrogenolysis of biomass-derived furfural and 5-hydroxymethylfurfural (HMF) to 2-methylfuran (MF) and 2,5-dimethylfuran (DMF), respectively. The selective hydrogenation of furfural to furfuryl alcohol (FA) is also discussed. The properties and significance of furfural, HMF, MF, DMF and FA is also mentioned. This chapter also includes an introduction to the selective hydrogenation of cinnamaldehyde (CA), a representative of α,β-unsaturated carbonyl compounds. The industrial importance of CA hydrogenation products such as cinnamyl alcohol (CAL) and hydrocinnamaldehyde (HCA) is highlighted. It also describes various catalyst supports used like hydrotalcites, zeolites, carbon materials and nitrogen-doped carbons. Finally, the objectives of the thesis are outlined briefly.

Chapter 2: Catalyst synthesis and experimental techniques for characterization

Chapter 2 describes the catalysts preparation methods and experimental techniques employed for their characterization. The catalysts synthesized were Ru-doped hydrotalcites and

NaY zeolite supported Ru, Pt, Pd, Rh, Au, Ni and Cu catalysts. In addition, nitrogen-doped mesoporous carbons (NMC's) with different N-contents were prepared and were used as supports for Ru, Pt, Pd, Rh, Au, Ni and Cu metals. They were characterized by using various physico-chemical techniques including X-ray diffraction (XRD), N_2 sorption, H_2 chemisorption, scanning and transmission electron microscopy (SEM and TEM), Raman spectroscopy, X-ray photoelectron spectroscopy (XPS), temperature programmed desorption (TPD) of ammonia and CO_2, temperature programmed reduction (TPR) in H_2, inductively coupled plasma-optical emission spectrometry (ICP-OES), *etc*. Theory and experimental procedures of each of these techniques have been described in this chapter.

Chapter 3: Reductive upgradation of biomass-derived furanic compounds over supported metal catalysts using H_2

Chapter 3 starts with detailed literature review of hydrogenolysis of HMF to DMF, followed by the present work on hydrogenolysis of biomass components. This reaction is carried out on two types of supported Ru catalysts using molecular H_2. Therefore, the chapter is divided into two parts, i.e., 3A and 3B. Part 3A deals with the investigations pertaining to Ru-doped hydrotalcites as catalysts for hydrogenolysis of HMF to DMF. It presents the characterization of Ru-doped hydrotalcite catalysts using XRD, SEM and TEM to study their structure and morphology before and after Ru incorporation. The results of N_2 sorption, H_2 chemisorption, TPR and XPS are also discussed in detail. The activity of the catalysts in HMF hydrogenolysis and optimization of reaction conditions is also given in this part. Part 3B deals with the preparation of DMF from HMF using NaY zeolite supported metal catalysts. It exhibits the characterization results of catalysts using XRD, N_2 sorption, H_2 chemisorption, SEM, TEM, NH_3-TPD, TPR, XPS, *etc*. The experimental results for the preparation of DMF are also given. Moreover, this part also includes the results of studies related to the hydrogenation of furfural to FA.

The investigations show that highly dispersed Ru was obtained on calcination of hydrotalcite-like precursors, which were prepared through co-precipitation. Catalyst containing only 0.56 wt% Ru yielded 58 mol% of DMF, showing that smaller Ru crystallites are needed for higher DMF yield, as consecutive ring hydrogenation is suppressed. Higher DMF yields were obtained when 2-propanol was used as the solvent, as a result of hydrogen transfer from 2-propanol to HMF. This catalyst was recyclable without any noticeable loss in activity.

Among various transition metal exchanged NaY catalysts, Ru-NaY showed relatively better activity and gave 78 mol% DMF yield in 1 h of reaction time. DMF yields were correlated with dispersion of Ru metal and its crystallite size. This catalyst exhibited excellent recyclability. Based on the results, a plausible reaction pathway for the DMF from HMF was proposed. The results clearly show that DMF is formed through hydrogenolysis of –OH groups in 2,5-bis(hydroxymethyl)furan (BHMF) followed by 5-methyl furfuryl alcohol (MFA). Under optimized reaction conditions, FA can be selectively produced (86.1 mol% yield) on furfural hydrogenation over 2wt% Ru-NaY catalyst. Conclusions were drawn based on the experimental results and given at the end of each section.

Chapter 4: Catalytic transfer hydrogenolysis of biomass-derived furanic compounds over nitrogen-doped mesoporous carbon supported metal catalysts

Chapter 4 described the characterization results of nitrogen-free mesoporous carbon (MC), NMC's with various N-contents and supported metal catalysts using XRD, N_2 sorption, XPS, Raman spectroscopy, TEM, CO_2-TPD, *etc*. The catalytic activity in transfer hydrogenolysis of HMF and furfural is also described in detail.

Catalytic transfer hydrogenolysis of furfural to MF and HMF to DMF was carried out over metal supported on NMC's. It was found that during hydrogenolysis reaction, temperature, hydrogen donor, nitrogen content, size of the Ru nanoparticles and catalyst support play vital role in the conversion of substrate to give desired product. Transfer hydrogenolysis activity was enhanced with increasing nitrogen content of the catalyst. Under optimized reaction conditions, 2wt% Ru-NMC catalyst with 11.6 wt% nitrogen content gave 84 and 87 mol% yield of DMF and MF, respectively with 2-propanol as the hydrogen donor. This catalyst was recyclable and its excellent performance was attributed to the high Ru dispersion and stabilization of Ru nanoparticles by the nitrogen present in the support. The characterization results were corroborated with the catalytic performance at the end of the chapter.

Chapter 5: Chemoselective hydrogenation of cinnamaldehyde over Pd and Au supported on nitrogen-doped mesoporous carbon

Chapter 5 begins with detailed literature review on the hydrogenation of CA to HCA and CAL followed by the present work on the selective hydrogenation of CA to HCA and CAL over supported metal catalysts using molecular H_2. This chapter is divided into two parts. Part 5A deals with selective hydrogenation of CA to HCA. It discusses characterization of supported Pd

catalysts using XRD, N$_2$ sorption, XPS, TEM, Raman spectroscopy, *etc*. The catalytic activity in selective hydrogenation of CA to HCA is also discussed in this part. Part 5B deals with selective hydrogenation of CA to CAL using NMC and metal oxide supported Au catalysts. The characterization of Au catalysts was carried out using various physico-chemical techniques. It also describes the catalytic activity of these catalysts in the conversion of CA to CAL.

Catalyst with 2wt% Pd on NMC shows remarkable catalytic activity and high HCA selectivity (93%) under mild reaction conditions (30 °C, 1 bar H$_2$). The observed high catalytic activity and better C=C hydrogenation selectivity was attributed to small particle size of Pd nanoparticles as a result of peculiar metal-support interaction between Pd and NMC and support mesoporosity that facilities easier diffusion of reactants and hydrogenated products. The 2wt% Pd-NMC catalyst was recyclable without any loss in catalytic activity and HCA selectivity.

Part 5B contains discussion on highly dispersed Au on NMC, which was prepared by sol-immobilization technique. Among the supported Au catalysts tested, 1wt% Au-NMC catalyst displayed superior hydrogenation activity and good CAL selectivity (78%). The presence of small Au nanoparticles are indispensable for achieving high activity, because of their higher number of d electrons, which favors the selective hydrogenation of C=O bond in CA. Moreover, the basicity of NMC support also facilitate the adsorption of CA through their C=O group and thereby improve catalytic activity and CAL selectivity. The catalytic performance of 1wt% Au-NMC remains same in recyclability study. The conclusions were drawn from the above studies which are included at the end of each section.

Chapter 6: Summary and conclusions

This chapter describes the inferences and conclusions drawn upon the investigations conducted with regard to various catalysts employed in the selective hydrogenation and hydrogenolysis of biomass-derived compounds for obtaining chemicals and fuels. It also includes the conclusions obtained upon the study associated with selective hydrogenation of CA. Since, it is also mandatory to summarize the work for the benefit of the reader; this chapter summarizes the results of this work. Further, at the end of this chapter, it offers some suggestions for further research in these areas.

1.14. References

1. (a) S. Green, Industrial Catalysis, Macmillan Company, New York, 1928; (b) J. J.

Berzelius, Arsberattelse Om Framstegen I Fysik Och Kemi, Royal Swedish Academy of Sciences, 1835; (c) J. J. Berzelius, Reseanteckningar, P. A. Norstedt and Söner, Stockholm, 1903.

2. B. H. Davis, G. Ertl, H. Knözinger, J. Weitkamp (Eds.), Handbook of Heterogeneous Catalysis, Vol. 1, VCH, Weinheim, 1997.

3. B. Lindstroma and L. J. Petterson, *Cat. Tech.,* 2003, **7**, 130.

4. J. Hagen, Industrial Catalysis: A Practical Approach, 2nd ed. VCH, Weinheim, 2006.

5. C. G. Brundtland, Our Common Future, The World Commission on Environmental Development, Oxford University Press, Oxford, 1987.

6. P. Anastas and J. C. Warner, *Green Chemistry: Theory and Practice,* Oxford University Press, Oxford, 1998.

7. D. A. Simonetti and J. A. Dumesic, *ChemSusChem, 2008,* **1**, 725.

8. Energy Information Administration (EIA) International Energy Outlook, 2007. http://www.eia.doe.gov/oiaf/ieo/index.html

9. D. Y. Goswami and F. Kreith, Handbook of Energy Efficiency and Renewable Energy, CRC Press/Taylor & Francis, Boca Raton, 2007.

10. https://en.wikipedia.org/wiki/Global_warming

11. A. Pandey, Handbook of plant based biofuels, CRC Press/Taylor & Francis, Boca Raton, 2008.

12. (a) R. H. He, P. Ye, B. C. English and J. A. Satrio, *Bioresour. Technol.*, 2009, **100**, 5305; (b) Y. Y. Wu, Z. H. Fu, D. L. Yin, Q. Xu, F. L. Liu, C. L. Lu and L. Q. Mao, *Green Chem.*, 2010, **12**, 696.

13. National Renewable Energy Laboratory, Conceptual biorefinery, 2005 http://www.nrel.gov/biomass/biorefinery.html

14. S. Lima, M. M. Antunes, M. Pillinger and A. A. Valente, *ChemCatChem,* 2011, **3**, 1686.

15. (a) D. M. Alonso, J. Q. Bond and J. A. Dumesic, *Green Chem.,* 2010, **12**, 1493; (b) J. B. Binder and R. T. Raines, *J. Am. Chem. Soc.*, 2009, **131**, 1979; (c) D. M. Alonso, S. G. Wettstein and J. A. Dumesic, *Chem. Soc. Rev.*, 2012, **41**, 8075.

16. C. E. Wyman, S. R. Decker, M. E. Himmel, J. W. Brady, C. E. Skopec and L. Viikari, In Polysaccharides, 2nd ed., S. Dumitriu, Marcel Dekker (Eds.) New York, 2005.

17. A. C. O'Sullivan, *Cellulose,* 1997, **4**, 173.

18. T. A. Hsu, M. R. Ladisch and G. T. Tsao, *Chem. Technol.,* 1980, **10**, 315.

19. http://www.eere.energy.gov/biomass/feedstock_glossary.html

20. R. J. Evans, T. A. Milne and M. N. Soltys, *J. Anal. Appl. Pyrolysis,* 1986, **9**, 207.

21. E. Adler, *Wood Sci. Technol.*, 1977, **11,** 169.

22. Y. Zhao, L. Deng, B. Liao, Y. Fu and Q. X. Guo, *Energy Fuels,* 2010, **24**, 5735.

23. J. P. Lange, *Biofuels Bioprod. Bioref.,* 2007*,* **1**, 39.

24. M. E. Dry, *Catal. Today,* 2002, **71**, 227.

25. K. Klier, *Adv. Catal.,* 1982, **31**, 243.

26. E. L. Kunke, R. R. Soares, D. A. Simonetti and J. A. Dumesic, *Appl. Catal. B,* 2009, **90**, 693.

27. S. Koppatz, C. Pfeifer, R. Rauch, H. Hofbauer, T. Marquard-Moellensted and M. Specht, *Fuel Process. Technol.,* 2009, **90**, 914.

28. C. N. Hamelinck, R. A. Surs and A. P. C. Faaij, *Biomass Bioenergy,* 2005, **29**, 114.

29. D. Mohan, C. U. Pittman and P. H. Steele, *Energy Fuels,* 2006, **20**, 848.

30. D. C. Elliott, *Energy Fuels,* 2007, **21**, 1792.

31. T. R. Carlson, T. P. Vispute and G. W. Huber, *ChemSusChem,* 2008, **1**, 397.

32. Y. Shun and J. Cheng, *Bioresour. Technol.,* 2002, **83**, 1.

33. A. Carroll and C. Somerville, *Annu. Rev. Plant Biol.,* 2009, **60**, 165

34. (a) S. Lima, M. M. Antunes, M. Pillinger and A. A. Valente, *ChemCatChem,* 2011, **3**, 1686; (b) T. Stahlberg, W. J. Fu and J. M. Woodley, *ChemSusChem,* 2011, **4,** 451.

35. F. W. Lichtenthaler, In Methods and Reagents for Green Chemistry: An Introduction, P. Tundo, A. Perosa and F. Zecchini (Eds.), John Wiley & Sons, Inc., New York, 2007.

36. A. Boisen, T. B. Christensen, W. Fu, Y. Y. Gorbanev, T. S. Hansen, J. S. Jensen, S. K. Klitgaard, S. Pedersen, A. Riisager, T. Ståhlberg and J. M. Woodley, *Chem. Eng. Res. Des.,* 2009, **87**, 1318.

37. M. E. Zakrzewska, E. B. Lukasik and R. B. Lukasik, *Chem. Rev.,* 2011, **111**, 397.

38. J. N. Cheda, G. W. Huber and J. A. Dumesic. *Angew. Chem. Int. Ed.,* 2007, **46**, 7164.

39. M. J. Climent, A. Corma and S. Iborra, *Green Chem.,* 2011, **13**, 520.

40. X. Tong, Y. Ma and Y. Li, *Appl. Catal. A,* 2010, **385**, 1.

41. C. Luo, S. A. Wang and H. C. Liu, *Angew. Chem.,* 2007, **119**, 7780.

42. M. S. Holm, S. Saravanamurugan and E. Taarning, *Science,* 2010, **328**, 602.

43. T. Werpy and G. Petersen, "Top Value Added Chemicals from Biomass: Vol. 1-Results of Screening for Potential Candidates from Sugars and Synthesis Gas", Report No. NREL/TP-510-35523; National Renewable Energy Laboratory, Golden, CO, 2004. http://www.osti.gov/bridge.

44. A. Corma, S. Iborra and A. Velty, *Chem. Rev.,* 2007, **107**, 2411.

45. E. L. Kunkes, D. A. Simonetti, R. M. West, J. C. Serrano-Ruiz, C. A. Gärtner and J. A. Dumesic, *Science,* 2008, **322**, 417.

46. (a) R. Karinen, K. Vilonen and M. Niemela, *ChemSusChem*, 2011, **4**, 1002; (b) J. B. Binder, J. J. Blank, A. V. Cefali and R. T. Raines, *ChemSusChem,* 2010, **3**, 1268; (c) C. Aellig and I. Hermans, *ChemSusChem,* 2012, **5**, 1737.

47. M. Murkovic and N. Pichler, *Mol. Nutr. Food Res.*, 2006, **50**, 842.

48. A. A. Rosatella, S. P. Simeonov, R. F. Frade and C. A. Afonso, *Green Chem.,* 2011, **13**, 754.

49. B. Hucker and P. Varelis, *Food Chemistry*, 2011, **126,** 1512.

50. S. Sitthisa, W. An and D. E. Resasco, *J. Catal.,* 2011, **284**, 90.

51. M. Hronec and K. Fulajtarová, *Catal. Commun.,* 2012, **24**, 100.

52. N. K. Gupta, S. Nishimura, A. Takagaki and K. Ebitani, *Green Chem.,* 2011, **13**, 824.

53. R. Alamillo, M. Tucker, M. Chia, Y.P. Torres and J. A. Dumesic, *Green Chem.,* 2014, **14**, 1413.

54. Y. Román-Leshkov, C. J. Barrett, Z. Y. Liu and J. A. Dumesic, *Nature,* 2007, **447**, 982.

55. J. Tuteja, H. Choudhary, S. Nishimura and K. Ebitani, *ChemSusChem,* 2014, **7**, 96.

56. B. Girisuta, L. P. Janssen and H. J. Heeres, *Green Chem.,* 2006, **8**, 701.

57. M. Chia and J. A. Dumesic, *Chem. Commun.,* 2011, **47**, 12233.

58. (a) R. V. Sharma, U. Das, R. Sammynaiken and A. K. Dalai, *Appl. Catal. A,* 2013, **454**, 127; (b) S. G. Kulkarni, V. S. Bagalkote, S. S. Patil, U. P. Kumar and V. A. Kumar, *Propell. Explos. Pyrot.,* 2009, **34**, 520.

59. A. Bohre, S. Dutta, B. Saha, and M. M. Abu-Omar, *ACS Sustainable Chem. Eng.,* 2015, **3**, 1263.

60. (a) C. Wang, H. Xu, R. Daniel, A. Ghafourian, J. M. Herreros, S. Shuai and X. Ma, *Fuel,* 2013, **103**, 200; (b) S. Song, R. Daniel, H. Xu, J. Zhang, D. Turner, M. L. Wyszynski and P. Richards, *Energy Fuels*, 2010, **24**, 2891.

61. (a) C. L. Williams, C. C. Chang, P. Do, N. Nikbin, S. Caratzoulas, D. G. Vlachos, R. F. Lobo, W. Fan and P. J. Dauenhauer, *ACS Catal.,* 2012, **2**, 935; (b) D. Wang, C. M. Osmundsen, E. Taarning and J. A. Dumesic, *ChemCatChem*, 2013, **5**, 2044; (c) C. C. Chang, S. K. Green, C. L. Williams, P. J. Dauenhauer and W. Fan, *Green Chem.,* 2013, **16**, 585.

62. K. van Gorp, E. Boerman, C. V. Cavenaghi and P. H. Berben, *Catal. Today,* 1999, **52**, 349.

63. W. H. Jones, W. F. Benning, P. Davis, D. M. Mulvey, P. I. Pollok, J. C. Schaeffer, R. Tull, L. M. Weinstock, Ann. N. Y. *Acad. Sci.,* 1969, **158**, 471.

64. M. Akinori, M. Yumi, O. Eri, H. Tomoko, M. Tomohiro and S. Hironao, *Org. Lett.,* 2006, **8,** 3279.

65. R. Noyori and T. Ohkuma. *Pure Appl. Chem.,* 1999, **71**, 1493.

66. (a) K. Bauer and D. Garbe, Common Fragrance and Flavor Materials, VCH, Weinheim, 1985; (b) K. Bauer and D. Garbe, in Ullman Encyclopedia, VCH, New York, 1988, 141; (c) K. Weissermel and H. J. Arpe, Industrial Organic Chemistry, Verlag Chemie, Weinheim, 1978.

67. (a) P. Maki-Arvela, J. Hajek, T. Salmi and D. Y. Murzin, *Appl. Catal. A,* 2005, **292**, 1; (b) S. Mahmoud, A. Hammoudeh, S. Gharaibeh and J. Melsheimer, *J. Mol. Catal. A,* 2002, **178**, 161.

68. (a) P. Claus, *Top Catal.,* 1998, **5**, 51; (b) T. Vergunst, F. Kapteijn and J. A. Moulijn, *Catal. Today,* 2001, **66**, 381.

69. P. Gallezot and D. Richard, *Catal. Rev. Sci. Eng.,* 1998, **40**, 81.

70. F. Delbecq and P. Sautet, *J. Catal.,* 1995, **152**, 217.

71. M. J. Climent, A. Corma, S. Iborra and A. Velty, *J. Catal.*, 2004, **221**, 474.

72. (a) M. J. Climent, A. Corma, S. Iborra and J. Primo, *J. Catal.,* 1995, **151**, 60; (b) W. T. Reichle, S. Y. Kang and D. S. Everhardt, *J. Catal.,* 1986, **101**, 352.

73. (a) W. Kagunya and W. Jones, *Appl. Clay Sci.,* 1995, **10**, 95; (b) E. Suzuki and Y. Ono, *Bull. Chem. Soc. Jpn.,* 1988, **61**, 1008.

74. R. M. Barrer, Hydrothermal Chemistry of Zeolites academic press, New York, 1982.

75. L. V. C. Rees, *Nature,* 1992, **296,** 492.

76. W. M. Meier and D. H. Olson, Atlas of Zeolite Structure Types, Butterworths, 1987.

77.   K. F. Fischer and W. M. Meier, *Fortschr. Mineral,* 1965, **42**, 50.

78.   E. M. Flanigen, In Proceedings of the fifth International Conference of Zeolites, (L.V.C Rees Eds.) Naples, Italy, June 2-6, 1980, 760.

79.   L. B. Sand, *Econ. Geol.*, 1967, 161.

80.   (a) https://en.wikipedia.org/wiki/Faujasite

        (b) http://www.personal.utulsa.edu/~geoffrey-price/zeolite/fau.htm

81.   http://www.invsee.asu.edu/nmodules/Carbonmod

82.   (a) https://en.wikipedia.org/wiki/Amorphous_carbon

        (b) https://en.wikipedia.org/wiki/Graphite

        (c) https://en.wikipedia.org/wiki/Diamond

        (d) https://en.wikipedia.org/wiki/Activated_carbon

        (e) https://en.wikipedia.org/wiki/Buckminsterfullerene

        (f) https://en.wikipedia.org/wiki/Carbon_nanotube

83.   A. K. Geim and K. S. Novoselov, *Nat. Mater.,* 2007, **6**, 183.

84.   R. J. White, R. Luque, V. L. Budarin, J. H. Clark and D. J. Macquarrie, *Chem. Soc. Rev.,* 2009, **38**, 481.

85.   S. Crossley, J. Faria, M. Shen and D. E. Resasco, *Science,* 2010, **327**, 68.

86.   V. Z. Radkevich, T. L. Senko, K. Wilson, L. M. Grishenko, A. N. Zaderko and V. Y. Diyuk, *Appl. Catal. A,* 2008, **335**, 241.

87.   Y. K. Zhou, K. Neyerlin, T. S. Olson, S. Pylypenko, J. Bult, H. N. Dinh, T. Gennett, Z. P. Shao and R. O'Hayre, *Energy Environ. Sci.,* 2010, **3**, 1437.

88.   Z. B. Lei, L. Z. An, L. Q. Dang, M. Y. Zhao, J. Y. Shi, S. Y. Bai and Y. D. Cao, *Microporous Mesoporous Mater.,* 2009, **119**, 30.

89.   Xin-Hao Li and M. Antonietti, *Chem. Soc. Rev.,* 2013, **42**, 6593.

90.   Y. Motoyama, Y. Lee, K. Tsuji, S.-H. Yoon, I. Mochida and H. Nagashima, *ChemCatChem,* 2011, **3**, 1578.

91.   Y. Lee, Y. Motoyama, K. Tsuji, S.-H. Yoon, I. Mochida and H. Nagashima, *ChemCatChem,* 2012, **4**, 778.

Chapter 2
Catalyst synthesis & characterization

2.1. Introduction

A good heterogeneous catalyst should exhibit admirable catalytic activity, 100% selectivity to the desired product and should have excellent on-stream stability. The material characterization is extremely important in the context of development of novel catalysts, as it provides insights into the relation between physico-chemical features of the catalyst and its performance. Catalyst performance can be improved if the composition and structure of a catalyst is correlated with its activity and selectivity.

This chapter describes the preparation of various catalyst materials used in this thesis and experimental techniques utilized for their physico-chemical characterization. Hydrotalcite (HT) and Ru doped HT, NaY and HY zeolite supported transition metal (Ru, Pt, Rh, Pd, Au, Ni and Cu) catalysts, nitrogen-doped mesoporous carbons (NMC's) with different nitrogen content, nitrogen-free mesoporous carbon (MC), NMC's and MC supported transition metal and metal oxide supported transition metal catalysts were prepared for the present study. For detailed characterization of these catalyst materials; X-ray diffraction, scanning and transmission electron microscopy, Raman spectroscopy, X-ray photoelectron spectroscopy and methods based on adsorption and desorption of probe molecules were used. These investigations are expected to give information about crystallinity, phase structure, crystallite size, surface structure, textural properties, nature of active sites, morphology, metal particle size, acidity, basicity and other characteristic features. The structure-activity relationship can be better understood by these techniques, which finally helps to improve the catalyst performance for various applications.

2.2. Catalyst preparation

2.2.1. Preparation of hydrotalcite and Ru-doped hydrotalcites by co-precipitation method

Ru-doped HT catalyst precursors were prepared by co-precipitation method at a constant pH of 9.5-10.[1] In a typical synthesis, a mixture of aqueous solution containing $Mg(NO_3)_2 \cdot 6H_2O$ (0.25 mol), $Al(NO_3)_3 \cdot 9H_2O$ (0.083 mol) and $Ru(NO)(NO_3)_3$ (1.5 wt%, Ru content 15 mg/mL) was prepared in 50 mL double distilled deionized water. This solution was added dropwise to a second solution containing Na_2CO_3 (0.125 M) in 50 mL double distilled deionized water under vigorous stirring at 30 °C. The pH of the mixture was maintained constant by adding aqueous 0.25 M NaOH. The precipitate formed was filtered, washed thoroughly and dried at 100 °C for 10 h. Subsequently, it was calcined in air at 450 °C for 4 h followed by reduction in H_2 stream

(30 mL/min) at 350 °C for 3 h. These samples with different Ru contents were designated as RH-1, RH-2 and RH-3. A similar procedure was adopted for the preparation of Mg-Al HT sample with Mg/Al mole ratio 3 without using $Ru(NO)(NO_3)_3$ solution. The Ru-impregnated catalyst (RH-imp) was prepared by dry-impregnation method. For this, an aqueous solution of $Ru(NO)(NO_3)_3$ was added dropwise to the freshly dried HT sample. The resultant wet solid was initially dried at ambient temperature for 12 h and subsequently dried at 100 °C for 10 h. Finally, the catalyst was calcined in air at 450 °C for 4 h followed by reduction in H_2 (30 mL/min) at 350 °C for 3 h.

2.2.2. Preparation of NaY zeolite supported metal catalysts by ion exchange method
2.2.2.1. Preparation of M-NaY (M= Ru, Pt, Rh, Pd, Au, Ni and Cu) catalysts

NaY zeolite (CBV-100, Si/Al ratio = 2.5) supported metal catalysts were prepared by ion exchange method (Scheme 2.1). For Ru-NaY catalyst, 1.96 g of NaY zeolite was dispersed in 40 mL of deionized water in a 100 mL round bottom flask. To this, 8 mL of $RuCl_3$ solution (Ru content 5 mg/mL, for 2wt% Ru-NaY) was added and the resulting slurry was stirred for 3 h at 80 °C. The mixture was then cooled, filtered and washed until no chloride ions were detected (confirmed by $AgNO_3$ test). The remnant was dried in hot air oven at 100 °C for 10 h. Subsequently, $NaBH_4$ ($Ru/NaBH_4$ = 1:4 mol mol^{-1}) in ethanol was added with continuous stirring at room temperature for 2 h to get Ru in its metallic state. The sample was filtered, washed and dried at 100 °C for 10 h. Similar procedure was adopted for the preparation of 1wt% Ru-NaY, 3wt% Ru-NaY, 2wt% Pt-NaY, 2wt% Rh-NaY, 2wt% Pd-NaY, 2wt% Au-NaY, 5wt% Ni-NaY and 5wt% Cu-NaY catalysts.
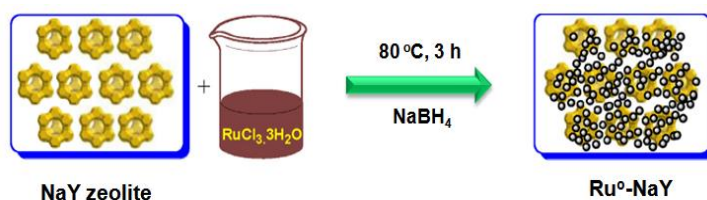
Scheme 2.1 Schematic illustration for synthesis of Ru-NaY catalyst by ion-exchange method.

2.2.2.2. Preparation of Ru-X-NaY (X= K, Rb and Cs) catalysts
2.2.2.2.1. Preparation of 5% K-NaY catalyst

NaY zeolite (5 g) was dispersed in 100 mL of deionized water in a 250 mL round bottom flask along with 1.059 g of KNO_3 and the resulting slurry was stirred for 3 h at 80 °C. The

mixture was then cooled, filtered, washed with deionized water and the remnant was dried in oven at 100 °C for 10 h. The material obtained was calcined in air at 400 °C for 4 h. Similar procedure was used for the preparation of 5% Rb-NaY and 5% Cs-NaY.

2.2.2.2.2. Preparation of Ru-K-NaY catalyst

5% K-NaY (3.92 g) was dispersed in 100 mL of deionized water along with 16 mL of RuCl$_3$ solution (Ru is 5 mg/ml for 80 mg of Ru) and the resulting slurry was stirred for 3 h at 80 °C. The mixture was then cooled, filtered, washed until no chloride ions were detected (confirmed by AgNO$_3$ test) and the remnant was dried at 100 °C for 10 h. The sample was reduced by NaBH$_4$ (Ru/NaBH$_4$ = 1:4 mol mol^{-1}) in ethanol with continuous stirring at room temperature for 2 h. The material was filtered, washed thrice with 50 mL of deionized water and dried at 100 °C for 10 h. Similar procedure was adopted to prepare 2wt% Ru-Rb-NaY from 5% Rb-NaY and 2wt% Ru-Cs-NaY from 5% Cs-NaY.

2.2.3. Preparation of HY zeolite supported Ru catalyst

HY zeolite supported Ru catalyst (2wt% Ru-HY) was prepared by ion exchange of NH$_4$Y zeolite (CBV-500, Si/Al ratio = 2.6) with RuCl$_3$ at 80 °C for 3 h. The mixture was then cooled, filtered, washed with deionized water until no chloride ions were detected (confirmed by AgNO$_3$ test) and was dried in oven at 100 °C for 10 h. This crystalline material was subsequently calcined in air at 300 °C and reduced using NaBH$_4$ (Ru/NaBH$_4$ = 1:4 mol mol^{-1}) in ethanol with continuous stirring at room temperature for 2 h. The material was filtered, washed thrice with 50 mL of deionized water and dried at 100 °C for 10 h.

2.2.4. Preparation of nitrogen-doped mesoporous carbons (NMC's)

The NMC's were prepared by colloidal silica assisted sol-gel process, using melamine as nitrogen source (Scheme 2.2).[2] In a typical synthesis procedure, 3.67 g of phenol (39 mmol) and 6.33 g of formaldehyde (37 wt%, 78 mmol) were added dropwise to 50 mL of NaOH solution (0.2 M, 10 mmol) under stirring. This mixture was stirred at room temperature for 20 min and then heated to 70 °C in an oil bath and stirred for 40 minutes. About 4.92 g of melamine (39 mmol) and another part of formaldehyde (9.5 g, 107 mmol) were then added to the above solution under continuous stirring. This was followed by the addition of 50 g of Ludox SM-30 sol (30 wt% SiO$_2$) with vigorous stirring for 1 h. The suspension was then transferred to a sealed bottle and heated at 80 °C for 3 days. The gel obtained was dried at 80 °C and made into fine

powder. The material obtained was carbonized in N_2 flow at 800 °C for 3 h while raising the temperature at a heating rate of 5 °C/min. The NMC was obtained after dissolution of the silica in 2 M NaOH solution at 80 °C for 12 h. The resulting material was washed with deionized water until the pH is neutral and dried at 100 °C for 10 h. The NMC's with different nitrogen contents were prepared by changing the mole ratio of melamine to phenol. The nitrogen-free mesoporous carbon (MC) was also prepared by using above process without adding any melamine content.
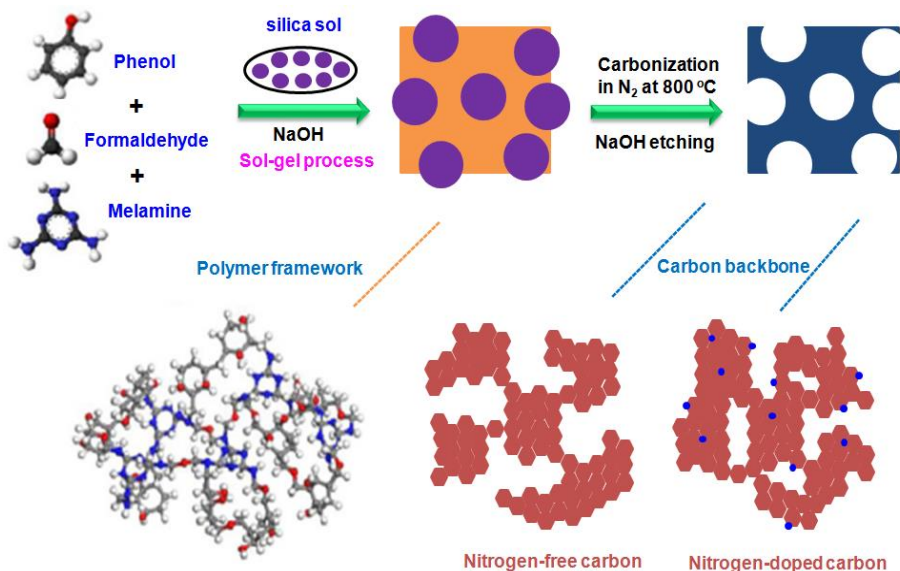
Scheme 2.2 Schematic illustration of NMC synthesis.

2.2.5. Preparation of NMC supported metal catalysts by ultrasonic-assisted method

2.2.5.1. Preparation of M-NMC (M= Ru, Pt, Rh, Pd, Au, Ni and Cu) catalysts

The NMC supported metal catalysts were prepared by a modified ultrasonic-assisted method (Scheme 2.3).[3] For Ru-NMC catalyst, 0.1 g of NMC was dispersed in 50 mL of deionized water in a 100 mL round bottom flask by ultrasonication (20 min). To it, 0.5 mL aqueous solution of $RuCl_3$ (Ru content 4 mg/mL, for 2wt% Ru) was added under agitation in an ultrasonicator. This mixture was stirred at 80 °C for 6 h and cooled to room temperature. To it, aqueous solution of $NaBH_4$ (Ru/$NaBH_4$ = 1:4 mol mol^{-1}) was added slowly under ultrasonication (30 min). The solution was filtered and washed with deionized water until no chloride was detected (confirmed through $AgNO_3$ test). The resulting 2wt% Ru-NMC catalyst was dried at 80 °C for 10 h. Catalyst samples with different Ru loadings were prepared using a similar procedure by using appropriate amounts of $RuCl_3$. Activated carbon and MC supported Ru and Pd catalysts were also prepared by following the above procedure. Furthermore, a similar procedure was

adopted for the preparation of 2wt% Pt-NMC, 2wt% Rh-NMC, 2wt% Pd-NMC, 2wt% Au-NMC, 5wt% Ni-NMC and 5wt% Cu-NMC catalysts.
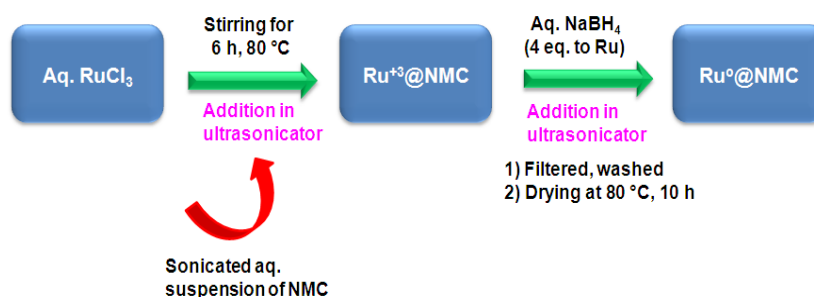
Scheme 2.3 Schematic illustration for synthesis of Ru-NMC catalyst by ultrasonic-assisted method.

2.2.6. Preparation of NMC supported Au catalysts by different methods

2.2.6.1. Preparation of Au-NMC catalyst by incipient wetness method

Catalyst 1wt% Au-NMC was synthesized by a modified incipient-wetness method (Scheme 2.4).[4] Typically, 0.1 g of NMC was dispersed in 50 mL of deionized water. To it, 0.25 mL of aqueous solution of $HAuCl_4$ (Au content 4 mg/mL, for 1wt% Au) was added under continuous stirring at room temperature. This mixture was stirred at 80 °C for 6 h and cooled to room temperature. Subsequently, aqueous $NaBH_4$ (Au/$NaBH_4$ = 1:4 mol mol^{-1}) was added dropwise under stirring for 2 h. The solution was filtered and washed with deionized water to remove chloride ions (confirmed by $AgNO_3$ test). The sample was dried in an oven at 100 °C for 10 h. The resulting catalyst was designated as 1wt% Au-NMC-IW.
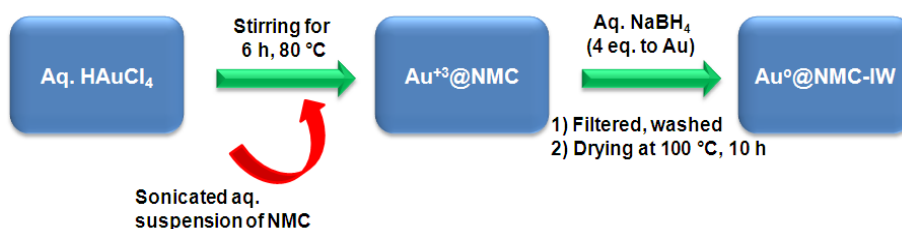
Scheme 2.4 Schematic illustration for synthesis of Au-NMC catalyst by incipient-wetness method.

2.2.6.2. Preparation of Au-NMC catalyst by deposition-precipitation method

Another 1wt% Au-NMC catalyst was prepared by a deposition-precipitation method (Scheme 2.5).[5] Typically, required aqueous $HAuCl_4$ solution (7.5 x 10^{-4} M) was heated to 70 °C under stirring. The pH of the solution was adjusted to 9 by dropwise addition of aqueous NaOH (0.2 M) and then sonicated aqueous suspension of NMC was dispersed in the above solution. The mixture was aged for 3 h at 70 °C and then aqueous $NaBH_4$ (Au/$NaBH_4$ = 1:4 mol mol^{-1})

solution was added dropwise to the above suspension under stirring at room temperature for 2 h. The solution was filtered and washed with deionized water to remove chloride ions (confirmed by AgNO₃ test). The material was dried in oven at 100 °C for 10 h. The resulting catalyst was designated as 1wt% Au-NMC-DP.
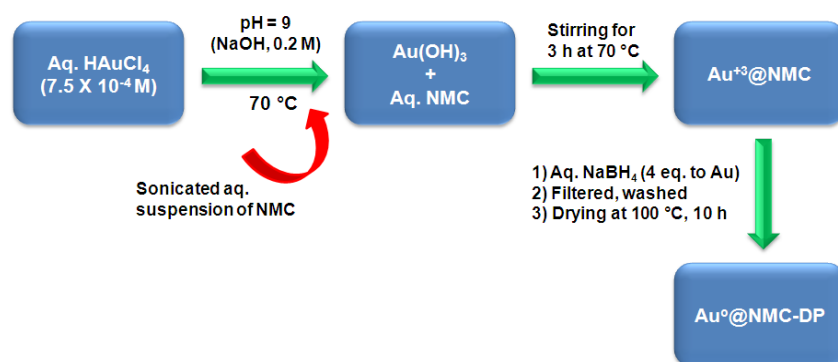
Scheme 2.5 Schematic illustration for synthesis of Au-NMC catalyst by deposition-precipitation method.

2.2.6.3. Preparation of Au-NMC catalyst by sol-immobilization method

Au was deposited on NMC support using sol-immobilization technique (Scheme 2.6).[6] HAuCl₄ (0.0076 mmol) was dissolved in deionized water (50 mL) and polyvinyl alcohol (PVA) was added to the solution by keeping Au/PVA ratio at 1:1 (wt/wt). After 10 min of stirring at room temperature, 0.1 M aqueous solution of NaBH₄ (Au/NaBH₄ = 1:4 mol mol⁻¹) was added to the above yellow solution under continuous stirring. A ruby red color was formed suggesting the formation of metallic Au. The required amount of NMC was suspended in 30 mL of deionized water and sonicated for 30 min and subsequently added to the Au sol. This slurry was stirred at room temperature for 2 h followed by filtration. The catalyst was washed with deionized water to remove chloride ions (confirmed by AgNO₃ test) and dried in an oven at 100 °C for 10 h. The resulting catalyst was designated as 1wt% Au-NMC-SI. Similar procedure was adopted to prepare MC supported Au catalyst and it was designated as 1wt% Au-MC-SI.
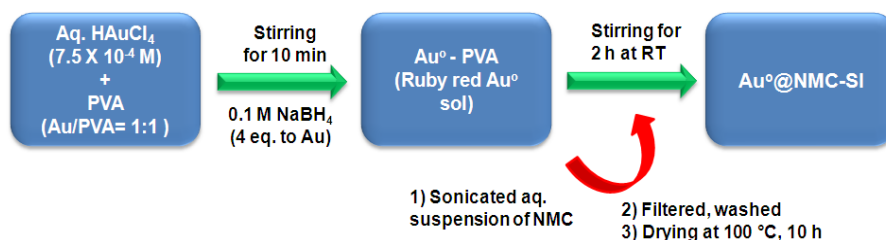
Scheme 2.6 Schematic illustration for synthesis of Au-NMC catalyst by sol-immobilization method.

2.2.7. Preparation of metal oxide (metal oxide= CeO₂, MgO, Mg(Al)O, γ-Al₂O₃ and TiO₂) supported Ru and Au catalysts by deposition-precipitation method

Metal oxide supported Ru and Au catalysts were prepared by a deposition-precipitation method.[5] In a typical preparation for metal oxide supported Ru catalyst, an appropriate amount of aqueous solution of $RuCl_3$ (7.5 x 10^{-4} M) was heated to 70 °C under stirring. The pH of the solution was adjusted to 9 by dropwise addition of aqueous NaOH (0.2 M) and then 1 g of metal oxide was dispersed in the above solution. The mixture was stirred for 3 h at 70 °C and cooled to room temperature. Subsequently, $NaBH_4$ (Ru/$NaBH_4$ = 1:4 mol mol^{-1}) in water was added dropwise to above suspension under continuous stirring at room temperature for 2 h. The solution was filtered and washed with deionized water to remove chloride ions (confirmed by $AgNO_3$ test). The catalyst was dried in an oven at 80 °C for 10 h. Similar procedure was used for the preparation of metal oxide supported Au catalysts.

2.3. Characterization of catalysts

Characterization of the above synthesized materials would help to understand the physico-chemical properties of the catalysts in a better way, so that requisite materials can be designed to meet the reaction needs. Hence, a brief account of the theory and principles of various characterization techniques used for the current study is given below, along with the detailed procedures used for each experimental technique for the characterization of above prepared materials.

2.3.1. X-ray diffraction (XRD)

XRD is one of the most widely used techniques for characterization of materials. It is an important tool for determining the structure of materials that are distinguished by long-range order.[7] X-rays are extremely intrusive electromagnetic radiation which are electrically neutral. Their wavelength is in the range of 0.04 to 1000 Å. X-rays with only shorter wavelengths (from few Å to 0.1 Å) are used for diffraction applications because these are comparable to the size of the atoms. Hence, the X-rays are ideally suited for deducing the structural arrangement of atoms in variety of materials.

The diffraction method involves interaction of the incident monochromatic X-rays (like Cu Kα) with the atoms of a periodic lattice. The X-rays are scattered by atoms constructively as

per Bragg's law (Fig. 2.1).[8] This law relates the wavelength (λ) of electromagnetic radiation to the lattice spacing and the diffraction angle in a crystalline material.

$$n\lambda = 2\ d\ \sin\theta;\ n = 1, 2, 3,\ldots\ldots \qquad (2.1)$$
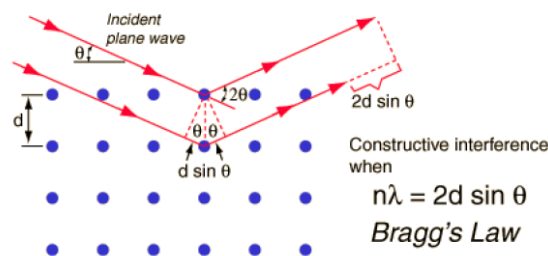
Fig. 2.1 Principle of Bragg's law.

Where, n is an integer called order of the reflection, λ is wavelength of the X-rays, d is the distance between two lattice planes and θ is the angle between the incoming X-rays and the normal to the reflecting lattice plane. The lattice spacing (d) can be obtained from Bragg's equation, which is characteristic of a particular material. Width of the diffraction peaks indicates the dimension of the reflecting planes. It is well-known that the width of a diffraction peak increases when the crystallite size is reduced below a certain limit (<100 nm). Hence, XRD patterns can be used for the estimation of an average crystallite size of small crystallites using XRD line broadening with the help of Scherrer formula.[9]

$$t = 0.9\lambda/\beta\ \cos\theta \qquad (2.2)$$

Where, t is the thickness of the crystallites (Å), λ is the wavelength of X-rays, β is the full width at half maxima of the diffraction peak and θ is the diffraction angle. The XRD patterns of all the samples reported in this thesis were collected using PANalytical X'pert Pro dual goniometer operating at 30 mA and 40 kV. The spectra were scanned using Cu Kα (λ= 1.5406 Å) radiation using a Ni filter. Data was recorded in 2θ range of 5-90° with 0.02° step size using a flat holder in Bragg-Brentano geometry.

2.3.2. N$_2$ Physisorption and H$_2$ chemisorption

The most accepted technique for measuring surface area of materials is the one that is based on the theory developed by Brunauer, Emmett and Teller in 1938 by taking into account the multilayer adsorption of adsorbate molecules on the adsorbent surface. Its assumptions are; *(i) there is no inter molecular interaction, (ii) adsorption energy remains constant from zero*

coverage to full coverage for the primary layer of the adsorbate and each successive layers above, (iii) a new layer can be initiated before the completion of the one under formation and (iv) enthalpy of adsorption is same for any other layer except the first one. The Brunauer-Emmett-Teller (BET) equation is [10];

$$P/V\ (P_0-P) = 1/\ CV_m + [(C-1)/CV_m]\ (P/P_0) \qquad (2.3)$$

Where, P is adsorption equilibrium pressure, V is volume of gas adsorbed at pressure P, P_0 is saturation vapor pressure of the adsorbate at the experimental temperature, V_m is the volume of adsorbate required for monolayer coverage and C is a constant related to the heat of adsorption and liquefaction. In order to quantify the amount of N_2 adsorbed, a linear relationship between $P/V(P_0-P)$ and P/P_0 is required. This linear portion of the curve is restricted to a limited portion of the isotherm, generally for P/P_0 of 0.05 to 0.30. *The slope of the straight line (A) is equal to $(C-1)/CV_m$ and the intercept (I) is equal to $1/CV_m$.* Both the parameters are used to calculate the monolayer volume, V_m *given by $1/(A+I)$.* The surface area of the catalyst (S_{BET}) is related to V_m by the equation,

$$S_{BET} = (V_m/22414)\ N_a\ \sigma \qquad (2.4)$$

Where, N_a is Avogadro number and σ is average cross sectional area of one adsorbate molecule. Nitrogen gas is most commonly used for surface area measurements as it exhibits intermediate C values (50-250) on most solid surfaces, impeding either localized adsorption or behavior as two dimensional gas. It has been demonstrated that the C influences the value of the cross sectional area of an adsorbate. Thus, the acceptable range of C for nitrogen makes it possible to calculate its cross sectional area from its bulk liquid properties.[11] For the hexagonal close-packed nitrogen monolayer at -196 °C, the cross sectional area (σ) for nitrogen is 0.16 nm^2.

In case of the supported metal catalysts, it is very essential to know what fraction of the active metal atoms are exposed. Since the atoms located in the interior of the metal particles do not participate in surface reactions, they may not be available for the catalytic processes. *"The metal dispersion 'D' is defined as the fraction of metal atoms present on the surface of active metal particles; it is expressed as a percentage of all metal atoms present in the sample"* The higher the dispersion, the more exposed a metal is and the more efficient is the catalyst. The value of D is obtained from the following equation,

$$D = N_m\ S\ M\ /100\ L \qquad (2.5)$$

Where, M and L are the atomic weight and percent loading of the supported metal, respectively, S is adsorption stoichiometry and N_m is monolayer uptake of chemisorbed gas.

The N_2 physisorption and H_2 chemisorption experiments were conducted using Quantachrome Autosorb IQ analyzer (Fig. 2.2). N_2 physisorption analysis was carried out at -196 °C after degassing the samples at 250 °C for 3 h in vacuum. The isotherms were analyzed in a conventional manner in the relative pressure range $P/P_0 = 0.0005$ to 1.0. The total pore volume of the samples was calculated at $P/P_0 = 0.9$. The BJH method was used to determine the pore size distribution from the adsorption/desorption branches of the isotherms. H_2 chemisorption experiments were conducted at 40 °C after reducing the catalyst in situ in H_2 flow.

Fig. 2.2 Quantachrome Autosorb IQ instrument used for N_2 physisorption and H_2 chemisorption.

2.3.3. Electron microscopy

The electron microscopy has many variants. In this section, we deal only with scanning electron microscopy and transmission electron microscopy. The former is very useful for the examination of physical features of the sample, like size and shape of crystals in the material. On the other hand latter is useful to study the nano structure of the material along with the metal particle distributions.

2.3.3.1. Scanning electron microscopy (SEM)

SEM is a type of electron microscopy technique that generates images of a sample by scanning it with a focused high-energy beam of electrons in a raster scan pattern. It is a simple technique to investigate the morphological characteristics of the samples. A probe of electrons (5-50 eV) is scans over a sample surface and the yield of either secondary or back-scattered electrons is detected as a function of the position of the primary beam. The interaction between the incident electrons with the atoms in the sample produces different types of signals, which

carry detailed information about the sample surface topography and the composition of the sample.[12] A major advantage of SEM is that bulk samples can also be directly studied by this technique.

The SEM images of the samples were recorded using a JEOL-JSM-5200 to study the morphology. The samples were prepared by dispersing them ultrasonically in 2-propanol and transferring a portion of it onto silicon wafer and then subsequently dried and gold coated before SEM analysis.

2.3.3.2. Transmission electron microscopy (TEM)

TEM is used for high resolution imaging of thin films of a solid sample for micro structural and compositional analysis. In this technique, a very thin sample is irradiated with high energy electron beam. The electron beam which is partially transmitted through an ultrathin specimen is diffracted by the lattices of a semi crystalline or crystalline material and propagates along different directions. Thus, the beam carries information about the structure of the specimen. This is followed by imaging and angular distribution analysis of the forward scattered electrons (unlike SEM where backscattered electrons are detected) and energy analysis of the emitted X-rays.[13] The image is then magnified by a series of magnetic lenses until it is recorded by hitting a fluorescent screen, photographic plate or light sensitive sensor such as a charge-coupled device (CCD) camera. The image detected by the CCD may be displayed in real time on a computer. The ability to determine the positions of atoms within the materials has made the TEM an interesting and very important tool for research in the fields of nano-technologies, development of semiconductor devices for electronics and photonics and heterogeneous catalysis.

The TEM images of the samples were collected using a FEI Technai TF-30 instrument operating at 300 kV. The samples for TEM measurements were prepared by placing a droplet of highly diluted suspension of the sample in 2-propanol on a carbon-coated copper grid (mesh 200) and allowed to dry at room temperature. The difference in the alignment of the SEM and TEM is depicted in Fig. 2.3.
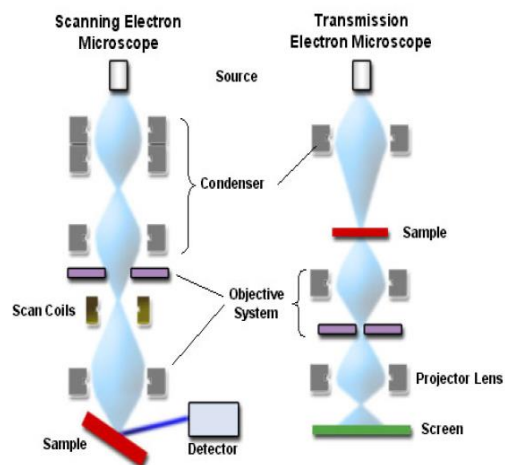
Fig. 2.3 Alignment of SEM and TEM instrument.
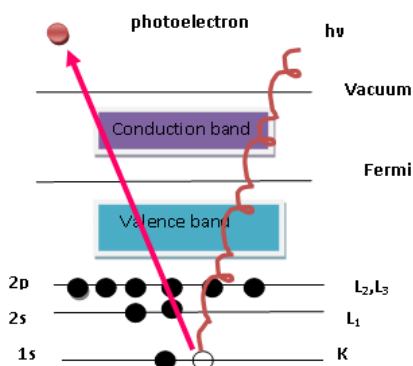
Fig. 2.4 Principle of XPS.

2.3.4. X-ray photoelectron spectroscopy (XPS)

The XPS technique is based on the photoelectric effect discovered by Heinrich Hertz and explained later by Albert Einstein (Fig. 2.4).[14] XPS spectra can be obtained by irradiating a sample with a beam of X-rays and measuring the kinetic energy of emitted photoelectrons. It is a widely used technique for finding the chemical information of various material surfaces. The emitted photoelectrons have different kinetic energies that are characteristic of the emitting atoms and their bonding states. XPS is a surface-sensitive technique and the sample depth is in the range of few nanometers. The shape of the peaks and the binding energy is slightly changed based on the chemical state of the emitting atom. Thus, XPS can provide information on chemical bonding. The number of catalytic properties such as oxidation state of active species,

interaction of a metal with the support, change in oxidation state upon activation of the catalyst, nature of surface impurities, *etc.* can be systematically studied using this technique.

XPS measurements were carried out using a VG Microtech Multilab ESCA 3000 with Mg Ka radiation (hv = 1253.6 eV). The base pressure in analyzing chamber was maintained at 3– 6 x 10^{-10} mbar. The peak corresponding to carbon 1s at 284.5 eV was taken as reference in estimating the binding energy values of various elements in the catalyst.

2.3.5. Raman spectroscopy

Raman spectroscopy is a technique employed to study the rotational, vibrational and other low-frequency transitions in molecules.[15] It is regularly used in chemistry as vibrational information is specific to the chemical bond and the symmetry of a molecule. Hence, it provides a fingerprint by which the molecule can be identified. A vibration is Raman active if it changes the polarizability of the molecule. Raman and infrared spectroscopy complement each other, in particular for highly symmetrical molecules e.g. CO_2. Raman spectroscopy is based on inelastic scattering of monochromatic light usually from a laser in the near ultra-violet, near infrared or visible range (Fig. 2.5). The laser light interacts with molecular vibrations or other excitation in the molecule. The frequency of the emitted laser photons being shifted up or down in comparison with original monochromatic frequency, which is called the Raman effect. From Raman spectra, we can determine the composition of the material, crystal symmetry and orientation, quality of crystal, stress or strain, *etc*.

The Raman spectra of the samples were collected using LabRAM HR800 (Jobin Yvon Horiba, France) with laser wavelength of 632.84 nm (He-Ne Laser, 20 mW of power) and 2 µm spot size.
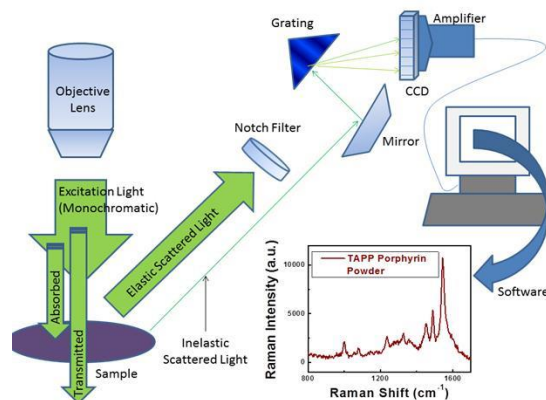
Fig. 2.5 Schematic illustration of Raman spectroscopy.

2.3.6. Inductively coupled plasma-optical emission spectrometry (ICP-OES)

ICP-OES is a powerful analytical technique used for the detection of trace elements in a myriad of sample types. This technique uses the inductively coupled plasma to generate excited atoms and ions, which emits radiation at characteristic wavelength of the element involved (Fig. 2.6).[16] The concentration of the element within the sample is indicated by the intensity of emitted radiation. The liquid and gas samples may be injected directly into the instrument, while solid samples require extraction or acid digestion so that the analytes will be present in solution.

The sample solution is delivered into the nebulizer using peristaltic pump where it converted into mist and introduced directly inside the plasma flame. The flame temperature is in the range of 5723 to 9727 °C, so the mist is quickly vaporized. Sufficient energy is normally available in order to convert the atoms to ions and subsequently promote the ions to excited states. Both the atomic and ionic excited state species may then relax to the ground state *via* the emission of photons. Thus, the wavelength of the emitted photons can be used to identify the elements from which they originated. Sample introduction in ICP-OES instrument is depicted in Fig. 2.6.

ICP-OES analysis was carried out using a Spectro Arcos instrument equipped with the Winlab software (FHS-12). Standard solutions containing different elements were used for the calibration purpose. The solid samples were digested with aqua-regia before ICP-OES analysis.
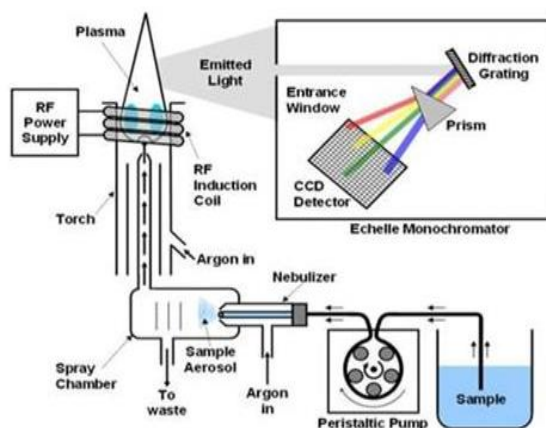
Fig. 2.6 Schematic illustration of sample introduction to ICP-OES.

2.3.7. Temperature programmed desorption (TPD)

TPD is a technique of monitoring desorbed molecules from a sample surface when the temperature is raised linearly with time.[17] The basic set up of a TPD consists of a reactor

charged with the catalyst in a furnace that can be temperature programmed and a thermal conductivity detector (TCD) to measure the conductivity of gas stream passing through the sample before and after interaction, to find out its change in concentration (Fig. 2.7). Mass spectrometer can be coupled with the detector for identification of various species formed or evolved during the desorption process.

TPD of NH_3 is used for characterizing the acid sites, whereas TPD of CO_2 is used for characterizing the basic sites of the catalyst. Performance of an acid-base catalyst can be understood by measuring the quantity and strength of its acidic/basic sites. The catalyst surface was contacted with the probe molecule (NH_3/CO_2), which is sorbed onto the surface either by chemisorption, physisorption or by the formation of chemical bonds, minimizing the energy of the species. With increasing the sample temperature, the species is desorbed from the surface. The amount of NH_3/CO_2 desorbed is proportional to the acidity/basicity.

The acidity of the samples was determined by TPD of NH_3 using a Micromeritics Autochem-2920 instrument. Before TPD run, the sample was activated at 400 °C in He flow (40 mL/min) for 1 h. Subsequently, the temperature was brought down to 80 °C and NH_3 was sorbed by exposing the sample to a stream of 10% NH_3 in He (30 mL/min) for 0.5 h. Then, the temperature was increased to 100 °C and physisorbed NH_3 was removed by flushing with He for 1 h. Desorption of NH_3 was carried out in He flow (40 mL/min) by increasing the temperature from 100 to 800 °C at a heating rate of 10 °C/min. The amount of NH_3 desorbed was monitored quantitatively by a TCD, which was calibrated before the TPD study.

The basicity of the samples was measured by TPD of CO_2 using a Micromeritics Autochem-2920 instrument. Before the analysis, the sample was activated at 300 °C in He flow (40 mL/min) for 1 h and the temperature was brought down to 50 °C. Subsequently, CO_2 was sorbed by exposing the sample to a stream of 10% CO_2 in He (30 mL/min) for 0.5 h. Then, the temperature was raised to 100 °C and physisorbed CO_2 was removed by flushing with He for 1 h. Desorption of CO_2 was carried out in He flow (40 mL/min) by rising the temperature from 100 to 800 °C at a heating rate of 10 °C/min. The amount of CO_2 desorbed was estimated quantitatively by a TCD, which was calibrated before the TPD study.

Fig. 2.7 Micromeritics Autochem 2920 used for TPD and TPR study.

2.3.8. Temperature programmed reduction (TPR)

The TPR is a technique used for the characterization of supported metal catalysts in order to find the most efficient reduction conditions.[18] The oxidized catalyst precursor is subjected to a programmed heating rise in the flow of reducing gas mixture. The TPR study was carried out using a Micromeritics Autochem 2920 equipped with a TCD detector. Before the TPR study, the sample was pre-treated at 300 °C for 1 h using 5% O_2 in He gas mixture at a heating rate of 10 °C/min. After cooling it to 40 °C, the gas flow was changed to 5% H_2 in He gas mixture (30 mL/min) and the sample was heated to 700 °C at a heating rate of 5 °C/min. The change in H_2 concentration at the outlet was measured quantitatively by a TCD that was calibrated before the TPR study.

2.4. References

1. S. K. Sharma, P. A. Parikh and R. V. Jasra, *J. Mol. Catal.,* 2010, **317**, 27.

2. H. Chen, F. Sun, J. Wang, W. Li, W. Qiao, L. Ling and D. Long, *J. Phys. Chem. C,* 2013, **117**, 8318.

3. X. Xu, Y. Li, Y. Gong, P. Zhang, H. Li and Y. Wang, *J. Am. Chem. Soc.,* 2012, **134**, 16987.

4. L. Delannoy, N. E. Hassan, A. Musi, N. N. L. To, J. M. Krafft and C. Louis, *J. Phys. Chem. B,* 2006**, 110***,* 22471.

5. M. -M. Wang, L. He, Y. -M. Liu, Y. Cao, H. -Y. He and K. -N. Fan, *Green Chem*., 2011, **13**, 602.

6. A. Villa, D. Wang, G. M. Veith, F. Vindigni and L. Prati, *Catal. Sci, Technol.,* 2013, **3**, 3036.

7.   J. W. Niemantsverdriet, Spectroscopic methods in heterogeneous catalysis, VCH, Weinheim, 1993.

8.   B. D. Cullity and S. R. Stock, Elements of X-ray diffraction, Prentice Hall, 3rd ed., 2001.

9.   N. F. M. Henry, J. Lipson and W. A. Wooster, The interpretation of X-ray diffraction photographs, Macmillan and Co Ltd., London, 1951.

10.   S. Brunauer, P. H. Emmett and E. Teller, *J. Am. Chem. Soc.,* 1938, **60,** 309.

11.   (a) A. V. Kiselev and Y. A. Eltekov, World Congress on Surface Activity, Vol. 2, p. 228, Butterworths, London, 1957; (b) S. Lowell, J. Shields, G. Charalambous and J. Manzione, *J. Colloid Interface Sci.*, 1982, **86**, 191.

12.   (a) J. I. Goldstein and H. Yakowitz, Practical Scanning Electron Microscopy, Plenum Press, New York, 1975; (b) G. Lawes, Scanning Electron Microscopy and X-Ray Microanalysis, John Wiley and Sons Ltd., Chichester, 1987.

13.   J. R. Fryer, Chemical Applications of Transmission Electron Microscopy, Academic Press, San Diego, 1979.

14.   (a) T. A. Carlson, X-ray Photoelectron Spectroscopy, Dowden, Hutchinson & Ross: Stroudsburg, PA, 1978; (b) D. Briggs and M. P. Seah, Practical Surface Analysis, Vol. 1: Auger and X-ray Photoelectron Spectroscopy, 2nd ed., Wiley, New York, 1990.

15.   D. J. Gardiner, Practical Raman spectroscopy. Springer-Verlag, 1989.

16.   C. B. Boss and K. J. Fredeen, Concept, Instrumentation and Techniques in Inductively Coupled Plasma Optical Emission Spectrometry, 2nd ed., Perkin-Elmer, Norwalk, CT, 1997.

17.   (a) D. A. King, *Surface Science,* 1975, **47**, 384; (b) E. Habenschaden and J. Küppers, *Surface Science,* 1984, **138**, 147.

18.   D. A. M. Monti and A. Baiker, *J. Catal.,* 1983, **83**, 323.

Chapter 3

Reductive upgradation of biomass-derived furanic compounds over supported metal catalysts using H$_2$

3.1. Introduction

At present, there is an alarmingly over dependence on fossil fuels, which is not sustainable. Moreover, their indiscriminate use is leading to ecological problems. Hence, utilization of biomass to produce renewable fuels and valuable chemical intermediates is gaining increasing attention.[1–4] Hydrogenolysis is an important process in biomass refinement, as biomass-derived compounds have high oxygen content.[5,6] 5-Hydroxymethylfurfural (HMF) is an important platform chemical that can be synthesized from hexoses. Hence, it has been identified as a key player in the bio-based renaissance. It can be converted to levulinic acid, ethyl levulinate, γ-valerolactone and the highly promising transportation liquid fuel 2,5-dimethylfuran (DMF).[7–12] DMF is particularity attractive due to its superior energy density (33.7 MJ/kg), higher research octane number (RON=119) and ideal boiling point (92-94 °C).[8] Further, DMF consumes only one-third of the energy in the evaporation stage, immiscible with water and also easier to blend with gasoline compared to ethanol.[8] Biomass-derived DMF has been tested as a biofuel in a single-cylinder gasoline direct-injection research engine.[13] The performance of DMF was satisfactory against gasoline in terms of ignition, emission and combustion characteristics. These attributes bode very well for the use of DMF as an alternative fuel for transportation. Moreover, DMF is also a renewable source for the production of p-xylene *via* Diels-Alder reaction.[14] As a result of above described applications, successful efforts were made to produce DMF through hydrogenation/hydrogenolysis using supported metal catalysts. Following sections provide detailed literature background of DMF synthesis from HMF.

3.2. Literature on the synthesis of DMF from biomass-derived HMF

One of the vital challenges for the upgradation of HMF to value added chemicals and fuels is the product selectivity because HMF possesses a hydroxyl group, an aldehyde group and a furan ring; hence it is a highly reactive molecule. As a result, hydrogenation of HMF can result in a mixture of ring- and side chain-hydrogenated products along with ring-opened products.[15] Decoupling these processes is highly important for using furans as renewable fuels and chemicals. To solve these issues, it is very essential to select an appropriate catalytic system. Hydrogenolysis of HMF into DMF was studied over various supported metal catalysts. These processes can be categorized in terms of type of hydrogen donor used.

1. Molecular hydrogen as hydrogen donor

2. Formic acid as hydrogen donor

3. Alcohols as hydrogen donor

4. Water as hydrogen donor

These processes are described below in detail.

3.2.1. Hydrogenolysis of HMF to DMF using molecular hydrogen

Roman-Leshkov *et al.* reported an important study on the selective hydrogenolysis of biomass-derived HMF to DMF over $CuCrO_4$ catalyst using molecular H_2 in 1-butanol. HMF conversion of 100% with 61% DMF yield was obtained at 220 °C after 10 h of reaction.[8] But, $CuCrO_4$ catalyst was easily deactivated by chloride ions present at ppm level in reaction medium. To address this poisoning, authors developed a chlorine-resistant bimetallic CuRu/C catalyst, which helped to increase DMF yield to 71% at 100% HMF conversion in 10 h at 220 °C and at 6.8 bar H_2 pressure.[8] In 2009, Raines *et al.* used above catalytic system consisting of CuRu/C, H_2 and 1-butanol for the hydrogenolysis of the crude HMF obtained from corn stover and achieved 49% DMF yield under similar reaction conditions.[16] Bell *et al.* obtained 15% DMF yield at 47% HMF conversion using Pd/C as a catalyst in ionic liquid 1-ethyl-3-methylimidazolium chloride ([EMIM]Cl) under H_2 pressure of 62 bar.[17] The lower yield of DMF was attributed to the low solubility of H_2 in ionic liquids. As a result, a high H_2 pressure has to be used, making the process highly energy intensive. Authors also found that the source of HMF had negligible effect on the product distribution and hydrogenation selectivity.

Zhang *et al.* reported 60.3% DMF yield in 1-butanol at 260 °C by using Ru/C catalyst.[18] Zu *et al.* obtained 93.4% DMF yield over Ru/Co_3O_4 catalyst in tetrahydrofuran (THF) after 24 h.[19] Gallo *et al.* studied HMF hydrogenolysis over RuSn/C catalyst to get 46% DMF yield.[20] Chatterjee *et al.* reported a novel catalytic strategy for HMF hydrogenolysis by using Pd/C catalyst in supercritical CO_2 and H_2O as reaction medium.[21] Selectivity to various products could easily be changed by changing the H_2 pressure and the CO_2 pressure. When 10 bar H_2 and 100 bar CO_2 were used, excellent DMF yield of 100% was obtained. It is important to note that DMF selectivity was found to be highly dependent on the mole ratio of CO_2 to H_2O. Wang *et al.* achieved very good yield of DMF (98%) with 100% HMF conversion by using bimetallic PtCo nanoparticles supported on hollow carbon sphere catalyst in the presence of 1-butanol and H_2 (10 bar) at 180 °C.[22] Huang *et al.* reported selective hydrogenation of HMF over activated carbon supported nickel-tungsten carbide catalyst ($Ni-W_2C/AC$) in THF and at 40 bar H_2 pressure; an

excellent DMF yield of 96% with 100% HMF conversion was achieved at 180 °C after 3 h of reaction.[23] Nishimura *et al.* studied the HMF hydrogenolysis over PdAu/C catalyst in presence of HCl under atmospheric H_2 pressure and obtained 96% DMF yield.[24]

3.2.2. Hydrogenolysis of HMF to DMF using formic acid

In 2010, Rauchfuss *et al.* proposed a mild reaction pathway for the selective hydrogenolysis of HMF to DMF, in which formic acid was used for the first time as a hydrogen donor.[25] When the reaction was carried out over Pd/C and H_2SO_4 as catalysts in the presence of formic acid and THF, 100% HMF conversion with 95% DMF yield was obtained at 70 °C in 15 h. One-pot process for the conversion of fructose to DMF was also investigated. Fructose was initially dehydrated in the presence of formic acid at 150 °C for 2 h and generated HMF was subsequently hydrogenated to DMF; using formic acid, Pd/C, H_2SO_4 and THF at 70 °C after 15 h. This process yielded up to 51% DMF. Notably, formic acid performed three distinct functions during this process; (i) Acted as an acid catalyst for the fructose dehydration to HMF, (ii) Acted as a reagent for the deoxygenation and (iii) worked as a hydrogen donor. In order to get high yield of DMF, simultaneous use of formic acid and H_2SO_4 is necessary. However, both the acids are highly corrosive and not environment friendly. To use formic acid as a hydrogen donor for DMF synthesis, special corrosion-resistant equipment are indispensable and that will add cost to the process. Hence, an extensive application of formic acid as a hydrogen donor is restricted.

3.2.3. Hydrogenolysis of HMF to DMF using alcohols as hydrogen donors

Riisager *et al.* followed a new approach for the hydrogenolysis of HMF, through catalytic transfer hydrogenation (CTH), in which methanol was used as a reaction medium as well as a hydrogen donor.[26] Over a Cu-doped porous metal oxide catalyst, 48% DMF yield with 100% HMF conversion was obtained at 260 °C for 3 h. It is important to note that compared to H_2 and formic acid, the overall production cost of DMF can be decreased and operational safety can be achieved to some extent with methanol as hydrogen donor. Vlachos *et al.* achieved 81% DMF yield by employing Ru/C as catalyst and 2-propanol as a hydrogen donor at 190 °C for 6 h.[27] However, when the recovered Ru/C catalyst was used for second cycle, significant drop in catalytic activity was observed (13% DMF yield with 47% HMF conversion). The observed catalyst deactivation for the first re-use was attributed to the blockage of active Ru sites by the deposition of high molecular weight by-products on the catalyst surface. Scholz *et al.* reported

CTH of HMF over Pd/Fe_2O_3 catalyst using 2-propanol as a hydrogen donor and achieved 100% HMF conversion with 72% DMF yield at 180 °C.[28] Morikawa *et al.* studied CTH of HMF using cyclohexane to obtain 60% DMF yield over Pd/C and $AlCl_3$ catalysts.[29] Aellig *et al.* used Cu-Al hydrotalcite catalyst and 1,4-butanediol as a hydrogen donor, which led to 100% HMF conversion with 72% DMF yield.[30]

3.2.4. Hydrogenolysis of HMF to DMF using water as hydrogen donor

Nilges *et al.* reported an electrocatalytic hydrogenation pathway, at room temperature and atmospheric pressure, for the conversion of HMF to DMF.[31] The process consists of a series of consecutive 2-proton and 2-electron reduction steps. The complete reduction process required total of six protons and six electrons. The results revealed that the copper electrode materials were more efficient compared to other electrode materials such as carbon, iron, aluminium, lead, nickel and platinum. Furthermore, the addition of ethanol or acetonitrile to the H_2SO_4 electrolyte solution not only decreased the H_2 formation, but also increased the DMF yield. Hence, when a combination of copper electrode and H_2SO_4 (0.5 M) with 1:1 mixture of ethanol and water was used, the DMF selectivity of up to 35.6% was achieved. Electrochemical hydrogenation technique offers a pathway to convert electrical energy obtained from renewable resources such as wind power into biofuels. In addition, it also provides a strategy to replace the use of H_2 in the manufacture of renewable chemicals.

Thus, it may be visualized that DMF synthesis has been explored using various hydrogen donors and over a wide range of supported metal catalysts. However, most of the reported processes do not offer good space time DMF yield and have other drawbacks such as high metal content of the catalyst, recyclability issues and the need of high H_2 pressure. Use of catalysts with high precious metal content is not favorable to the overall process economics of the production of transportation fuels from biomass-derived compounds.[32] Commercial application of the HMF to DMF process will be feasible only when minimal precious metal content is used in the catalyst. Hence, there is a need to develop an economically viable and environmental friendly process for the selective conversion of HMF to DMF. This chapter deals with the hydrogenolysis of HMF to DMF and hydrogenation of furfural to furfuryl alcohol (FA) using molecular H_2 as a hydrogen donor. The results of this chapter are divided into two parts. Part-3A deals with the hydrogenolysis of HMF to DMF over Ru-doped hydrotalcite (HT) catalysts, while

part-3B deals with the hydrogenolysis of HMF to DMF and hydrogenation of furfural to FA over NaY zeolite supported metal catalysts.

3.3. Part 3A: Hydrogenolysis of HMF to DMF over Ru-doped hydrotalcite catalysts using molecular H_2

Ruthenium-doped HT catalysts were tested for the selective hydrogenolysis of biomass-derived HMF to DMF. Effect of Ru content as well as various reaction parameters was optimized with the objective of increasing the DMF yield.

3.3.1. Experimental procedures

3.3.1.1. Materials

All the chemicals were reagent grade and used without further purification. HMF (99%), DMF (99%), 2,5-dimethyltetrahydrofuran (DMTHF, 99%), 2-methylfuran (MF, 99%), 2-methyltetrahydrofuran (MTHF, 99%) and THF (98%) were procured from Sigma-Aldrich. 5-Methyl furfural (MFU, 99%) and $Ru(NO)(NO_3)_3$ were purchased form Alfa Aesar. Toluene, 2-propanol, $Mg(NO_3)_2 \cdot 6H_2O$, $Al(NO_3)_3 \cdot 9H_2O$, NaOH, Na_2CO_3 and 1,2-dimethoxyethane were obtained from Loba chemie, Mumbai.

3.3.1.2. Evaluation of catalysts

Evaluation of catalysts was carried out using a 100 mL Parr autoclave (SS316). In a typical experiment, 1 mmol of HMF, 25 mL of solvent along with required amount of the freshly reduced catalyst were introduced into the reactor vessel. After closing the reactor, it was purged 2-3 times with H_2 gas and filled with the same gas to reach required H_2 pressure. Subsequently, the reaction vessel was heated under stirring to the desired temperature. During the reaction, the liquid samples were withdrawn periodically and analyzed by GC (Agilent 7890A) equipped with flame ionization detector (FID) and CP Sil 8 CB capillary column (30 m length, 0.25 mm diameter). Product identification was done using authentic standards and by using GC-MS (Varian, Saturn 2200). The FID sensitivity of BHMF and MFA was assumed to be equal to that of HMF and MFU, respectively.

3.3.2. Results and discussion

3.3.2.1. Catalyst characterization

3.3.2.1.1. X-ray diffraction (XRD)

The XRD profiles of the as-synthesized Ru-doped HT samples (RH-1, RH-2 and RH-3) and HT precursor are given in the Fig. 3.1a. The XRD profiles have characteristic peaks of pure HT ($d_{(003)}$ = 7.65 Å). No extraneous peaks belonging to other phases (JCPDS no. 70-2151) were seen. These results show that Ru may be present in the brucite-like lattice of HT, as no peaks corresponding to any of Ru or its oxide phases were seen. The intensities of reflections pertaining to the layered structure decreased with increasing Ru content of the sample. The XRD patterns of the calcined–reduced Ru-doped HT-derived catalysts (RH-1, RH-2 and RH-3) are given in Fig. 3.1b, which also includes the spectra of the Ru-impregnated sample (RH-imp). The RH-imp sample has Ru content similar to that of RH-1. The reflections belonging to the periclase phase of Mg(Al)O (JCPDS no. 4-829) were seen predominantly. In addition to the mixed metal oxide phase, metallic Ru peaks were also present in the case of the catalyst of higher Ru content (RH-3).
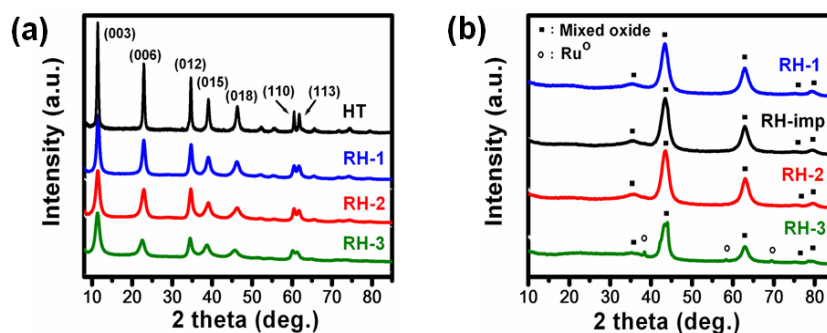
Fig. 3.1 XRD of (a) the as-synthesized precursors and (b) the calcined–reduced catalysts.

3.3.2.1.2. BET surface area

The BET surface areas of calcined HT (HT$_{cal}$) and calcined-reduced Ru-containing catalysts are given in Table 3.1. The surface areas of HT$_{cal}$, RH-1, RH-2, RH-3 and RH-imp were 210, 194, 180, 142 and 185 m^{2}g^{-1}, respectively. The surface area has decreased with increasing Ru content of the sample, as compared to HT$_{cal}$. The decrease in surface area may either be attributed to the poor crystallinity, as reflected in lower XRD intensities (Fig. 3.1) or to the blockage of pores by the segregated Ru oxide phases of the sample.[33]

Catalyst[a]	Synthesis composition Mg:Al:Ru	Ru content[b] (wt%)	BET surface area[c] (m²/g)	Ru metal dispersion[d] (%)	Average Ru crystallite size[d] (nm)	Average Ru particle size[e] (nm)	Ru metal surface area[d] (m²/g)
HT$_{cal}$	3:1:0	0	210	--	--	--	--
RH-1	3:0.97:0.03	0.56	194	47.6	2.8	3.1	0.97
RH-2	3:0.94:0.06	1.0	180	33.1	4.0	4.3	1.20
RH-3	3:0.90:0.10	1.7	142	10.3	12.9	14.0	0.56
RH-imp[f]	3:0.97:0.03	0.58	185	32.4	4.1	--	1.18

Table 3.1 Chemical composition and structural characteristics of the catalysts.

[a] Catalyst precursors prepared by co-precipitation method. [b] Estimated by ICP-OES. [c] Calcined-reduced samples. [d] Determined by H_2 chemisorption. Prior to chemisorption at 40 °C, the catalyst was reduced in situ in H_2 flow at 350 °C. [e] Calculated based on surface area averaged TEM particle size. [f] Prepared by dry-impregnation method.

3.3.2.1.3. H₂ Chemisorption study

Dispersion of Ru in the Ru-containing catalysts was investigated by H_2 chemisorption. The Ru metal dispersion, average Ru crystallite size and the metal surface areas are included in Table 3.1. The metal dispersions were: RH-1, 47.6%; RH-2, 33.1%; RH-3, 10.3% and RH-imp, 32.4%. Good Ru dispersion in the RH-1 catalyst (47.6%) confirms the homogeneous distribution of Ru on the metal oxide support with an average Ru crystallite size of 2.8 nm (Table 3.1).

3.3.2.1.4. Scanning electron microscopy (SEM)

The morphologies of the HT and Ru-doped HT precursors were investigated by SEM. Some of their representative images are shown in Fig. 3.2. The micrographs demonstrate the flower-like morphology [34] of parent HT, which was not changed even after Ru incorporation.
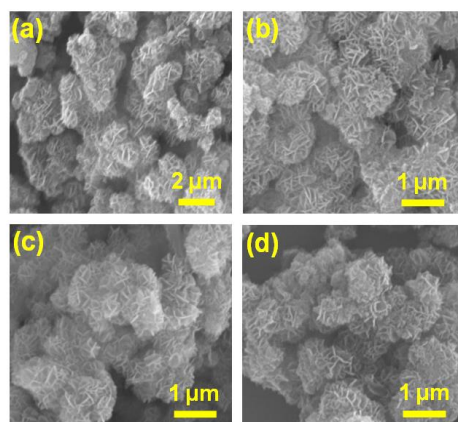
Fig. 3.2 SEM images of as synthesized (a) HT, (b) RH-1, (c) RH-2 and (d) RH-3 catalyst.

3.3.2.1.5. Transmission electron microscopy (TEM)

The Ru nanoparticles sizes as well as their distribution were also investigated by TEM. These results are shown in Fig. 3.3. Micrographs of RH-1 show that Ru nanoparticles are in the 2-6 nm range, dispersed over the HT derived metal oxide support. The average particle size of Ru was 3.1 nm, calculated through surface area averaged TEM particle size by assuming that the Ru particles are hemispherical in shape, with the flat side on the support. These values for the three catalysts, RH-1, RH-2 and RH-3, are in close agreement with the values obtained from H_2 chemisorption (Table 3.1).
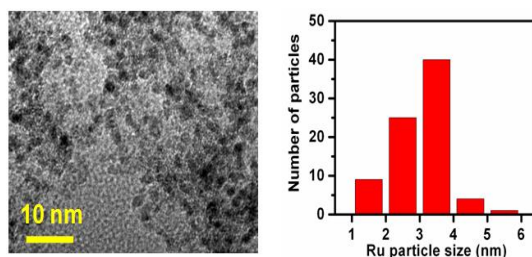
Fig. 3.3 TEM micrograph and Ru particle size distribution of the RH-1 catalyst.

3.3.2.1.6. Temperature programmed reduction (TPR)

In order to understand the reducibility of the Ru supported on mixed oxides, TPR studies were carried out. TPR profiles (Fig. 3.4) showed two H_2 consumption peaks. The first reduction peak is in the range of 120–190 °C, while the second peak is in the 200–330 °C range. These peaks are attributed to the different interactions of the RuO_x species with the support.[35] The low temperature peak is probably due to the weak interaction of Ru with the support, whereas the high temperature peak may be due to the stronger interaction of Ru with the support. In the case of RH-1, the intensity of the low temperature peak was weak. But, its intensity enhanced with increasing Ru content, implying that the concentration of loosely bound Ru increased. There is also a shift of the high temperature peak towards low temperature at high Ru content, particularly in the case of the impregnated catalyst. For RH-imp sample, both low and high temperature peaks have merged.
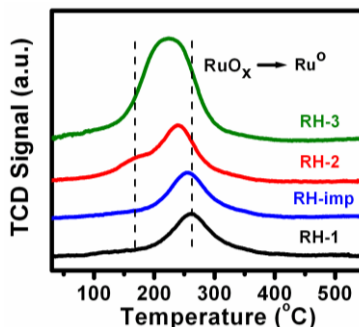
Fig. 3.4 TPR profiles of various Ru catalysts.

3.3.2.1.7. X-ray photoelectron spectroscopy (XPS)

The XPS plot of Ru 3d in RH-1 catalyst is given in Fig. 3.5. The peaks centered at 280.1 and 284.2 eV were attributed to metallic Ru (Ru^o), corresponding to Ru^o $3d_{5/2}$ and Ru^o $3d_{3/2}$, respectively.[36] Whereas, the peaks at 281.6 and 285.9 eV are assigned to the Ru in the +4 oxidation state (RuO_2), hence belong to Ru^{4+} $3d_{5/2}$ and Ru^{4+} $3d_{3/2}$, respectively.[36] Based on XPS results, the relative percentage of Ru metal and Ru oxide were 73 and 27%, respectively. The single peak at 284.5 eV is assigned to carbon 1s coming from the carbon contamination of the sample surface.
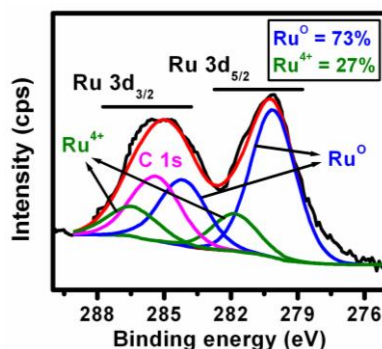
Fig. 3.5 XPS spectrum of Ru 3d for RH-1 catalyst.

3.3.2.2. Catalytic activity in hydrogenolysis of HMF to DMF

3.3.2.2.1. Effect of reaction temperature

The influence of reaction temperature on HMF conversion and DMF yield over the RH-1 catalyst was investigated by varying the reaction temperature in the 180–230 °C temperature range. The HMF conversions and DMF yields are shown in Fig. 3.6a and Fig. 3.6b, respectively. It can be clearly seen (Fig. 3.6a) that the temperature played an important role with regard to HMF conversion, as it has increased with increasing reaction temperature. In addition, HMF

conversion also increased with reaction time. After 4 h of reaction, HMF conversion increased from 70 to 100 mol%, as the reaction temperature increased from 180 to 210 °C. On the other hand, complete conversion of HMF could be seen within 2 h of reaction time, when the reaction was carried out at 220 and 230 °C.
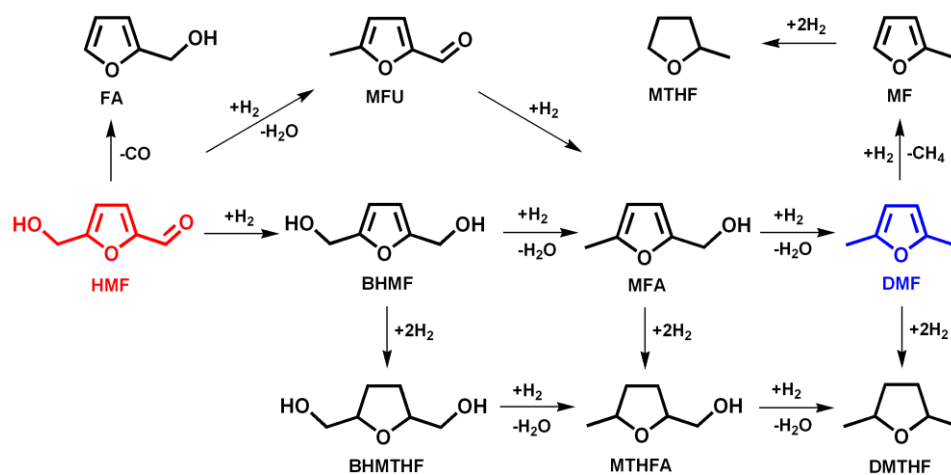
Scheme 3.1 Reaction network for hydrogenolysis of HMF to DMF.

Compounds: 5-Hydroxymethylfurfural (HMF); 2,5-bis(hydroxymethyl)furan (BHMF); 5-methyl furfural (MFU); 5-methyl furfuryl alcohol (MFA); furfuryl alcohol (FA); 2,5-bis(hydroxymethyl)tetrahydrofuran (BHMTHF); 5-methyl tetrahydrofurfuryl alcohol (MTHFA); 2,5-dimethylfuran (DMF); 2,5-dimethyltetrahydrofuran (DMTHF); 2-methylfuran (MF); 2-methyl tetrahydrofuran (MTHF).

The reaction temperature has a profound influence on DMF yield, as may be seen in Fig. 3.6b. The DMF yield increased continuously as a function of reaction time, when the reaction temperature was raised from 180 to 210 °C, indicating that intermediates like 2,5-bis(hydroxymethyl)furan (BHMF), 5-methyl furfuryl alcohol (MFA) and 5-methyl furfural (MFU) that formed during the course of the reaction were converted to DMF with increasing reaction temperature as well as with reaction time (Scheme 3.1).[19] On further increasing the reaction temperature to 220 °C, high DMF yield of 58 mol% could be reached after 4 h of reaction time. However, on further increasing the reaction time, the DMF yield has decreased (Fig. 3.6b). This decrease in the DMF yield could be attributed to its ring hydrogenation, leading to the formation of DMTHF. The DMF yield decreased continuously at higher reaction temperature (230 °C), which clearly implies that the ring hydrogenation is predominant at higher reaction temperatures (Table 3.3, entries 4, 5 and 6), leading to the formation of DMTHF as a principal product.[19] Thus, 220 °C seems to be the optimum temperature to obtain good yield of DMF after 4 h of reaction.
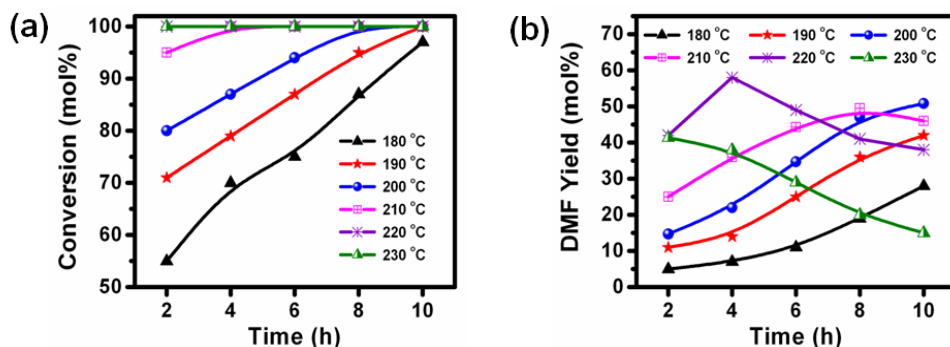
Fig. 3.6 Effect of reaction temperature on (a) HMF conversion and (b) DMF yield as a function of reaction time. <u>Reaction conditions:</u> HMF (1 mmol); catalyst (RH-1, 50 mg); H_2 (10 bar); solvent (2-propanol, 25 mL).

3.3.2.2.2. Effect of solvent

Effect of solvent on the catalytic activity in the liquid-phase hydrogenolysis of HMF to DMF was examined over the RH-1 catalyst at 220 °C and at 7 bar H_2 pressure. Solvents of different chemical nature, such as protic (2-propanol), aprotic polar (THF and 1,2-dimethoxyethane (1,2-DME)) and non-polar (toluene) solvents, were used to investigate the influence of solvent on hydrogenolysis activity and DMF yields.
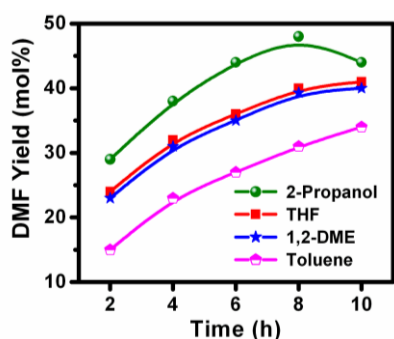
Fig. 3.7 Effect of solvent on DMF yield as a function of reaction time.
<u>Reaction conditions:</u> HMF (1 mmol); catalyst (RH-1, 50 mg); temperature (220 °C); solvent (25 mL); H_2 pressure (7 bar).

The results given in Fig. 3.7 clearly show that the RH-1 activity is heavily solvent dependent. It can be seen that the catalytic activity follows the order: 2-propanol > THF ≈ 1,2-DME > toluene. The lower HMF hydrogenolysis activity in toluene could be explained on the basis of the competitive adsorption between the reactant and the solvent on the active catalytic sites. Moreover, with toluene as a solvent, hydrogenated compounds of toluene were observed under the reaction conditions studied. Competitive adsorption between toluene and HMF on the active catalytic sites results in reduced availability of active sites for HMF. As a result, the HMF

hydrogenolysis activity drops down. The strength of toluene adsorption is controlled by the degree of overlap of the carbon π molecular orbitals with the d bands of the Ru metal.[37]

To understand the reason behind the superior activity in the presence of 2-propanol, experimental runs were carried out in the absence of H_2 at 220 °C under 5 bar N_2 pressure over RH-1, RH-2, RH-3 and RH-imp catalysts (Fig. 3.8). Catalyst RH-1 exhibited superior activity in terms of CTH, compared to other catalysts, probably due to the smaller Ru crystallite size. The results of the CTH experiments, using RH-1 in the absence of H_2, with different solvents are given in Fig. 3.9. About 14 mol% DMF yield was seen after 5 h of reaction with 2-propanol as a solvent. Acetone was detected as one of the products in this experiment, implying hydrogen transfer from 2-propanol. However, the 2-propanol consumed for the purpose of CTH was low (<1 mol%), as it was used as a solvent at a high solvent-to-substrate molar ratio (>300). No CTH was seen when THF or 1,2-DME was used as a solvent under similar conditions. These results strongly suggest that in 2-propanol, HMF is hydrogenated over the RH-1 catalyst via an additional reduction mechanism involving hydrogen transfer from 2-propanol to HMF in the presence of the Ru metal catalyst.[37] Thus, HMF is hydrogenated by molecular H_2 as well as by hydrogen transfer from 2-propanol over the catalyst. However, the rate of HMF hydrogenation using molecular H_2 is comparatively much higher than that of CTH (difference in DMF yield in Fig. 3.7 and 3.9). To understand this aspect further, effect of temperature (Fig. 3.10), effect of Ru content (Fig. 3.11) and the effect of H_2 pressure (Fig. 3.12) were investigated with THF as a solvent, as THF is not expected to be reactive in the given reaction conditions. Unlike with 2-propanol, variation of any of the reaction parameters did not improve the DMF yield, clearly demonstrating the advantage of 2-propanol as a solvent. In view of the higher apparent catalytic activity and superior DMF yield, 2-propanol was chosen as the solvent for further investigations. It is well known that there are differences between heterogeneous catalytic hydrogenation using hydrogen donor molecules as the source of hydrogen and hydrogenation using molecular H_2.[38] The CTH reaction could occur through direct hydride transfer from 2-propanol to HMF.

Fig. 3.8 Yield of DMF on various catalysts in the absence of hydrogen.
Reaction conditions: HMF (1 mmol); catalyst (50 mg); temperature (220 °C); solvent (2-propanol, 25 mL); N_2 pressure (5 bar).
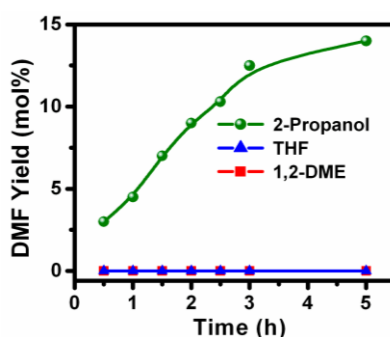
Fig. 3.9 CTH of HMF as a function of reaction time over the RH-1 catalyst.
Reaction conditions: HMF (1 mmol); catalyst (50 mg); temperature (220 °C); solvent (25 mL); N_2 pressure (5 bar).
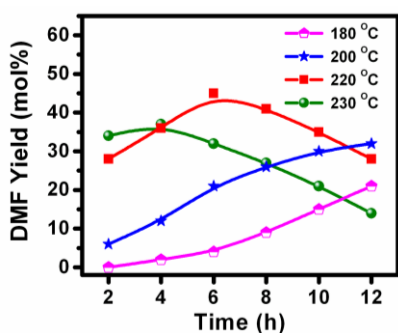
Fig. 3.10 Effect of temperature on DMF yield under non-CTH conditions over RH-1 catalyst.
Reaction conditions: HMF (1 mmol); catalyst (50 mg); H_2 pressure (10 bar); solvent (THF, 25 mL).
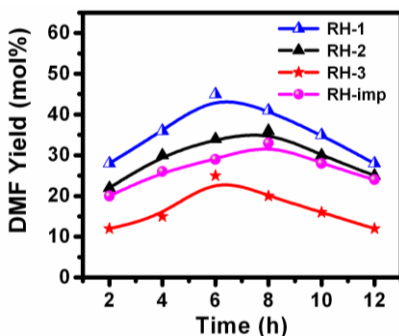
Fig. 3.11 Effect of Ru content on DMF yield over various catalysts under non-CTH conditions.
<u>Reaction conditions:</u> HMF (1 mmol); catalyst (50 mg); temperature (220 °C); H_2 pressure (10 bar); solvent (THF, 25 mL).
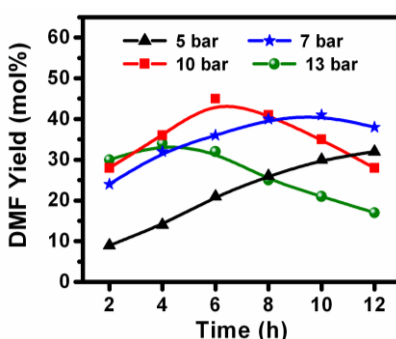
Fig. 3.12 Effect of H_2 pressure on DMF yield over RH-1 catalyst under non-CTH conditions.
<u>Reaction conditions:</u> HMF (1 mmol); catalyst (50 mg); temperature (220 °C); solvent (THF, 25 mL).

3.3.2.2.3. Effect of Ru metal content of the catalysts

To optimize the Ru content of the catalyst, a series of catalysts with different wt% of Ru were prepared and evaluated for HMF hydrogenolysis. The HMF conversions and product yields are summarized in Table 3.2. Catalyst RH-1 showed the highest activity in terms of HMF hydrogenolysis, yielding 58 mol% DMF at 100 mol% HMF conversion (Table 3.2, entry 1). However, under similar reaction conditions, DMF yields were only 48, 35 and 45 mol% over RH-2, RH-3 and RH-imp catalysts, respectively. When Ru content was low (RH-1 with 0.56 wt% Ru), lesser yields of the hydrogenated products of BHMF and DMF were observed, leading to high yield of DMF. On the other hand, over catalysts with high Ru content (RH-2 and RH-3), a significant increase in the yields of ring hydrogenated products such as 2,5-bis(hydroxymethyl)tetrahydrofuran (BHMTHF) and 2,5-dimethyltetrahydrofuran (DMTHF) was observed. This could be a result of the larger Ru crystallite size in these catalysts (Table 3.1). However, the total metal surface areas of RH-2 and RH-imp per gram of catalyst were higher than that of RH-1 (Table 3.1). Even then, RH-1 was found to be superior, as the smaller

crystallite size (2.8 nm) suppresses ring hydrogenation, thus leading to a better DMF yield over RH-1. This is a welcome result, as the hydrotalcite catalyst with low Ru content (RH-1) can achieve a high DMF yield (58 mol%), which may be helpful for the economic production of transportation fuels from biomass.

To ascertain the desirability of Ru in the catalyst, HMF hydrogenolysis was carried out in its absence, using only HT_{cal}, which gave <1 mol% DMF yield (Table 3.2, entry 5). Blank experiment with HMF in 2-propanol, in the absence of a catalyst, showed no activity for DMF formation (Table 3.2, entry 6). But, minor amounts of by-products, probably as a result of HMF polymerization and condensation reactions, were observed in the absence of the catalyst.

Table 3.2 Product distributions during HMF hydrogenolysis over different catalysts.[a]

Entry	Catalyst	HMF conv. (mol%)	Product Yields (mol%)								
			DMF	DMTHF	BHMF	MFA	MFU	BHMTHF	MF	Others[b]	TOF[c] (h^{-1})
1	RH-1	100	58	6	5	8	4	2	3	14 (3)	52.3
2	RH-2	100	48	10	8	11	5	6	1	11 (4)	24.4
3	RH-3	92	35	9	8	8	4	15	2	11 (7)	10.4
4	RH-imp	100	45	8	7	12	4	7	2	15 (4)	39.0
5	HT_{cal}	32	<1	0	1	1	0	0	0	29 (29)	--
6	none	8	0	0	0	0	0	0	0	8 (8)	--

[a] <u>Reaction conditions:</u> HMF (1 mmol); catalyst (50 mg); temperature (220 °C); H_2 pressure (10 bar); solvent (2-propanol, 25 mL); reaction time (4 h). [b] It includes 5-methyl tetrahydrofurfuryl alcohol (MTHFA), furfuryl alcohol (FA), 5,5'-(oxybis(methylene))bis(2-methylfuran) (OMBM), 2,5-bis(hydroxymethyl)tetrahydrofuran (BHMTHF) and other unidentified products (values in brackets). [c] TOF = turnover frequency (moles of DMF produced per mole of Ru per hour).

3.3.2.2.4. Effect of H$_2$ pressure

The influence of H_2 pressure on the HMF hydrogenolysis was studied by varying the pressure in the range of 3–13 bar over RH-1 catalyst (Fig. 3.13). When the reaction was carried out in the low pressure range (3 to 7 bar), the intermediate products such as BHMF, MFA and MFU formed in significant quantities, showing that the hydrogenolysis was incomplete. As a result, only 48 mol% DMF yield was obtained even after 8 h of reaction under 7 bar H_2 pressure. On increasing the H_2 pressure to 10 bar, the DMF yield reached the maximum (58 mol%) over the RH-1 catalyst within 4 h of reaction. But, the DMF yield decreased on continuation of the

reaction for further duration (Fig. 3.13 and Table 3.3, entry 3). Similarly, increasing the H_2 pressure further to 13 bar has an adverse affect on the DMF yield, mostly due to the increased rate of consecutive ring hydrogenation of DMF, leading to the formation of DMTHF in considerable quantities (Table 3.3, entries 8, 9 and 10). Moreover, the concentration of other unwanted by-products such BHMTHF and 5-methyl tetrahydrofurfuryl alcohol (MTHFA) increased at higher pressure (13 bar). These results clearly show that at higher H_2 pressures, ring hydrogenation is the predominant reaction, leading to the lower yield of DMF (Table 3.3). Hence, 10 bar of H_2 pressure being optimum was used for further investigations.

The cis- and trans-DMTHF isomers have different physical properties, e.g. boiling points, which can be distinguished and quantified by GC-FID. Our experiments show that the formation of cis-DMTHF is favoured over trans-DMTHF, with a cis : trans molar ratio of ≈6.5 : 1 under the given experimental conditions (Table 3.3).[26] This may be explained in terms of steric crowding. During the course of the reduction reaction, addition of the second hydrogen molecule takes place on the same face as the first would result in less steric hindrance, whereas the hydrogen molecule may be sterically crowded by the methyl group, restricting the formation of trans-DMTHF (Scheme 3.2).

				DMTHF	cis : trans
Entry	Time (h)	Temp (°C)	DMF yield (mol%)	yield (mol%)	ratio of DMTHF
1	4	210	36	3	6.3
2	4	220	58	6	6.2
3	6	220	49	15	6.7
4	4	230	38	17	6.6
5	6	230	29	26	6.4
6	8	230	20	32	6.5
7[b]	4	220	38	2	6.1
8[c]	2	220	47	7	6.8
9[c]	4	220	41	12	6.6
10[c]	6	220	35	21	6.6
11[d]	4	220	30	19	6.7

Table 3.3 Effect of reaction temperature and H_2 pressure on DMTHF yield.[a]

[a] Reaction conditions: HMF (1 mmol); catalyst (RH-1, 50 mg); H_2 pressure (10 bar); solvent (2-propanol, 25 mL). [b] H_2 pressure (7 bar). [c] H_2 pressure (13 bar). [d] H_2 pressure (16 bar).
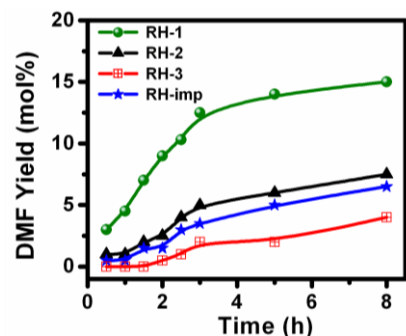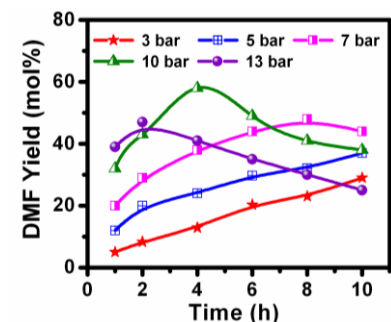
Fig. 3.13 Effect of H$_2$ pressure on DMF yield as a function of reaction time.
<u>Reaction conditions:</u> HMF (1 mmol); catalyst (RH-1, 50 mg); temperature (220 °C); solvent (2-propanol, 25 mL).
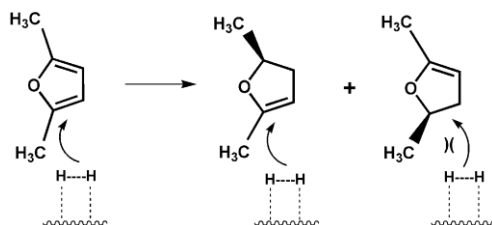
Scheme 3.2 Mechanism for the preferential formation of the cis-DMTHF isomer over the trans-DMTHF isomer from DMF over the RH-1 catalyst.[26]

3.3.2.2.5. Effect of catalyst content

The amount of catalyst used in the reaction is an important parameter that needs to be optimized to get high DMF yield. Experiments were conducted by varying the amount of the RH-1 catalyst from 15 to 70 mg at 220 °C, while maintaining the same HMF content (Fig. 3.14). These experiments showed that the DMF yield increased initially with catalyst content. When the catalyst was 15 mg, the DMF yield reached a maximum of 40 mol% after 12 h of reaction, which declined on further increasing the reaction time. When 30 mg of catalyst was used, the DMF yield reached 46 mol% in a slightly shorter duration (10 h) of reaction time. With 50 mg of catalyst, a maximum DMF yield of 58 mol% was accomplished only in 4 h of reaction time, but it decreased when the reaction was continued further, mostly due to ring hydrogenation of DMF. However, when the catalyst content was further increased to 70 mg, a much lower DMF yield of 44 mol% was achieved after 4 h, which decreased with further increasing time on stream. These results show that with increased duration of reaction even at low catalyst content, DMF undergoes consecutive hydrogenation, leading to DMTHF formation. At higher catalyst content, more active sites are available, which drive the formation of side products such as 2-methylfuran

(MF) and 2-methyl tetrahydrofuran (MTHF) in addition to the hydrogenated products MTHFA and DMTHF, leading to a lower DMF yield. Hence, optimization of catalytic sites and reaction time is essential to obtain the maximum DMF yield. Based on these studies, 50 mg of catalyst was found to be the optimum under the given reaction conditions.
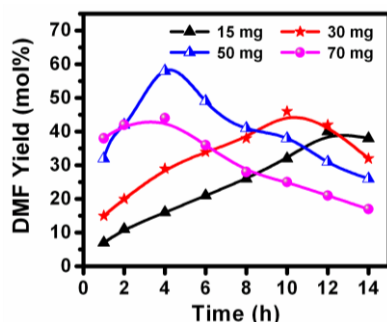
Fig. 3.14 Effect of catalyst content on DMF yield as a function of reaction time over the RH-1 catalyst. Reaction conditions: HMF (1 mmol); temperature (220 °C); H_2 pressure (10 bar); solvent (2-propanol, 25 mL).

3.3.2.2.6. Recyclability study

Catalyst recyclability is of great importance, if the process has to be upscale to an industrial process. The recyclability of the RH-1 catalyst in HMF hydrogenolysis to DMF was evaluated by repeating the reaction with the same catalyst at least five times without any regeneration/activation (Fig. 3.15). The results show that the catalyst remains active even after five cycles, though a minor drop in DMF yield was observed probably due to blockage of some catalytic sites. These results indicate good stability of the catalyst. The product mixture at the end of each recycle was analyzed by ICP-OES, for the presence of any Ru due to leaching out of the catalyst. No such leaching was observed. Moreover, the concentration of Ru in the catalyst was similar to that of the starting catalyst even after five cycles.
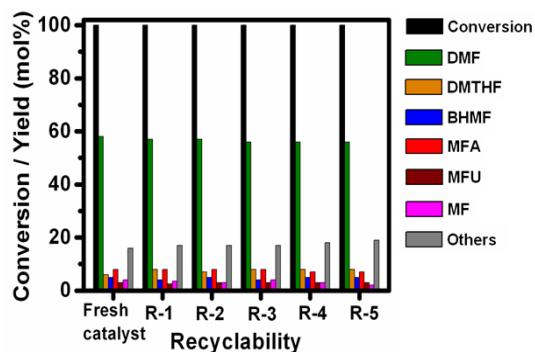
Fig. 3.15 Recyclability experiments of the RH-1 catalyst in HMF hydrogenolysis. Reaction conditions: molar ratio of HMF to Ru (360); solvent (2-propanol, 25 mL); temperature (220 °C); H_2 pressure (10 bar); reaction time (4 h).

3.3.3. Conclusions

The present investigations demonstrate that highly dispersed Ru-containing mixed metal oxide catalysts can be obtained by the calcination of hydrotalcite-like precursors, which were obtained through co-precipitation method. As a result, even catalysts with low Ru metal (0.56 wt%) content were highly active in the conversion of HMF to DMF. Analysis of intermediate products at different stages of reaction showed that DMF is formed via BHMF followed by MFA. Under optimized reaction conditions, a maximum DMF yield of 58 mol% was achieved at 220 °C, at 10 bar H_2 pressure with 2-propanol as the solvent. The catalyst can be recycled up to five times without any significant loss in activity. Higher DMF yields were seen with 2-propanol as the solvent, as a result of hydrogen transfer from 2-propanol to HMF over the Ru metal. This study clearly shows that Ru-containing mixed metal oxide derived catalysts have an excellent potential for the conversion of biomass oxygenates to biofuels.

3.4. Part 3B: Hydrogenolysis of HMF to DMF and hydrogenation of furfural to furfuryl alcohol over Ru-NaY catalysts using molecular H_2

Ruthenium doped hydrotalcite catalysts could effectively catalyze the hydrogenolysis of HMF giving good yield of DMF. But, the challenge is to get a catalyst that is easy to synthesize and also capable of giving high space time DMF yield. Hence, we prepared Ru supported on NaY zeolite catalyst via a simple ion-exchange method and tested for HMF hydrogenolysis. The Ru-NaY catalyst was reported as an active catalyst for the hydrogenation of cinnamaldehyde[39a], hydrogenation of benzene[39b], CO methanation[39c], nitriles hydrogenation[39d] and so on. Herein, we have studied the effectiveness of Ru-NaY catalyst for the hydrogenolysis of HMF to DMF and hydrogenation of furfural to FA in the presence of THF solvent (it can be prepared from biomass-derived furfural). Various process parameters were optimized with an aim to improve the DMF and FA yields.

3.4.1. Experimental procedures

3.4.1.1. Materials

All the chemicals used in this study were reagent grade, hence used without further purification. HMF (99%), DMF (99%), DMTHF (99%), MF (99%), MTHF (99%), $RuCl_3 \cdot 3H_2O$ and THF (98%) were procured from Sigma-Aldrich. MFU (99%), $PdCl_2 \cdot 2H_2O$, $H_2PtCl_6 \cdot 6H_2O$, $RhCl_3 \cdot 3H_2O$, $HAuCl_4 \cdot 3H_2O$, $CuCl_2 \cdot 2H_2O$, $NiCl_2 \cdot 6H_2O$, n-decane and $AgNO_3$ were purchased

from Alfa Aesar. NaY zeolite (CBV-100, Si/Al ratio = 2.5) and NH_4Y zeolite (CBV-500, Si/Al ratio = 2.6) were obtained from Zeolyst International, USA. Toluene, 2-propanol, CH_3CN, DMSO, $NaBH_4$ and 1,2-DME were procured from Loba chemie, Mumbai.

3.4.1.2. Evaluation of catalysts

All the reactions were carried out using 100 mL parr autoclave (SS316). In a typical experiment, the reactor was charge with 1 mmol of HMF (or 4 mmol of furfural), solvent (25 mL), n-decane (0.2 g, internal standard) and required amount of freshly reduced catalyst. The reactor contents were mixed thoroughly and the reactor was sealed, purged 2-3 times with H_2 gas and filled with the same gas to the required H_2 pressure. Subsequently, the reaction vessel was heated under stirring (800 rpm) to the required temperature. Liquid samples were withdrawn periodically during the reaction and analyzed by GC (Agilent 7890A) equipped with FID and CP Sil 8 CB capillary column (30 m length, 0.25 mm diameter). Product identification was done using authentic standards and GC-MS (Varian, Saturn 2200). The FID sensitivity of BHMF and MFA was assumed to be equal to that for HMF and MFU, respectively.

3.4.2. Results and discussion

3.4.2.1. Catalyst characterization

3.4.2.1.1. X-ray diffraction (XRD)

XRD profiles of Ru exchanged NaY zeolite and parent NaY zeolite are shown in Fig. 3.16. The similarity in diffraction pattern of Ru exchanged NaY zeolite sample and NaY zeolite show that the NaY zeolite has retained its crystalline structure after Ru exchange.[39b] Diffraction peaks corresponding to Ru metal were not observed, signifying that the Ru nanoparticles are highly dispersed on NaY zeolite support.
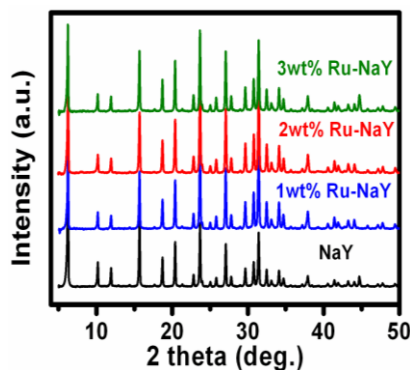
Fig. 3.16 XRD profiles of the NaY and various Ru exchanged NaY zeolite catalysts.

3.4.2.1.2. BET surface area

Similarity in the BET surface area values for Ru containing NaY catalyst and the NaY zeolite suggest that the NaY zeolite did not undergo any changes on Ru exchange (Table 3.4, entry 1, 2, 3 and 4). However, there is significant decrease in the surface area of the Ru catalysts as we move from 2wt% Ru-NaY (851 m^2/g) to 2wt% Ru-Cs-NaY (602 m^2/g). This decrease in surface area may be attributed to the larger size of Cs^+ (167 pm) that replaced smaller Na^+ (102 pm), which is also reflected in continuous decrease in pore volume (Table 3.4, entry 3, 5, 6 and 7). Structural characteristics and chemical compositions of the other supported metal catalysts are also given in Table 3.4.

Table 3.4 Structural characteristics and chemical composition of supported metal catalysts.							
Entry	Samples	BET surface area (m^2/g)	Total pore volume[a] (cm^3/g)	Metal content[b] (wt%)	Metal dispersion[c] (%)	Average metal crystallite size[c] (nm)	Metal surface area[c] (m^2/g)
1	NaY zeolite	886	0.35	--	--	--	--
2	1wt% Ru-NaY	861	0.34	0.97	47.4	2.8	1.72
3	2wt% Ru-NaY	851	0.34	1.98	53.2	2.5	3.86
4	3wt% Ru-NaY	827	0.33	2.95	19.3	6.9	2.11
5	2wt% Ru-K-NaY	776	0.30	1.92	48.5	2.7	3.54
6	2wt% Ru-Rb-NaY	686	0.27	1.95	45.2	3.0	3.23
7	2wt% Ru-Cs-NaY	602	0.23	1.91	41.1	3.2	3.01
8	2wt% Pt-NaY	795	0.31	1.84	--	--	--
9	2wt% Pd-NaY	811	0.32	1.91	--	--	--
10	2wt% Rh-NaY	788	0.31	1.90	--	--	--
11	2wt% Au-NaY	810	0.32	1.82	--	--	--
12	2wt% Ru-HY	751	0.27	1.86	--	--	--
13	5wt% Ni-NaY	771	0.29	4.72	--	--	--
14	5wt% Cu-NaY	813	0.32	4.59	--	--	--
[a] Total pore volume at $P/P_0 = 0.899$. [b] Estimated by ICP-OES. [c] Determined by H_2 chemisorption. Prior to chemisorption at 40 °C, the catalyst was reduced in situ in H_2 flow at 250 °C.							

3.4.2.1.3. H₂ Chemisorption study

Dispersion of Ru, average Ru crystallite size and metal surface area of Ru catalysts were investigated by H_2 chemisorption using freshly reduced samples (Table 3.4). The Ru metal dispersions were: 1wt% Ru-NaY, 47.4%; 2wt% Ru-NaY, 53.2%; 3wt% Ru-NaY, 19.3%; 2wt%

Ru-K-NaY, 48.5%; 2wt% Ru-Rb-NaY, 45.2% and 2wt% Ru-Cs-NaY, 41.1%. The high dispersion of Ru in 2wt% Ru-NaY (53.2%) catalyst confirms the homogeneous distribution of Ru nanoparticles on NaY support with an average Ru crystallite size of 2.5 nm.

3.4.2.1.4. Scanning electron microscopy (SEM)

The morphology of the NaY zeolite and Ru-containing NaY catalysts were studied by SEM (Fig. 3.17). The SEM micrographs demonstrate that the morphology of Ru-containing catalysts did not undergo any change with respect to the parent NaY zeolite.
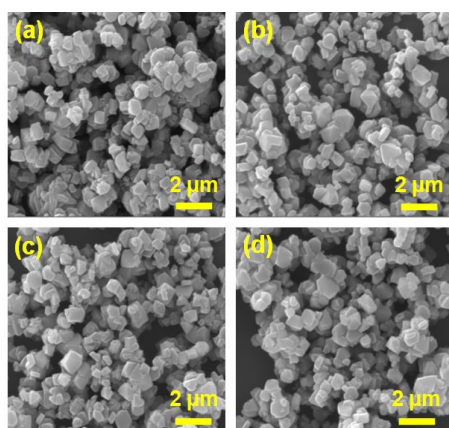
Fig. 3.17 SEM image of (a) NaY zeolite, (b) 1wt% Ru-NaY, (c) 2wt% Ru-NaY and (d) 3wt% Ru-NaY catalysts.

3.4.2.1.5. Transmission electron microscopy (TEM)

The Ru nanoparticles sizes as well as their distribution on 2wt% Ru-NaY catalyst were also investigated by TEM (Fig. 3.18). The micrographs show that Ru nanoparticles are well-dispersed and are in the 1-5 nm range over NaY support. The calculated average Ru nanoparticles sizes were in 2.7 nm range, which is in accordance with H_2 chemisorption results (Table 3.4, entry 3).
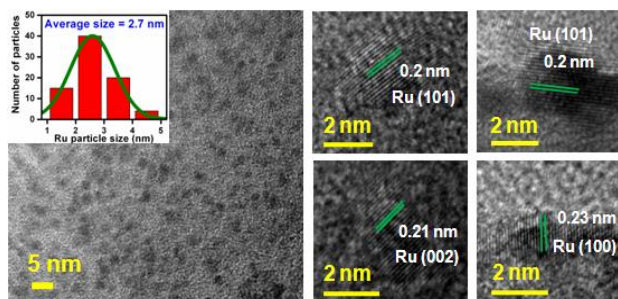
Fig. 3.18 TEM micrograph and Ru particles size distribution of 2wt% Ru-NaY catalyst.

3.4.2.1.6. Temperature programmed reduction (TPR)

In order to understand the reducibility of the supported Ru catalysts, TPR studies in dilute H_2 flow were carried out. TPR profiles of Ru exchanged NaY zeolite and alkali metal modified (K, Rb and Cs) Ru-NaY samples are given in Fig. 3.19a and 3.19b, respectively. Only one broad H_2 consumption peak in the temperature range 70-150 °C was observed, which may be attributed to the reduction of RuO_x species.[40] However, two peaks were seen for 3wt% Ru-NaY in the temperature range of 80-170 °C, probably due to the two different locations of RuO_x species in zeolite cavities.
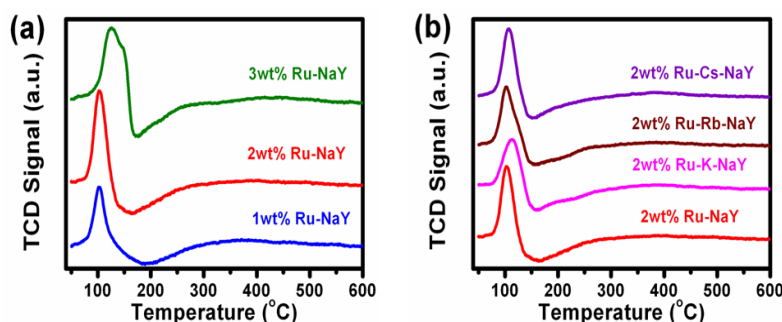
Fig. 3.19 TPR profiles of the (a) Ru-containing NaY catalysts and (b) Ru-containing alkali metal modified Ru-NaY catalysts.

3.4.2.1.7. X-ray photoelectron spectroscopy (XPS)

The XPS spectrum of Ru 3d in 2wt% Ru-NaY catalyst is given in Fig. 3.20. The peaks centered at 280.2 and 284.3 eV were assigned to metallic Ru (Ru^o), corresponding to Ru^o $3d_{5/2}$ and Ru^o $3d_{3/2}$, respectively.[36] Whereas, the peaks at 281.5 and 285.9 eV are attributed to the Ru in the +4 oxidation state (RuO_2), hence assigned to Ru^{4+} $3d_{5/2}$ and Ru^{4+} $3d_{3/2}$, respectively.[36] Based on XPS results, the relative percentage of Ru metal and Ru oxide were 76 and 24%, respectively. The single peak at 284.5 eV is assigned to carbon 1s originating from the carbon contamination of the sample surface.
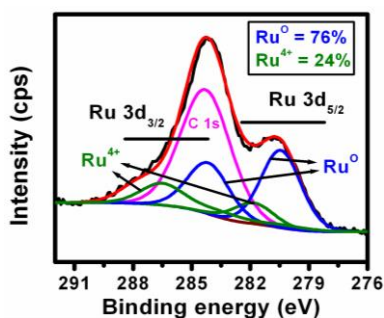
Fig. 3.20 XPS spectrum of Ru 3d for 2wt% Ru-NaY catalyst.

3.4.2.2. Catalytic activity in hydrogenolysis of HMF to DMF

3.4.2.2.1. Hydrogenolysis of HMF over different supported metal catalysts

The hydrogenolysis of HMF was investigated using Pt, Pd, Rh, Ru, Au, Ni and Cu catalysts supported on NaY zeolite. The HMF conversions and product yields are summarized in Table 3.5 (and Fig. 3.21). Under the reaction conditions studied (temperature = 220 °C, reaction time = 1 h and H_2 pressure = 15 bar), mainly four products were observed: DMF, DMTHF, BHMF and MFA. The HMF conversion was in the range of 30.1 to 100 mol% and the reactivity followed the order Cu < Ni < Au < Rh < Pd = Pt = Ru (Table 3.5). Though 100 mol% HMF conversion was seen for Pt-NaY and Pd-NaY catalysts, the DMF yields were low at 30.4 and 49.3 mol% respectively, when compared to their Ru counterpart (Table 3.5, entry 1 and 2). Similarly, with Rh-NaY, Au-NaY, Ni-NaY and Cu-NaY catalysts, poor catalytic activity as well as low DMF selectivity's were observed, resulting to 40.1, 8.2, 2.6 and 3.2 mol% DMF yields at 92, 65.6, 35.5 and 30.1 mol% HMF conversions, respectively (Table 3.5, entry 3, 5, 6 and 7). It is gratifying to note that excellent DMF yield of 78 mol% with 100 mol% HMF conversion was achieved with 2wt% Ru-NaY catalyst (Table 3.5, entry 4). These findings are in good agreement with the literature, which generally reports that the Ru based catalysts are highly selective for the conversion of HMF to DMF.[41]

When the hydrogenolysis reaction was carried out over Ru supported HY (proton exchanged) zeolite, HMF conversion as well as the product distributions changed significantly (Table 3.5, entry 8). The HMF conversion has dropped to 85.5 mol% on this catalyst, giving only 40.5 mol% DMF yield and the most of the HMF was converted to polyols (≈ 25 mol%). The Brønsted acid sites of HY zeolite in 2wt% Ru-HY catalyst (acidity = 2.43 mmol/g) may be responsible for the enhancement in side reactions, eg. ring opening through breakage of furanic C-O bond, which is normally catalyzed by Brønsted acid sites.[42] On the other hand, Lewis acid sites of 2wt% Ru-NaY catalyst (acidity = 1.12 mmol/g) are expected to increase deoxygenation ability of the catalyst and thus help to improve the DMF yield. Recently, Fu *et al.* reported synergy between hydrogenating Ni sites and deoxygenating Lewis acid sites, in nickel-tungsten carbide catalysts, for obtaining very high yield of DMF from HMF.[23]

To ascertain the desirability of Ru in the catalyst, HMF hydrogenolysis was carried out in its absence, using only NaY zeolite, it converted only 20.2 mol% of HMF, but hardly yielded any DMF in the product (Table 3.5, entry 9). Similarly, blank experiment in the absence of catalyst

did not show any activity for DMF formation (Table 3.5, entry 10). It is important to note that the complete hydrogenolysis of HMF to DMF was mainly catalyzed by Ru nanoparticles. Since, high yield of DMF at high HMF conversion was achieved; it was decided to carry out further investigations using 2wt% Ru-NaY catalyst.

Table 3.5 Product distributions during HMF hydrogenolysis over different supported metal catalysts.[a]

Entry	Catalyst	HMF conv. (mol%)	Product Yields (mol%)					TOF[c] (h^{-1})
			BHMF	MFA	DMF	DMTHF	Others[b]	
1	2wt% Pt-NaY	100	7.8	14.0	30.4	4.0	43.8 (5.1)	60.8
2	2wt% Pd-NaY	100	15.6	19.0	49.3	1.1	15.0 (2.4)	98.6
3	2wt% Rh-NaY	92.0	11.5	12.8	40.1	10.7	16.9 (3.4)	80.2
4	2wt% Ru-NaY	100	0	0	78.0	11.8	10.2 (1.2)	156.0
5	2wt% Au-NaY	65.6	25.5	5.5	8.2	0	26.4 (3.7)	16.4
6	5wt% Ni-NaY	35.5	6.4	5.2	2.6	0	21.3 (2.4)	5.2
7	5wt% Cu-NaY	30.1	5.5	1.5	3.2	0	19.9 (5.6)	6.4
8	2wt% Ru-HY[d]	85.5	2.5	2.2	40.5	3.0	37.3 (8.5)	81.0
9	NaY zeolite	20.2	0	0	0	0	20.2 (20.2)	0
10	none	6.3	0	0	0	0	6.3 (6.3)	0

[a] Reaction conditions: molar ratio of HMF to metal (200); temperature (220 °C); H$_2$ pressure (15 bar); solvent (THF, 25 mL); reaction time (1 h). [b] It includes furfuryl alcohol (FA), 5-methyl furfural (MFU), 2-methylfuran (MF), 2,5-bis(hydroxymethyl)tetrahydrofuran (BHMTHF), 5-methyl tetrahydrofurfuryl alcohol (MTHFA), hexanediol and some unidentified products (values in brackets). [c] TOF = turnover frequency (moles of DMF produced per mole of metal per hour). [d] 2wt% Ru-HY (acidity = 2.43 mmol/g), ≈ 25 mol% of polyols were obtained with 2wt% Ru-HY catalyst.
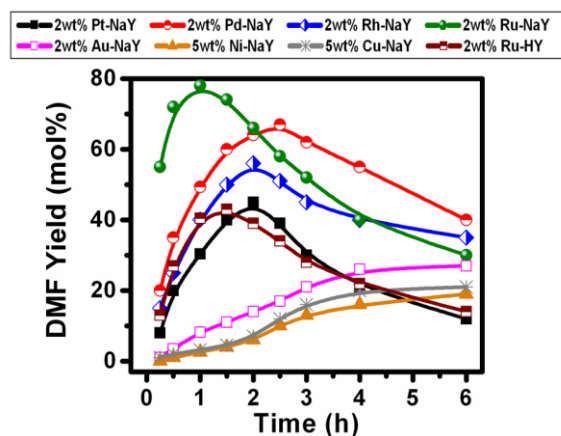
Fig. 3.21 Effect of reaction time on DMF yield over supported metal catalysts.
Reaction conditions: molar ratio of HMF to metal (200); temperature (220 °C); H$_2$ pressure (15 bar); solvent (THF, 25 mL).

3.4.2.2.2. Effect of reaction temperature

The influence of reaction temperature on the HMF conversion and product yields was studied by varying the temperature in the 180-230 °C range over 2wt% Ru-NaY catalyst at 10 bar H_2 pressure (Fig. 3.22). When the reaction was performed at 180 °C, the HMF conversion was low (65.5 mol%), while it has increased at higher temperatures to reach maximum of 100 mol% at 210 °C. At lower temperature (180 °C), the main product was BHMF (45 mol%) and the yield of DMF was considerably low (5 mol%). However, the DMF yield improved substantially with increasing reaction temperature, which reached 69.5 mol% at 220 °C. But, when the reaction temperature was further increased to 230 °C, the yield of DMF dropped (50.1 mol%) and the ring hydrogenation of DMF became prominent,[26,43] yielding 33.2 mol% of DMTHF. These results demonstrate that the low temperatures (180 and 200 °C) are not suitable to achieve good yield of DMF, while high temperature (230 °C) assisted the consecutive hydrogenation of DMF leading to high DMTHF yield. Therefore, 220 °C temperature was found to be optimum for selective conversion of HMF to DMF.
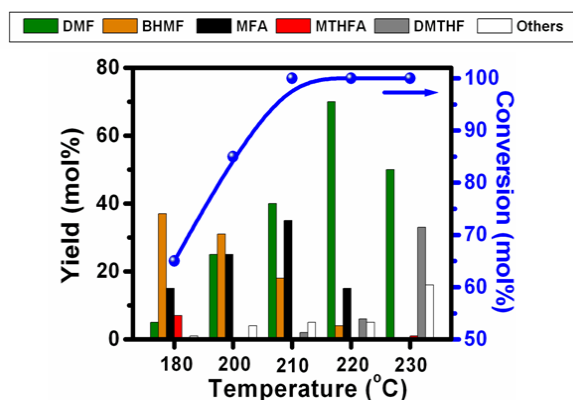
Fig. 3.22 Effect of reaction temperature on HMF conversion and product yields.
Reaction conditions: molar ratio of HMF to Ru (200); H_2 pressure (10 bar); solvent (THF, 25 mL); reaction time (1 h).

3.4.2.2.3. Effect of solvent

The influence of solvent in the liquid-phase hydrogenolysis of HMF to DMF was investigated over 2wt% Ru-NaY catalyst at 220 °C and at 10 bar H_2 pressure (Fig. 3.23). Solvents of different chemical nature, such as non-polar (toluene), aprotic polar (THF, 1,2-dimethoxyethane (1,2-DME), dimethyl sulfoxide (DMSO) and acetonitrile (CH_3CN)) and protic (2-propanol) solvents, were used to study the effect of solvent on HMF hydrogenolysis. The results shown in Fig. 3.23 clearly show that the catalytic activity is strongly solvent dependent,

which follows the order: THF > 1,2-DME > toluene > 2-propanol > CH_3CN > DMSO. Lower activity seen for DMSO, CH_3CN and toluene solvents could be explained on the basis of the competitive adsorption between the solvent and the reactant molecules on the active catalytic sites. Solvents containing nitrogen (CH_3CN) or sulfur (DMSO) are known to deactivate the Ru based catalysts, as a result of interaction of lone pair of electrons on nitrogen/sulfur with the empty d orbitals of Ru metal.[44] Strong adsorption of DMSO and CH_3CN would completely block Ru active sites for HMF adsorption, thus inhibiting HMF hydrogenolysis. When toluene was used as solvent, hydrogenated compounds of toluene were observed in the product mixture under the reaction conditions studied.[45] This shows that toluene and HMF compete for the same active sites, which leads to the lower availability of active sites for HMF adsorption, thus suppressing HMF hydrogenolysis rate. On the other hand, formation of undesirable condensed products (ethers and acetals, ≈16 mol%) were observed with 2-propanol as solvent, which may be facilitated by the residual acidity of 2wt% Ru-NaY catalyst.[46] This brings down the concentration of HMF in the solution, leading to reduced rate of HMF hydrogenolysis. The highest activity was observed in THF solvent giving 69.5 mol% yield of DMF at 100 mol% HMF conversion.

Fig. 3.23 Effect of solvent on HMF conversion and product yields.
Reaction conditions: molar ratio of HMF to Ru (200); temperature (220 °C); solvent (25 mL); H_2 pressure (10 bar); reaction time (1 h).

3.4.2.2.4. Effect of H_2 pressure

The effect of H_2 pressure on the DMF yield was studied over 2wt% Ru-NaY catalyst by varying it in the pressure range of 5-30 bar at 220 °C (Fig. 3.24). When the reaction was carried out at low pressure (5 bar), intermediate products such as BHMF and MFA formed in major

quantities, which are converted to DMF on prolonging the reaction time.[43] When H_2 pressure was increased further (10 and 12 bar); the DMF yield reaches maximum after certain reaction time, but decreased thereafter on continuation of the reaction for further duration. The highest yield of the targeted DMF (78 mol%) was obtained at 15 bar H_2 pressure within 1 h of reaction time. The decrease in DMF yield is due to its ring hydrogenation, a consecutive reaction, leading to the formation of DMTHF. Hence, increasing the H_2 pressure to 20 and 30 bar, the DMF yield was adversely affected. At higher H_2 pressure, DMF yield suppressed mostly due to the formation of DMTHF in significant amounts.[19,43] Moreover, the concentration of other undesirable by-products such as MTHFA, BHMTHF and hexanediol also increased at higher H_2 pressure.[43] Hence, an optimum H_2 pressure of 15 bar was chosen to obtain high yield of DMF.
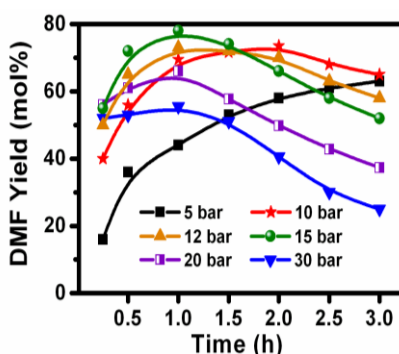
Fig. 3.24 Effect of H_2 pressure on DMF yield as a function of reaction time.
Reaction conditions: molar ratio of HMF to Ru (200); temperature (220 °C); solvent (THF, 25 mL).

3.4.2.2.5. Effect of Ru content

To optimize the Ru content of the catalyst, catalysts with different wt% of Ru supported on NaY zeolite were prepared and evaluated for HMF hydrogenolysis (Fig. 3.25). Since, all NaY supported Ru catalysts gave 100 mol% HMF conversion within half an hour of the reaction, only DMF yield as a function of reaction time is compared. Catalyst with 2wt% Ru (2wt% Ru-NaY) showed the highest activity yielding 78 mol% DMF within 1 h of the reaction time. However, under similar reaction conditions, DMF yields were only 67 and 45 mol% over 1wt% and 3wt% Ru-NaY catalysts, respectively. More importantly, significant increase in the yields of ring hydrogenated products such as DMTHF and 2,5-bis(hydroxymethyl)tetrahydrofuran (BHMTHF) were observed over 3wt% Ru-NaY catalyst. This could be attributed to larger Ru crystallite size (6.9 nm) over this catalyst.[43] On the other hand, the main by-product was MTHFA over 1wt% Ru-NaY catalyst, as a result of hydrogenation of MFA. The superior activity exhibited by 2wt%

Ru-NaY in terms of DMF yield could be attributed to its smaller Ru crystallite size (2.5 nm) and higher Ru metal surface area (3.86 m^2/g). The smaller Ru crystallite size suppresses the ring hydrogenation, thus leading to better DMF yield.[43]
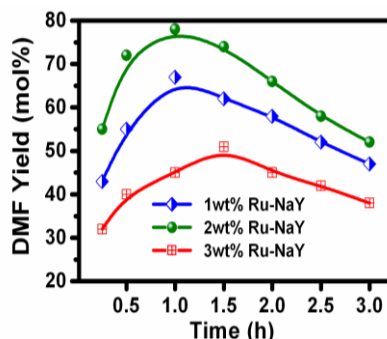
Fig. 3.25 Effect of Ru content of the catalyst on DMF yield.
Reaction conditions: molar ratio of HMF to Ru (200); temperature (220 °C); H$_2$ pressure (15 bar); solvent (THF, 25 mL).

3.4.2.2.6. Effect of HMF to Ru molar ratio

Effect of HMF/Ru molar ratio on DMF yields with 2wt% Ru-NaY catalyst was also studied and the results are given in Fig. 3.26. At higher HMF to Ru molar ratio (335), even prolonging the reaction beyond a point did not improve the DMF yield. This is due to the consecutive reaction of DMF to give DMTHF. Lower HMF to Ru molar ratios (63 and 100) were also not beneficial to get high yield of DMF, as higher Ru led to consecutive hydrogenation of DMF giving unwanted byproducts such as DMTHF, MF and MTHF. When HMF/Ru molar ratio was 200, it gave optimum high yield (78 mol%) of DMF within 1 h of reaction time. Therefore, to attain maximum yield of DMF, optimum HMF/Ru molar ratio and reaction time are essential.
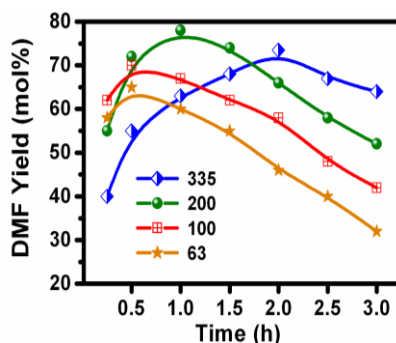
Fig. 3.26 Effect of HMF to Ru molar ratio on DMF yield over 2wt% Ru-NaY catalyst.
Reaction conditions: temperature (220 °C); H$_2$ pressure (15 bar); solvent (THF, 25 mL).

3.4.2.2.7. Hydrogenolysis of HMF to DMF over alkali metal modified Ru-NaY catalysts

Effect of alkali metal (Na, K, Rb and Cs) on Y zeolite supported Ru catalysts was tested for hydrogenolysis of HMF to DMF (Table 3.6). Higher activity was observed for 2wt% Ru-NaY catalyst, giving 78 mol% DMF yield with 100 mol% HMF conversion. However, under similar reaction conditions DMF yields were only 66.8, 58 and 49 mol% over 2wt% Ru-K-NaY, 2wt% Ru-Rb-NaY and 2wt% Ru-Cs-NaY catalyst, respectively. The superior activity exhibited by 2wt% Ru-NaY catalyst in terms of DMF yield could be due to its higher Ru dispersion (53.2 %), smaller Ru crystallite size (2.5 nm) and higher Ru metal surface area (3.86 m^2/g).

Table 3.6 Catalytic performance of alkali metal modified Y zeolite supported Ru catalysts in hydrogenolysis of HMF to DMF.[a]

Catalyst	HMF conv. (mol%)	Product Yields (mol %)						
		DMF	DMTHF	BHMF	MFA	MFU	MF	Others[b]
2wt% Ru-NaY	100	78	11.8	0	0	0	2.3	10.2
2wt% Ru-K-NaY	100	66.8	1.9	1.7	14.5	1.3	1.4	12.4
2wt% Ru-Rb-NaY	100	58	2.6	1.4	12.6	1.2	1.6	22.6
2wt% Ru-Cs-NaY	100	49	3.3	3.7	8.5	2.2	3.4	30.9

[a] Reaction conditions: molar ratio of HMF to Ru (200); temperature (220 °C); H_2 pressure (15 bar); solvent (THF, 25 mL); reaction time (1 h). [b] It includes furfuryl alcohol (FA), 2,5-bis(hydroxymethyl)tetrahydrofuran (BHMTHF), 5-methyl tetrahydrofurfuryl alcohol (MTHFA), hexanediol and some unidentified products.

3.4.2.2.8. Proposed reaction pathway for DMF from HMF

To understand the reaction path in the hydrogenolysis of HMF to DMF, the reaction was carried out at 200 °C under 10 bar H_2 pressure using 2wt% Ru-NaY catalyst. The reaction intermediates formed during the course of the reaction were analyzed by GC-MS and using authentic standards. The variations in concentration of reactant (HMF) and different products formed during the course of reaction are given in the Fig. 3.27. Under the reaction conditions used, a very short reaction time (10 min) provided low HMF conversion (20 mol%), which gradually increased to 100 mol% as the time progressed to 90 min, while the product distributions changed in a complex manner with progress of the reaction. The BHMF yield reached maximum at 40 mol% after 90 min and then deceased with increasing time. Similar

profile was also observed for MFA to that of BHMF, passing through the maxima at 120 min. The yield of DMF increased continuously up to certain reaction time, increasing to a maximum, which then decreased with increasing reaction time. The yield of MFU was very low (< 2 mol%) over the entire duration of the reaction. The low yield of MFU may be due to the fact that its formation is not rapid enough. Based on the results discussed above and the reported literature,[21,27] we hypothesize that the reaction proceeds through the hydrogenation of –CHO in HMF, followed by the hydrogenolysis of the –OH functionalities in BHMF to give DMF via MFA. In a consecutive step, DMF was hydrogenated to DMTHF along with the formation of other by-products such as MF, MTHF and 2-hexanol, on prolonging the reaction time.
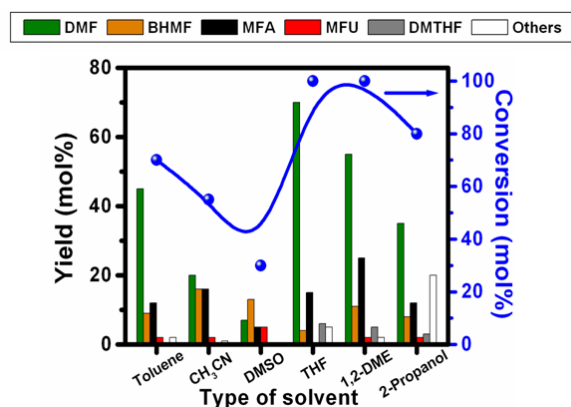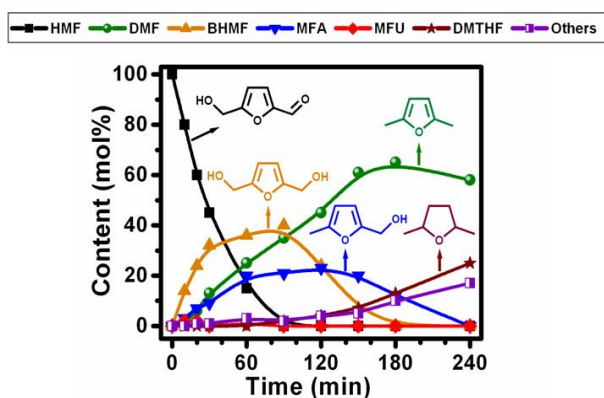

Fig. 3.27 Effect of reaction time on HMF conversion and product yields over 2wt% Ru-NaY. Reaction conditions: molar ratio of HMF to Ru (200); temperature (200 °C); solvent (THF, 25 mL); H_2 pressure (10 bar).

3.4.2.2.9. Recyclability study

The recyclability study of the 2wt% Ru-NaY catalyst was carried out by repeating the HMF hydrogenolysis reaction with the same used catalyst (Fig. 3.28). The catalyst recyclability studies were carried out as follows. After the first run, the content of the reactor was transferred to a centrifuge tube. The liquid phase was decanted, analyzed by GC-FID and the catalyst was washed three times with 20 mL of THF. After centrifugation, the liquid phase was discarded and the catalyst was dried at 100 °C for 6 h and was reused directly with fresh HMF for the hydrogenolysis reaction. This procedure was repeated for four more times. The results in Fig. 3.28 clearly show that the catalytic performance remains same even after being reused for five times. These results indicate good stability of the catalyst. Chemical analysis using ICP-OES also showed no leaching of Ru after each recycle. Moreover, the amount of Ru in the catalyst after five cycles was found to be same as that of starting catalyst.
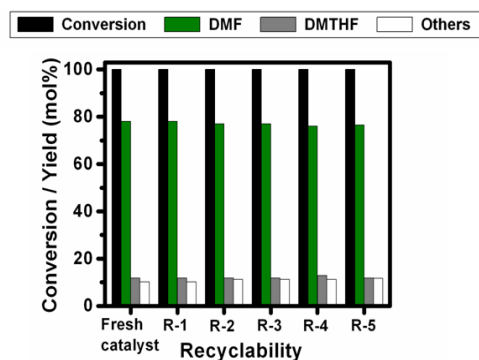
Fig. **3.28** Recyclability experiments with 2wt% Ru-NaY catalyst in the hydrogenolysis of HMF to DMF. Reaction conditions: molar ratio of HMF to Ru (200); solvent (THF, 25 mL); temperature (220 °C); H_2 pressure (15 bar); reaction time (1 h).

Table 3.7 Hydrogenation of furfural to furfuryl alcohol over 2wt% Ru-NaY catalyst.[a]

Entry	Temp (° C)	Time (h)	Furfural conv. (mol%)	FA yield (mol%)	THFA yield (mol%)	Others[e] (mol%)
1[b]	150	4	34.4	28.2	1.1	5.1
2	150	5	58.7	42.2	2.0	14.5
3	165	4	63.5	58.0	3.7	1.8
4	165	6	78.1	72.5	3.4	2.2
5	165	8	94.3	86.1	5.1	3.1
6	175	4	69.0	62.9	3.1	3.0
7	175	6	84.8	77.0	5.3	2.5
8	175	8	100	79.5	10.0	10.5
9[c]	175	6	100	46.7	24.1	29.2
10[d]	175	6	100	5.8	53.5	40.7
11	180	5	94.3	61.5	6.5	26.3

[a] Reaction conditions: furfural (4 mmol); catalyst (2wt% Ru-NaY, 30 mg); H_2 pressure (10 bar); solvent (THF, 25 mL). [b] 5 bar. [c] 15 bar. [d] 20 bar. [e] Includes MF, furan, THF and MTHF.

3.4.2.3. Catalytic activity in hydrogenation of furfural to furfuryl alcohol

The hydrogenation of furfural to furfuryl alcohol (FA) was studied over 2wt% Ru-NaY catalyst and the results are given in Table 3.7. The effect of reaction temperature on the furfural conversion and product yields was investigated by varying the temperature in the 150-180 °C range at 10 bar H_2 pressure. The reaction temperature of 165 °C was found to be optimum to achieve 94.3 mol% furfural conversion and 86.1 mol% FA yield (Table 3.7, entry 5). When the

reaction temperature was further increased to 180 °C, the yield of FA dropped (61.5 mol%) and side reactions become prominent leading to the formation of MF, MTHF, THF and furan (Table 3.7, entry 11). At higher H_2 pressure (15 and 20 bar), FA yield suppressed mostly due to the formation of tetrahydrofurfuryl alcohol (THFA) in significant amount (Table 3.7, entry 9 and 10).

3.4.3. Conclusions

Transition metal exchanged NaY catalysts, including Ru-NaY catalysts were synthesized through simple ion exchange method and used for the hydrogenolysis of HMF to DMF and hydrogenation of furfural to FA. Ruthenium based catalysts were found to be superior compared to other transition metal catalysts supported on NaY zeolite. Based on the results of investigations, a plausible reaction pathway for the conversion of HMF to DMF was proposed. The experimental results clearly show that DMF is formed through the hydrogenolysis of –OH groups in BHMF followed by MFA. Under optimized reaction conditions, DMF and FA can be selectively produced with 78 and 86.1 mol% yield, respectively, over 2wt% Ru-NaY catalyst. The catalyst can be reused for 5 times without loss in activity. This study shows that Ru-NaY catalyst, due to its high activity and excellent recyclability has tremendous potential for the conversion of biomass oxygenates to biofuels.

3.5. References

1. G. W. Huber, S. Iborra and A. Corma, *Chem. Rev.,* 2006, **106**, 4044.
2. A. Corma, S. Iborra and A. Velty, *Chem. Rev.,* 2007, **107**, 2411.
3. J. N. Chheda, G.W. Huber and J. A. Dumesic, *Angew. Chem. Int. Ed.,* 2007, **46**, 7164.
4. K. Shimizu and A. Satsuma, *Energy Environ. Sci.,* 2011, **4**, 3140.
5. E. L. Kunkes, D. A. Simonetti, R. M. West, J. C. Serrano-Ruiz, C. A. Gärtner and J. A. Dumesic, *Science,* 2008, **322**, 417.
6. A. J. Ragauskas, C. K. Williams, B. H. Davision, G. Britovsek, J. Cairney, C. A. Eckert, W. J. Frederick Jr., J. P. Hallett, D. J. Leak, C. L. Liotta, J. R. Mielenz, R. Murphy, R. Templer and T. Tschaplinski, *Science,* 2006, **311**, 484.
7. B. F. M. Kuster, *Starch,* 1990, **42**, 314.
8. Y. Román-Leshkov, C. J. Barrett, Z. Y. Liu and J. A. Dumesic, *Nature,* 2007, **447**, 982.
9. L. Deng, J. Li, D. M. Lai, Y. Fu and Q. X. Guo, *Angew. Chem. Int. Ed.,* 2009, **48**, 6529.

10. J. Q. Bond, D. M. Alonso, D. Wang, R. M. West and J. A. Dumesic, *Science*, 2010, **327**, 1110.

11. I. T. Horváth, J. Mehdi, V. Fábos, L. Boda and L. T. Mika, *Green Chem.*, 2008, **10**, 238.

12. J. P. Lange, W. D. van de Graaf and R. J. Haan, *ChemSusChem,* 2009, **2**, 437.

13. S. Song, R. Daniel, H. Xu, J. Zhang, D. Turner, M. L. Wyszynski and P. Richards, *Energy Fuels,* 2010, **24**, 2891.

14. (a) C. L. Williams, C. C. Chang, P. Do, N. Nikbin, S. Caratzoulas, D. G. Vlachos, R. F. Lobo, W. Fan and P. J. Dauenhauer, *ACS Catal.,* 2012, **2**, 935; (b) D. Wang, C. M. Osmundsen, E. Taarning and J. A. Dumesic, *ChemCatChem*, 2013, **5**, 2044; (c) C. C. Chang, S. K. Green, C. L. Williams, P. J. Dauenhauer and W. Fan, *Green Chem.,* 2013, **16**, 585.

15. (a) J. D. Garber, R. E. Jones and U. Torleif, US3083236A, 1963; (b) R. Alamillo, M. Tucker, M. Chia, Y. Pagán-Torres and J. Dumesic, *Green Chem.,* 2012, **14**, 1413; (c) Y. Nakagawa, M. Tamura and K. Tomishige, *ACS Catal.,* 2013, **3**, 2655.

16. J. B. Binder and R. T. Raines, *J. Am. Chem. Soc.,* 2009, **131**, 1979.

17. M. Chidambaram and A. T. Bell, *Green Chem.,* 2010, **12**, 1253.

18. J. Zhang, L. Lin and S. Liu, *Energy Fuels,* 2012, **26**, 4560.

19. Y. Zu, P. Yang, J. Wang, X. Liu, J. Ren, G. Lu and Y. Wang, *Appl. Catal. B,* 2014, **146**, 244.

20. J. M. R. Gallo, D. M. Alonso, M. A. Mellmer and J. A. Dumesic, *Green Chem.,* 2013, **15**, 85.

21. M. Chatterjee, T. Ishizaka and H. Kawanami, *Green Chem.,* 2014, **16**, 1543.

22. G.-H. Wang, J. Hilgert, F. H. Richter, F. Wang, H.-J. Bongard, B. Spliethoff, C. Weidenthaler and F. Schuth, *Nat. Mater.,* 2014, **13**, 293.

23. Y. B. Huang, M. Y. Chen, L. Yan, Q. X. Guo and Y. Fu, *ChemSusChem,* 2014, **7**, 1068;

24. S. Nishimura, N. Ikeda and K. Ebitani, *Catal. Today,* 2014, **232**, 89;

25. T. Thananatthanachon and T. B. Rauchfuss, *Angew. Chem. Int. Ed.,* 2010, **49**, 6616.

26. T. S. Hansen, K. Barta, P. T. Anastas, P. C. Ford and A. Riisager, *Green Chem.,* 2012, **14**, 2457.

27. J. Jae, W. Zheng, R. F. Lobo and D. G. Vlachos, *ChemSusChem,* 2013, **6**, 1158.

28. D. Scholz, C. Aellig and I. Hermans, *ChemSusChem,* 2014, **7**, 268.

29.   S. Morikawa, *Noguchi Kenkyusho Jiho*, 1980, **23**, 39.

30.   C. Aellig, F. Jenny, D. Scholz, P. Wolf, I. Giovinazzo, F. Kollhoff and I. Hermans, *Catal. Sci. Technol.,* 2014, **4**, 2326.

31.   P. Nilges and U. Schröder, *Energy Environ. Sci.,* 2013, **6**, 2925.

32.   D. J. Braden, C. A. Henao, J. Heltzel, C. C. Maravelias and J. A. Dumesic, *Green chem.*, 2011, **13**, 1755.

33.   F. Basile, L. Basini, G. Fornasari, M. Gazzano, F. Trifiro and A. Vaccari, *Chem Comm.*, 1996, 2435.

34.   Q. Wang, H. H. Tay, Z. Guo, L. Chen, Y. Liu, J. Chang , Z. Zhong, J. Luo and A. Borgna, *Appl. Clay Sci.,* 2012**, 55**, 18.

35.   (a) R. Lanza, S. G. Jaras and P. Canu, *Appl. Catal. A: Gen.*, 2007, **325**, 57; (b) M. G. Cattania, F. Parmigiani and V. Ragaini, *Surf. Sci.,* 1989, **211**, 1097; (c) S. -H. Lee and D. J. Moon, *Catal. Today,* 2011, **174**, 10.

36.   N. Chakroune, G. Viau, S. Ammar, L. Poul, D. Veautier, M. M. Chehimi, C. Mangeney, F. Villain and F. Fievet, *Langmuir*, 2005, **21**, 6788.

37.   N. M. Bertero, A. F. Trasarti, C. R. Apesteguía and A. J. Marchi, *Appl. Catal. A: Gen.*, 2011, **394**, 228.

38.   R. A. W. Johnstone, A. H. Wilby and I. D. Entwistle, *Chem. Rev.,* 1985, **85**, 129.

39.   (a) J. Hajek, N. Kumar, P. Maki-Arvela, T. Salmi and D. Y. Murzin, *J. Mol. Catal. A*, 2004, **217**, 145; (b) M. Zahmakiran, T. Kodaira and S. Ozkar, *Appl. Catal. B*, 2010, **96**, 533; (c) A. M. Abdel-Mageed, S. Eckle, H. G. Anfang and R. J. Behm, *J. Catal.* 2013, **298**, 148; (d) Y. Huang, V. Adeeva and W. M. H. Sachtler, *Appl. Catal. A*, 2000, **196**, 73.

40.   T. J. McCarthy, C. M. P. Marques, H. Trevino and W. M. H. Sachtler, *Catal. Lett.,* 1997, **43**, 11.

41.   L. Hu, X. Tang, J. X. Xu, Z. Wu, L. Lin and S. J. Liu, *Ind. Eng. Chem. Res.*, 2014, **53**, 3056.

42.   (a) N. Nikbin, S. Caratzoulas and D. G. Vlachos, *ChemSusChem*, 2013, **6**, 2066; (b) L. Bui, H. Luo, W. R. Gunther and Y. Roman-Leshkov, *Angew. Chem. Int. Ed.,* 2013, **52**, 8022; (c) J. Tuteja, H. Choudhary, S. Nishimura and K. Ebitani, *ChemSusChem,* 2014, **7**, 96.

43.   A. S. Nagpure, A. K. Venugopal, N. Lucas, M. Manikandan, T. Raja and S. Chilukuri,

Catal. Sci. Technol., 2015, **5**, 1463.

44. H. Takagi, T. Isoda, K. Kusakabe and S. Morooka, *Energy Fuels,* 1999, **13**, 1191.

45. M. Fang, N. Machalaba and R. A. Sanchez-Delgado, *Dalton Trans.,* 2011, **40**, 10621.

46. J. Hajek, N. Kumar, P. Maki-Arvela, T. Salmi, D. Y. Murzin, I. Paseka, T. Heikkila, E. Laine, P. Laukkanen and J. Vayrynen, *Appl. Catal. A,* 2003**, 251**, 385.

Chapter 4

Catalytic transfer hydrogenolysis of biomass derived furanic compounds over nitrogen-doped mesoporous carbon supported metal catalysts

4.1. Introduction

In view of the diminishing oil reserves and the clear visible signs of climate change attributed to greenhouse gas emissions to the atmosphere, utilization of renewable biomass sources for the production of fuels and chemicals has become imperative.[1] Worldwide, there is intense research activity in this area for the development of processes and catalysts for transforming abundant lignocellulosic biomass into liquid fuels for the transportation sector as well as to prepare platform chemicals. If these efforts have to translate into commercial reality; the developed process has to be economically feasible in terms of catalyst cost and ease of scalability. Hydrogenolysis reaction holds great promise for the proposed bio-refinery concept, as biomass-derived substrates possess very high oxygen content, which need to be reduced to get useful chemicals and fuels.[2] The selective hydrogenolysis of furfural and 5-hydroxymethylfurfural (HMF) to 2-methylfuran (MF) and 2,5-dimethylfuran (DMF), respectively, holds great promise for the production of liquid fuel substitutes/additives from renewable compounds (Scheme 4.1). Furfural and HMF can be obtained from the acid-catalyzed dehydration of hemicellulose and cellulose-derived carbohydrates, respectively.[3] Both DMF and MF have desirable chemical and physical properties to be used as transportation fuels; with nearly 40% more energy density (33.7 MJ/kg, 31.2 MJ/kg) than ethanol.[4] They also have high research octane number (RON = 119 and RON = 103), very little solubility in water (2.3 g/L, 7.0 g/L) and ideal boiling points (92-94 °C, 64.7 °C).[4] Furthermore, DMF consumes only one-third of the energy for separation by distillation, compared to that of required for the separation of ethanol from fermented broth.[5] The DMF and MF have been successfully tested as biofuels in a single cylinder spray guided direct-injection spark-ignition engine.[6] Their performance was satisfactory against gasoline in terms of ignition, emission and combustion properties. These excellent characteristics make DMF and MF as promising renewable fuels for transportation.

Hydrogenolysis of HMF and furfural into DMF and MF, respectively, were studied over various supported metal catalysts by using molecular H_2.[5,7,8] But, most of the reported processes were conducted under high H_2 pressure and elevated reaction temperatures. Such type of processes are energy intensive, thus difficult to commercialize. It is desirable to minimize the use of external H_2 required for biofuel production, especially if this H_2 has to be prepared from fossil fuels. In this work, we report an alternative process route for the hydrogenolysis of HMF to DMF and furfural to MF by catalytic transfer hydrogenation (CTH), in which hydrogen donor is used

as a hydrogen source, instead of molecular H_2. The CTH process for reducing the substrates has advantages compared to processes involving molecular H_2. Several investigators employed CTH process for the conversion of HMF to DMF and furfural to MF over different supported metal catalysts. Instead of molecular H_2, secondary alcohols, supercritical methanol, cyclohexane or 1,4-butanediol were used as a hydrogen source as well as reaction media.[4,9] Rauchfuss *et al.* reported DMF yield up to 95% using Pd/C as catalyst and formic acid as a hydrogen donor.[10] However, this process needs simultaneous use of formic acid and H_2SO_4 to get high yield of DMF. Use of acids is not environment friendly and also requires corrosion-resistant equipment for the process that will add cost to the process. Moreover, the reported CTH processes include the use of mineral acids as co-catalysts to improve the hydrogenation activity, which are difficult to separate from the reaction mixture and are responsible for undesirable side reactions.[10,11]
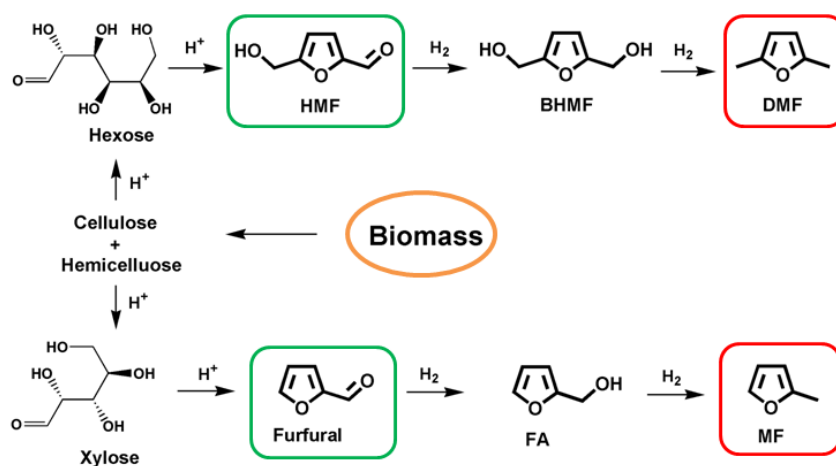
Scheme 4.1 Reductive upgradation pathways of biomass-derived compounds.

Compounds: FA (furfuryl alcohol); MF (2-methylfuran); HMF (5-hydroxymethylfurfural); BHMF (2,5-bis(hydroxymethyl)furan); DMF (2,5-dimethylfuran).

We have studied the CTH of HMF and furfural by using alcohols as hydrogen donor over nitrogen-doped mesoporous carbon (NMC) supported metal catalysts without using any co-catalyst. The catalysts were subjected to detailed characterization for better understanding of their catalytic activity. Various process parameters were optimized for CTH reaction with an aim to improve the DMF and MF yields.

4.2. Synthesis of DMF and MF over nitrogen-doped mesoporous carbon supported metal catalysts

4.2.1. Experimental procedures

4.2.1.1. Materials

All the chemicals were reagent grade and used without further purification. HMF (99%), DMF (99%), DMTHF (99%), MF (99%), MTHF (99%), $RuCl_3 \cdot 3H_2O$, THF (98%) and Ludox SM-30 colloidal silica (30 wt% SiO_2 in water) were procured from Sigma-Aldrich. MFU (99%), $PdCl_2 \cdot 2H_2O$, $H_2PtCl_6 \cdot 6H_2O$, $RhCl_3 \cdot 3H_2O$, $HAuCl_4 \cdot 3H_2O$, $CuCl_2 \cdot 2H_2O$, $NiCl_2 \cdot 6H_2O$, n-decane, melamine and $AgNO_3$ were purchased form Alfa Aesar. Methanol, ethanol, 1-propanol, 2-propanol, 1-butanol, 2-butanol, phenol, formaldehyde, NaOH and $NaBH_4$ were obtained from Loba chemie, Mumbai.

4.2.1.2. Evaluation of catalysts

All the reactions were carried out using 100 mL Parr autoclave (SS316). In a typical experiment, the reactor was charged with 1 mmol HMF (or 5 mmol furfural), hydrogen donor (25 mL), n-decane (0.2 g, internal standard) and required amount of freshly prepared catalyst. The reactor contents were mixed thoroughly and the reactor was sealed, purged 2-3 times with N_2 and pressurized to 20 bar N_2 pressure. Subsequently, the reaction vessel was heated under stirring at required temperature for a desired duration. Liquid samples were withdrawn periodically during the reaction and analyzed by GC (Agilent 7890A) equipped with a FID having CP Sil 8CB capillary column (30 m length, 0.25 mm diameter). Product identification was done using authentic standards and GC-MS (Varian, Saturn 2200) analysis.

4.2.2. Results and discussion

4.2.2.1. Catalyst characterization

4.2.2.1.1. X-ray diffraction (XRD)

The XRD patterns of nitrogen-free carbon (MC), nitrogen-doped carbon samples (NMC-1, NMC-2 and NMC-3) and as-synthesized 2wt% Ru deposited on various supports are shown in Fig. 4.1. These samples exhibited very similar diffraction features. Broader diffraction peaks are observed at around 25.2 (2θ) and 43.7° (2θ) that corresponds to the (002) and (100) planes of graphite, respectively.[12] The (002)-diffraction peak gradually broadens with the increasing nitrogen content of the sample (Fig. 4.1 and Table 4.1). The intensity of (100)-diffraction peak related to interlayer organization gradually deceases with increasing nitrogen content and even disappears when nitrogen content reaches 11.6 wt% (NMC-3). However, the positions of two peaks (25.2 and 43.7°) did not change with the nitrogen content. The formation of highly

dispersed Ru nanoparticles was proven by XRD (Fig. 4.1), as no diffraction peaks pertaining to metallic Ru were detected. Moreover, no change in diffraction peaks of the supports on Ru loading was observed, indicating that the Ru loading has no effect on the structure of the supports.
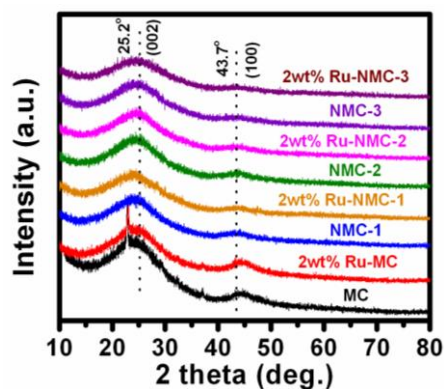
Fig. 4.1 XRD of various carbon samples and supported Ru catalysts.

4.2.2.1.2. N₂-Physisorption

The catalyst support materials and Ru containing samples show similar type IV adsorption-desorption isotherms with an H2 hysteresis loop, corresponding to the typical mesoporous structure of the materials (Fig. 4.2a). These results suggest that variation in nitrogen content does not strongly affect the mesoporous structure of the samples. Their BJH pore size distributions are similar in the range of 10-20 nm (Fig. 4.2b). The physico-chemical properties of various samples are summarized in Table 4.1 and 4.2. The micropores created by the release of volatile fragments during the pyrolysis under N_2 gas flow are dependent on the melamine to phenol ratio. Increasing nitrogen incorporation in carbon framework inhibits the formation of micropores during pyrolysis, resulting in decreased micropore volume (Table 4.1).
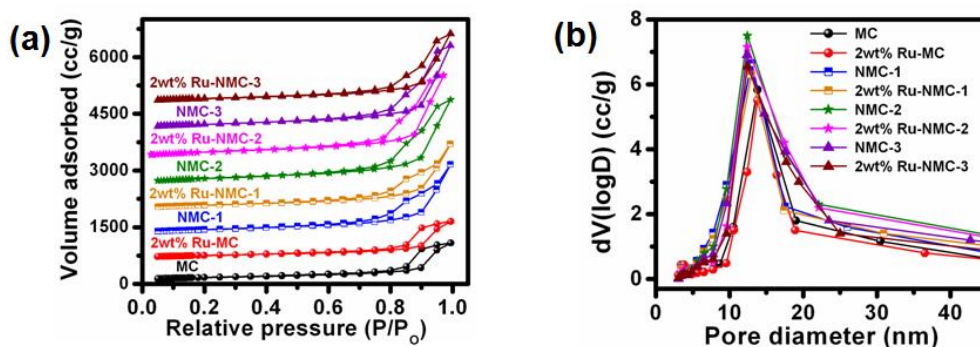
Fig. 4.2 (a) N₂ adsorption-desorption isotherms and (b) BJH pore size distribution of various samples.

Table 4.1 Pore parameters and chemical nature of the NMC's.

Sample	BET surface area (m²/g)	Total pore volume[a] (cc/g)	Micropore volume[b] (cc/g)	Elemental analysis (wt%)				Basicity[c] (mmol/g)
				C	N	H	O (cal.)	
MC	750	0.74	0.15	86.3	0	1.3	12.4	--
NMC-1	836	1.08	0.12	80.4	5.1	1.0	13.5	0.16
NMC-2	878	1.13	0.09	77.1	8.2	0.8	13.9	0.27
NMC-3	844	1.09	0.07	73.0	11.6	0.7	14.7	0.41

[a] Total pore volume at $P/P_0 = 0.9$. [b] Calculated by t-plot method. [c] Measured by CO_2-TPD.

Table 4.2 Physico-chemical properties of supported Ru catalysts.

Catalyst	Ru content[a] (wt%)	BET surface area (m²/g)	Total pore volume[b] (cc/g)
2wt% Ru-MC	1.92	722	0.71
2wt% Ru-NMC-1	1.89	792	1.04
2wt% Ru-NMC-2	1.91	849	1.10
2wt% Ru-NMC-3	1.95	805	1.05
2wt% Ru-AC	1.81	991	0.55
2wt% Ru-CeO₂	1.76	105	0.17
2wt% Ru-MgO	1.82	91	0.13
2wt% Ru-Mg(Al)O	1.79	130	0.22
2wt% Ru-TiO₂	1.86	36	0.07
2wt% Ru-γ-Al₂O₃	1.82	240	0.57

[a] Estimated by ICP-OES. [b] Total pore volume at $P/P_0 = 0.9$.

4.2.2.1.3. Raman spectroscopy

The formation of graphitic ordered carbon was proved by Raman spectroscopy (Fig. 4.3). Raman spectra show characteristic D- and G-bands of disordered graphitic carbon at 1335 and 1590 cm⁻¹, respectively. The D-band is a defects-induced Raman feature reflecting the non-perfect crystalline structure of the carbon, while G-band indicates the in-plane vibration of sp² carbon atoms.[13,14] There is no dependence of the position of the two bands on the nitrogen content. The D-band appears to be stronger than G-band, suggesting amorphization of the graphitic carbon. The intensity ratios of the D-band to the G-band (I_D/I_G, calculated from integral area of the peaks) are 1.6, 1.8, 2.1 and 2.3 for MC, NMC-1, NMC-2 and NMC-3, respectively.

These results show that the defects in graphite-like layers enhanced with increasing nitrogen content.[12]
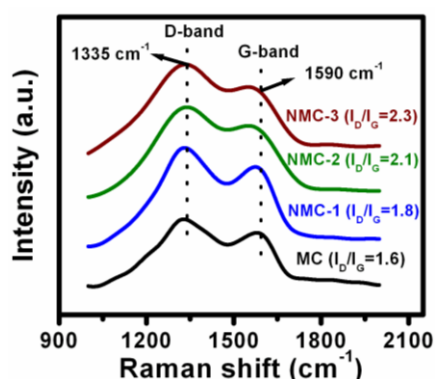
Fig. 4.3 Raman spectra of MC, NMC-1, NMC-2 and NMC-3.

4.2.2.1.4. Transmission electron microscopy (TEM)

The mesoporous structure of the MC and nitrogen–doped carbon samples can be further confirmed by TEM investigations (Fig. 4.4). In terms of TEM images, nitrogen containing samples (Fig. 4.4b,4.4c and 4.4d) have no differences when compared with their nitrogen-free counterpart (Fig. 4.4a), consisting of spherical mesopores with a disordered amorphous carbon structure. The Ru nanoparticle sizes as well as their distribution for various Ru containing catalysts were studied by TEM (Fig. 4.5). It was found that Ru nanoparticles were dispersed unevenly and large agglomerated Ru nanoparticles were detected on the surface of MC with an average particle size of 6.1 nm (Fig. 4.5a and 4.5b). On the other hand Ru nanoparticles were dispersed homogeneously over nitrogen-doped carbons with an average particle size of 3.1, 2.5 and 1.9 nm for 2wt% Ru-NMC-1, 2wt% Ru-NMC-2 and 2wt% Ru-NMC-3 catalyst, respectively (Fig. 4.5c,4.5d,4.5e,4.5f,4.5g and 4.5h). Thus, it can be concluded that the dominant contributor for stabilizing Ru nanoparticles is the nitrogen in the carbon structure and increasing nitrogen content in the sample led to decrease in the size of Ru nanoparticles.[15]
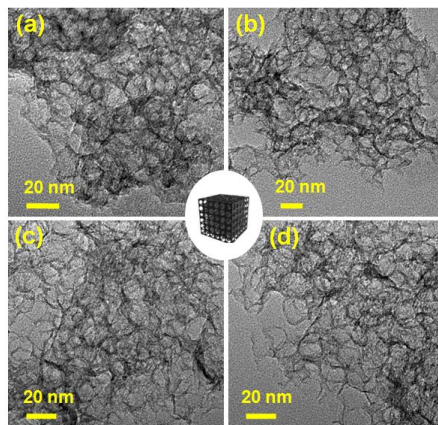
Fig. 4.4 TEM image of the (a) MC, (b) NMC-1, (c) NMC-2 and (d) NMC-3.
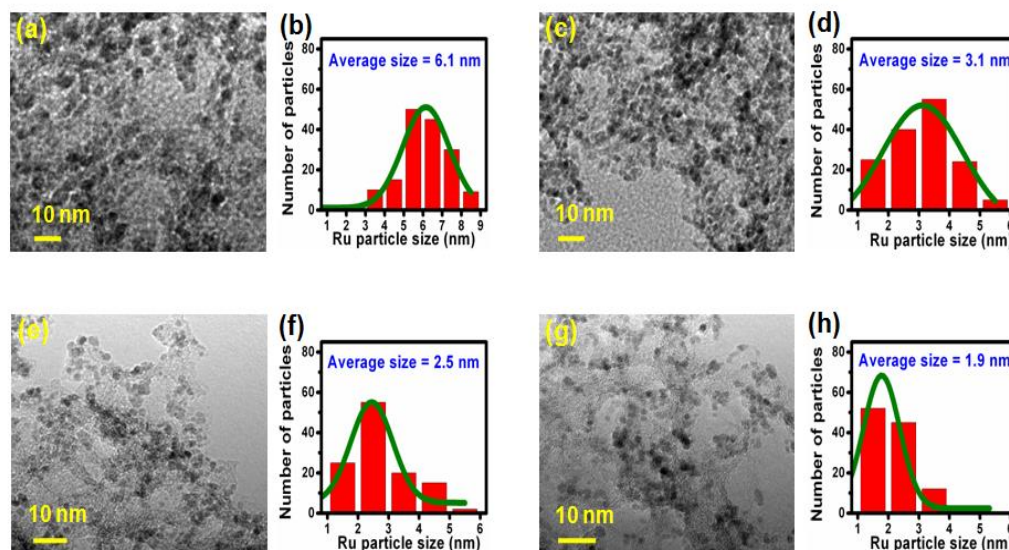
Fig. 4.5 TEM image and the Ru nanoparticle size distribution of 2wt% Ru-MC (4.5a and 4.5b), 2wt% Ru-NMC-1 (4.5c and 4.5d), 2wt% Ru-NMC-2 (4.5e and 4.5f) and 2wt% Ru-NMC-3 (4.5g and 4.5h), respectively.

4.2.2.1.5. Ru dispersion and metal surface area

The average Ru particle size of supported Ru catalysts (calculated based on TEM analysis) were used to determine Ru dispersion (%), assuming spherical shape of Ru particles and using the formula described by Scholten *et al*. [16] The Ru dispersion values were: 2wt% Ru-MC, 21.6%; 2wt% Ru-NMC-1, 42.5%; 2wt% Ru-NMC-2, 52.7% and 2wt% Ru-NMC-3, 69.3% (Table 4.3). The higher value of metal dispersion (69.3%) over NMC-3 support confirms the homogeneous distribution of Ru nanoparticles. These results clearly suggested that the Ru metal dispersion enhanced with increasing nitrogen content of the catalyst.[15] Ru metal surface area of catalysts was measured by assuming that the Ru nanoparticles are hemispherical in shape with

the flat side on the support (Table 4.3). These values for 2wt% Ru-MC, 2wt% Ru-NMC-1, 2wt% Ru-NMC-2 and 2wt% Ru-NMC-3 catalysts was calculated as 1.75, 3.16, 3.82 and 5.1 m^2/g, respectively.

Table 4.3 Ru dispersion and metal surface area of supported Ru catalysts.			
Catalyst	Average Ru particle size[a] (nm)	Ru metal dispersion[b] (%)	Ru metal surface area[c] (m^2/g)
2wt% Ru-MC	6.1	21.6	1.75
2wt% Ru-NMC-1	3.1	42.5	3.16
2wt% Ru-NMC-2	2.5	52.7	3.82
2wt% Ru-NMC-3	1.9	69.3	5.10
[a] Calculated from TEM analysis. [b] Estimated on the basis of average Ru particle size using TEM analysis by employing equation described by Scholten *et al*. in reference 16. [c] Calculated by assuming Ru metal particles in hemispherical shape with the flat side on the support.			

4.2.2.1.6. X-ray photoelectron spectroscopy (XPS)

The XPS was employed to investigate the nature of nitrogen species formed on the surface of carbon samples. Only peaks belonging to oxygen, carbon and nitrogen could be scanned (Fig. 4.6a). XPS of carbon 1s shows very similar peak at 284.6 eV, which is associated with the graphitic carbon,[12] suggesting that most of the carbon atoms are assembled in conjugated honeycomb lattices. The nitrogen 1s spectra (Fig. 4.6b) are curve-fitted into three peaks with the binding energies at 398.2, 400.4 and 401.8 eV that correspond to pyridinic N (N1), pyrrolic N (N2) and graphitic N (N3), respectively.[12] The peaks related to nitrogen bonded to oxygen (404-408 eV) were absent. It is important to note that the distribution of these nitrogen species is highly similar at similar pyrolysis temperature (800 °C), being independent of nitrogen content in the sample (Fig. 4.6c). As shown in Fig. 4.6c, regardless of nitrogen content, a majority of nitrogen atoms are localized at the edges of graphene sheets (N1 and N2) whereas small amount of nitrogen atoms are situated at the central region of graphene sheet (N3).
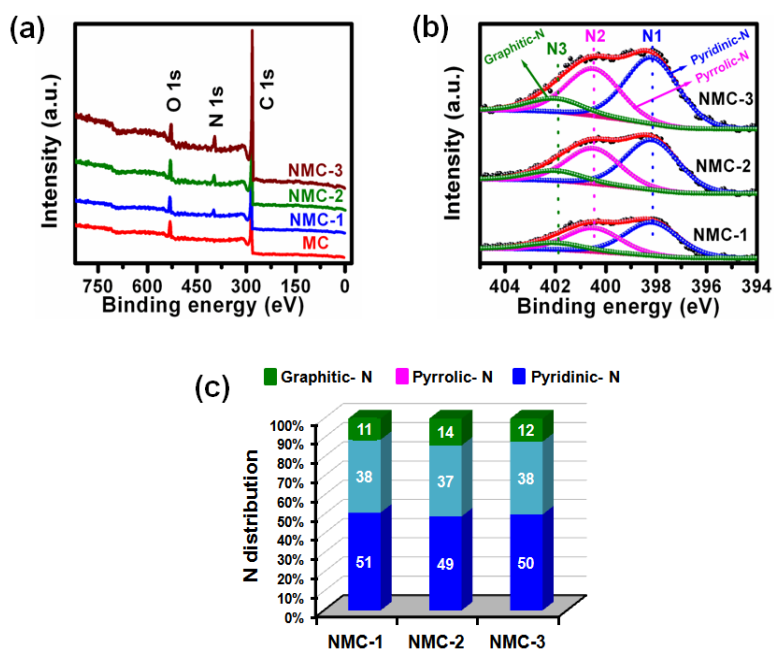
Fig. 4.6 (a) XPS survey and (b) high-resolution N 1s spectra of the NMC's. (c) The distribution of N species in the NMC's from resolving peaks of the N 1s spectra.

4.2.2.1.7. Temperature programmed reduction (TPR)

To study the reducibility of MC and NMC supported Ru catalysts, TPR in H_2 flow was carried out (Fig. 4.7). One H_2 consumption peak in the 70-100 °C temperature range was observed for all the catalysts, which may be attributed to the reduction of RuO_x species.[9a] Importantly, this peak was shifted to lower temperature with the increasing nitrogen content of the catalyst. This could be due to the fact that higher nitrogen containing carbon sample have more basicity (Table 4.1), which can help to reduced Ru at lower temperature (TPR peak at 74 °C for 2wt% Ru-NMC-3) compared to that of nitrogen-free carbon sample (TPR peak at 100 °C for 2wt% Ru-MC).
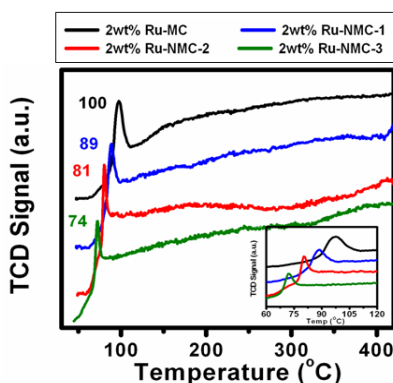
Fig. 4.7 TPR profiles of supported Ru catalysts.

4.2.2.2. Catalytic activity in CTH of HMF to DMF

4.2.2.2.1. Effect of reaction temperature

The effect of reaction temperature on CTH of HMF was investigated using 2-propanol as a hydrogen donor over 2wt% Ru-NMC-3 catalyst (Fig. 4.8). The CTH reaction occurs at a lower temperature (80 °C) and the DMF yield improved with increasing reaction temperature. At lower temperature, the primary product was 2,5-bis(hydroxymethyl)furan (BHMF) and upon increasing the temperature to 160 °C, BHMF is completely converted to DMF with a yield up to 84 mol% at 100 mol% HMF conversion (Scheme 4.2). Other products observed at 120 and 140 °C are hydrogenated furans: 5-methyl furfural (MFU), 5-methyl furfuryl alcohol (MFA), 2-methylfuran (MF) and furfuryl alcohol (FA). The formation of FA indicates the occurrence of decarbonylation reaction, however, the yield of FA was low (5 mol%). The formation of MFU suggested that hydrogenolysis of –OH group in HMF occur in parallel to the hydrogenation of the –CHO group. In addition, ethers are also observed at lower temperature (80 and 120 °C), which are formed via etherification of BHMF or MFA and 2-propanol. They are not observed upon increasing the reaction temperature (160 and 170 °C).
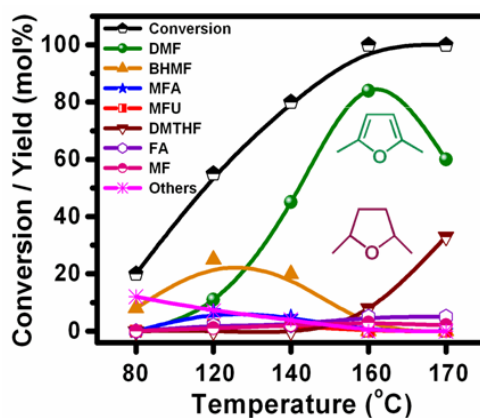
Fig. 4.8 Effect of reaction temperature on HMF conversion and product yields over 2wt% Ru-NMC-3. Reaction conditions: molar ratio of HMF to Ru (200); N_2 pressure (20 bar); solvent and hydrogen donor (2-propanol, 25 mL); reaction time (8 h). Other products include ethers.
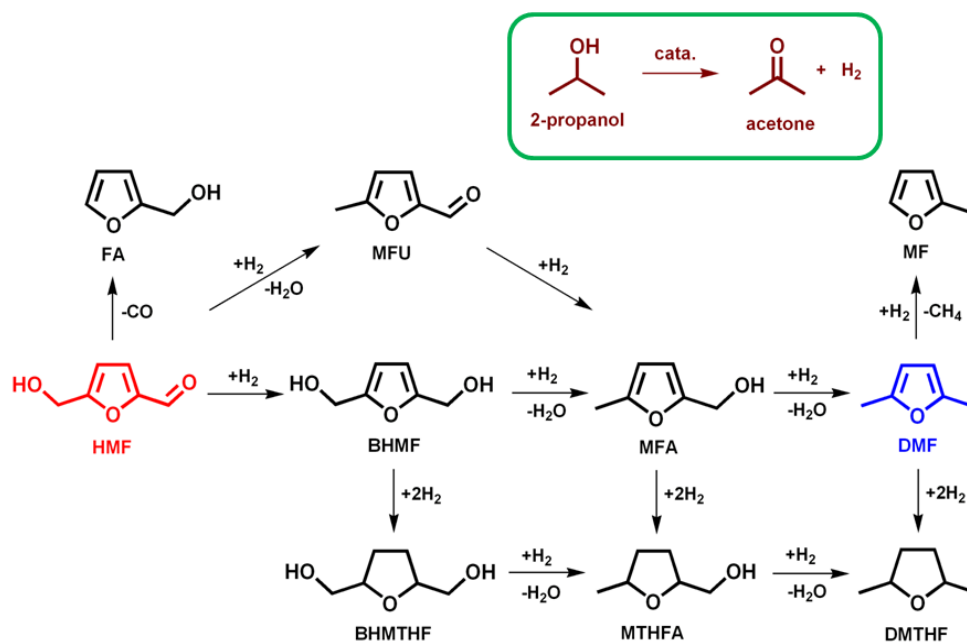
Scheme 4.2 Reaction network of the hydrogenolysis of HMF to DMF using 2-propanol on Ru-NMC.

Compounds: 5-Hydroxymethylfurfural (HMF); 2,5-bis(hydroxymethyl)furan (BHMF); 5-methyl furfural (MFU); 5-methyl furfuryl alcohol (MFA); furfuryl alcohol (FA); 2,5-bis(hydroxymethyl)tetrahydrofuran (BHMTHF); 5-methyl tetrahydrofurfuryl alcohol (MTHFA); 2,5-dimethylfuran (DMF); 2,5-dimethyltetrahydrofuran (DMTHF); 2-methylfuran (MF).

4.2.2.2.2. *Effect of hydrogen donor*

The effect of hydrogen donor on CTH reaction of HMF was studied over 2wt% Ru-NMC-3 catalyst at 160 °C (Fig. 4.9). The results clearly indicate that the CTH activity of catalyst greatly depends on the type of hydrogen donor used. The HMF conversion increased from 40 to 100 mol% with following reactivity order: methanol < 1-butanol < ethanol < 1-propanol < 2-butanol < 2-propanol. Among the hydrogen donors tested, 2-propanol showed superior activity giving 84 mol% DMF yield at 100 mol% HMF conversion. The formation of ethers was negligible in 2-propanol and 2-butanol but significant in other alcohols (2-14 mol%). This shows that etherification reaction favoured with lower chain alcohols (methanol, ethanol and 1-propanol) indicative of steric effect. These outcomes are in good agreement with the reported results, which shows that for CTH, aliphatic secondary alcohols gives relatively better activity than aliphatic primary alcohols.[4,9f] The higher tendency to release hydrogen from secondary alcohols has been attributed to the highest reduction potential of the corresponding dialkyl ketones (Scheme 4.3).[17]
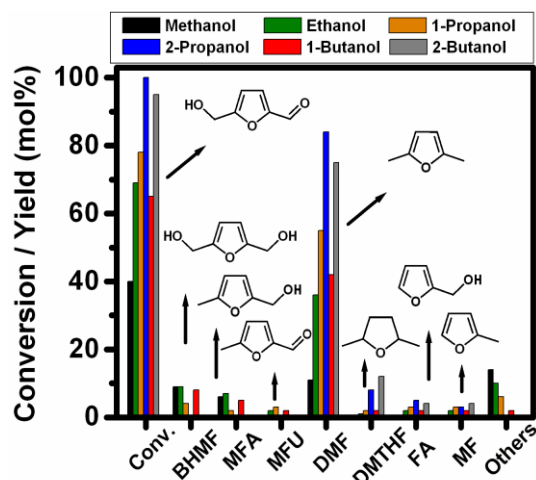
Fig. 4.9 Effect of hydrogen donor on HMF conversion and product yields over 2wt% Ru-NMC-3. <u>Reaction conditions:</u> Molar ratio of HMF to Ru (200); N$_2$ pressure (20 bar); solvent and hydrogen donor (25 mL); reaction time (8 h). Other products include ethers.
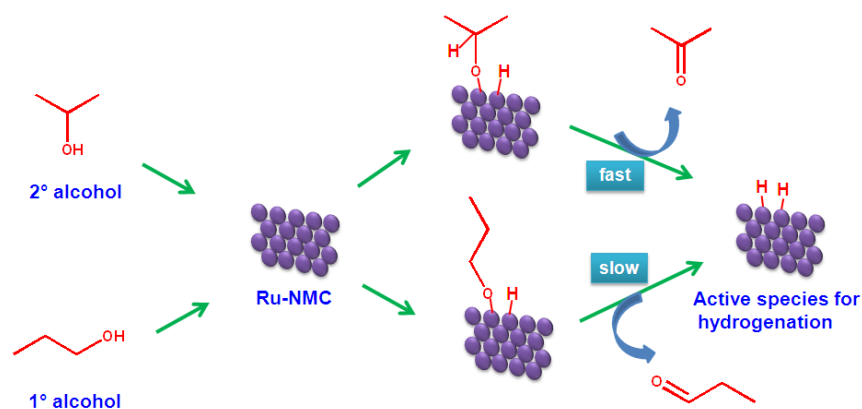
Scheme 4.3 Formation of active species for hydrogenation from 1° and 2° alcohol over Ru-NMC.

4.2.2.2.3. CTH of HMF over different supported metal catalysts

The activity and selectivity of various supported metal catalysts were investigated for the CTH reaction of HMF to get DMF using 2-propanol as the hydrogen source and solvent (Table 4.4). The reaction did not occur in the absence of the catalyst (entry 1, Table 4.4). When NMC-3 was used as the catalyst, poor catalytic activity was observed, leading to 1 mol% DMF yield at 15 mol% HMF conversion (entry 2, Table 4.4). The HMF conversions were 41, 61, 79 and 100 mol% with DMF yield at 11, 30, 55 and 84 mol% on 2wt% Ru-MC, 2wt% Ru-NMC-1, 2wt% Ru-NMC-2 and 2wt% Ru-NMC-3 catalysts, respectively (entries 3-6, Table 4.4). Therefore, it can be seen that the CTH activity is enhanced as the nitrogen content of the catalyst increased from 0 to 11.6 wt% (Table 4.1). The excellent performance of NMC-3 supported Ru catalyst

(2wt% Ru-NMC-3) in CTH reaction of HMF is probably due to the presence of more nitrogen content (11.6 wt%) and higher basicity (0.41 mmol/g, Table 4.1), which has been proved by the fact that increasing basicity increases the CTH activity (compare entries 3-6 in Table 4.4 and see Table 4.1 for basicity). It has been reported that the basicity of the catalyst plays an important role in CTH reaction and with increasing basicity, the catalytic activity in CTH can significantly improve.[18] Moreover, the superior activity of 2wt% Ru-NMC-3 catalyst was attributed to the uniqueness of the support-Ru interaction, i.e., N-doped mesoporous carbon-Ru heterojunction. The high nitrogen content in NMC-3 support (11.6 wt%) not only led to very stable and homogeneous dispersion of Ru but also can activate Ru nanoparticles,[19] which accelerates the CTH reaction, as compared to nitrogen-free catalyst (2wt% Ru-MC). Catalyst 2wt% Ru-NMC-3 is composed of small Ru nanoparticles (1.9 nm) that are surrounded by basic centers (nitrogen) provided by the support, which may favor ionic hydrogenation pathways during CTH process (Scheme 4.4). Sanchez-Delgado *et al.* reported heterolytic splitting of H_2 into H^+ and H^- (ionic hydrogenation pathway) over Ru nanoparticles, assisted by the basic pyridinic groups of the support (poly(4-vinylpyridine)).[20]

During the CTH process, H_2 was produced and the H_2 partial pressure in the closed reactor reached to 2 and 7 bar when the CTH reaction was carried out over 2wt% Ru-MC and 2wt% Ru-NMC-3, respectively. These results clearly show that the nitrogen plays a key role in the dehydrogenation of 2-propanol and with increasing nitrogen content of the support higher H_2 pressure was developed. It is possible that hydrogen species formed on dehydrogenation of 2-propanol during CTH process can directly hydrogenate HMF adsorbed on Ru nanoparticles instead of being released as H_2. To understand this prospect, HMF hydrogenation was performed at H_2 pressure of 7 bar (H_2 partial pressure developed during CTH reaction at 160 °C over 2wt% Ru-NMC-3 with 2-propanol) using tetrahydrofuran (THF) as solvent (entry 7, Table 4.4). The HMF conversion and DMF yield were 86 and 59 mol%, respectively, which were inferior to those using 2-propanol as hydrogen donor (compare entry 6 and 7 in Table 4.4). This result strongly suggests that HMF hydrogenation using hydrogen donors can be more efficient than that using external H_2.[9a] It is well known that there are differences between heterogeneous catalytic hydrogenation using hydrogen donor molecules as the source of hydrogen and hydrogenation using molecular H_2.[21] The CTH reaction could occur through direct hydride transfer from 2-propanol to HMF.
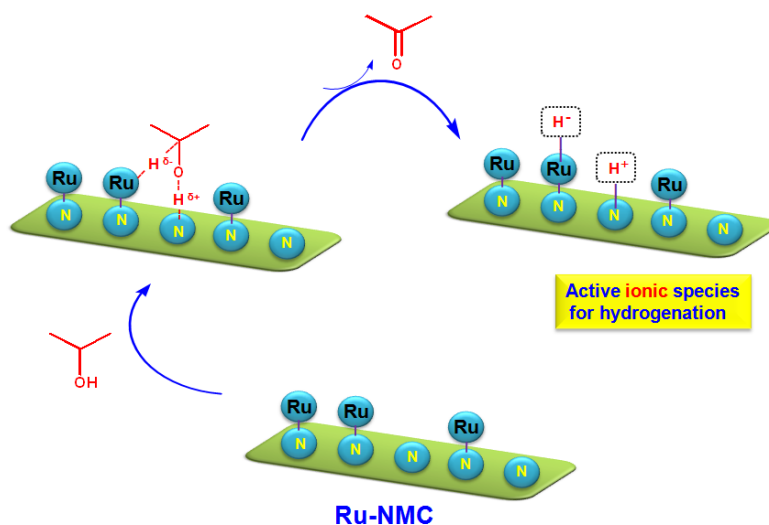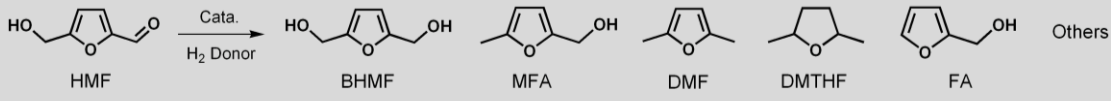
Scheme 4.4 Possible mechanism for the formation of active ionic species for hydrogenation from alcohol over NMC supported Ru catalyst.

The CTH of HMF was also studied using Pt, Pd, Rh, Au, Ni and Cu catalysts supported on NMC-3 (entries 8-13, Table 4.4). With Pt-NMC-3, Pd-NMC-3, Rh-NMC-3, Au-NMC-3, Ni-NMC-3 and Cu-NMC-3 catalysts, the DMF yields were 31, 15, 11, 2, 3 and 2 mol% at 75, 100, 66, 40, 25 and 21 mol% HMF conversion, respectively. Interestingly, when the CTH reaction was conducted with Pd catalyst, significant amount of decarbonylation product, FA was obtained (entry 9, Table 4.4). This shows that Pd is more suitable for HMF decarbonylation.[22] The CTH reaction using NMC-3 supported Ru catalyst achieved relatively better performance than the other supported metal catalysts (entry 6, Table 4.4). These findings are in good accordance with the previous work, which generally reports that the Ru based catalysts are highly efficient for the CTH process.[23]

Activated carbon (AC) and metal oxide (CeO$_2$, MgO, Mg(Al)O, TiO$_2$ and γ-Al$_2$O$_3$) supported Ru catalysts were also tested for CTH reaction (entries 14-19, Table 4.4). These results show that the metal oxide and AC supported Ru catalysts were not effective for CTH reaction of HMF, affording DMF in lower yields than the NMC-3 supported Ru catalyst. In case of Ru-TiO$_2$ and Ru-γ-Al$_2$O$_3$ catalysts the main product was BHMF, suggesting these catalysts have good ability towards carbonyl group hydrogenation, but have less ability for C-O bond hydrogenolysis (entries 18-19, Table 4.4). From these results, one could conclude that the nature of the catalyst support plays significant role in the activity and selectivity of Ru based catalysts in CTH reaction.

Table 4.4 Product distributions for CTH of HMF over different supported metal catalysts.[a]

Entry	Catalyst	HMF conv. (mol%)	Product Yields (mol%)						TOF[e] (h⁻¹)
			BHMF	MFA	DMF	DMTHF	FA	Others[d]	
1	No catalyst	8	0	0	0	0	0	8	--
2[b]	NMC-3	15	3	4	1	0	0	7	--
3	2wt% Ru-MC	41	7	6	11	0	4	13	2.7
4	2wt% Ru-NMC-1	61	7	22	30	0	1	1	7.5
5	2wt% Ru-NMC-2	79	5	14	55	2	2	1	13.7
6	2wt% Ru-NMC-3	100	0	0	84	8	5	3	21.0
7[c]	2wt% Ru-NMC-3	86	1	3	59	13	2	8	14.7
8	2wt% Pt-NMC-3	75	5	8	31	2	1	28	7.7
9	2wt% Pd-NMC-3	100	0	5	15	0	62	18	3.7
10	2wt% Rh-NMC-3	66	25	15	11	4	1	10	2.7
11	2wt% Au-NMC-3	40	25	3	2	0	2	8	0.5
12	5wt% Ni-NMC-3	25	6	1	3	0	1	14	0.7
13	5wt% Cu-NMC-3	21	3	3	2	0	2	11	0.5
14	2wt% Ru-AC	56	7	7	15	0	6	21	3.7
15	2wt% Ru-CeO₂	39	10	9	6	0	0	14	1.5
16	2wt% Ru-MgO	37	10	4	6	0	2	15	1.5
17	2wt% Ru-Mg(Al)O	48	15	6	5	1	3	18	1.2
18	2wt% Ru-TiO₂	45	26	1	0	0	0	18	0
19	2wt% Ru-γ-Al₂O₃	60	35	2	0	0	0	23	0

[a] <u>Reaction conditions:</u> molar ratio of HMF to metal (200); temperature (160 °C); N$_2$ pressure (20 bar); solvent and hydrogen donor (2-propanol, 25 mL); reaction time (8 h). [b] NMC-3 (25 mg). [c] 7 bar H$_2$ pressure was used instead of 2-propanol and THF (25 mL) as solvent. [d] It includes 2-methylfuran (MF), 2,5 bis(hydroxymethyl)tetrahydrofuran (BHMTHF), 5-methyl tetrahydrofurfuryl alcohol (MTHFA), ethers and some unidentified compounds. [e] TOF = turnover frequency (moles of DMF produced per mole of metal per hour).

4.2.2.2.4. Catalytic activity for the conversion of HMF to DMF using molecular H$_2$

The effect of H$_2$ pressure on the DMF yield was studied by varying the pressure from 2-15 bar at 160 °C in THF solvent over 2wt% Ru-NMC-3 catalyst (Fig. 4.10). When the reaction was carried out at low pressure (2 and 5 bar), the intermediate products such as BHMF and MFA formed in significant amounts, which are converted to DMF with the increasing reaction time. On further increasing H$_2$ pressure (7 bar); the DMF yield reached maximum (68 mol%), but the yield decreased on continuation of the reaction for further duration. This decrease in DMF yield

is due to ring hydrogenation, leading to the formation of 2,5-dimethyltetrahydrofuran (DMTHF). When H_2 pressure is raised further to 10 and 15 bar, it has an adverse effect on the DMF yield. At higher H_2 pressure, DMF yield decreased mostly due to the increased rate of consecutive ring hydrogenation of DMF, which led to the formation of DMTHF in considerable quantities. Furthermore, the amounts of by-products such as 5-methyl tetrahydrofurfuryl alcohol (MTHFA), 2,5-bis(hydroxymethyl)tetrahydrofuran (BHMTHF) and hexanediol also increased at higher H_2 pressure.
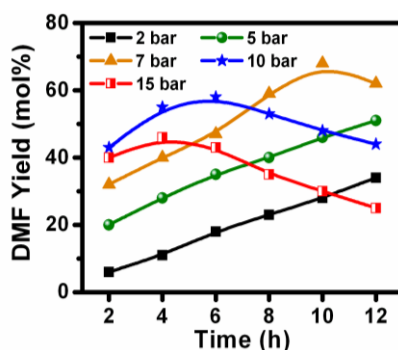
Fig. 4.10 Effect of H_2 pressure on DMF yield over 2wt% Ru-NMC-3 as a function of reaction time. <u>Reaction conditions:</u> molar ratio of HMF to Ru (200); temperature (160 °C); solvent (THF, 25 mL).

4.2.2.2.5. Recyclability study

The recyclability study of the 2wt% Ru-NMC-3 catalyst in CTH reaction of HMF to produce DMF was evaluated by repeating the reaction with the same catalyst (Fig. 4.11). The catalyst reusability studies were carried out as follows. After the first run, the content of the reactor was transferred to a centrifuge tube. The liquid phase was decanted, analyzed by GC-FID and the catalyst was washed two times with 20 mL of 2-propanol. After centrifugation, the liquid phase was discarded and the catalyst was dried at 100 °C for 4 h and was reused for the CTH reaction of HMF. The above procedure was repeated for three more times. The results in Fig. 4.11 show that the catalytic performance remains nearly same even after being reused for four times. In order to gain more insight into the catalytic activity, XRD and TEM analysis of used catalysts were carried out. XRD results show that the catalyst did not undergo any structural changes during the recyclability experiments (Fig. 4.12). The TEM image of the 2wt% Ru-NMC-3 catalyst after 4 recycles exhibited an average Ru nanoparticles size of 2 nm (Fig. 4.13), which is similar to that of the fresh catalyst (Fig. 4.5g and 4.5h). These results indicate an excellent stability of the catalyst. Chemical analysis using ICP-OES showed no leaching of Ru

after each recycle. Moreover, the amount of Ru in the catalyst after four cycles was found to be similar to that of starting catalyst.
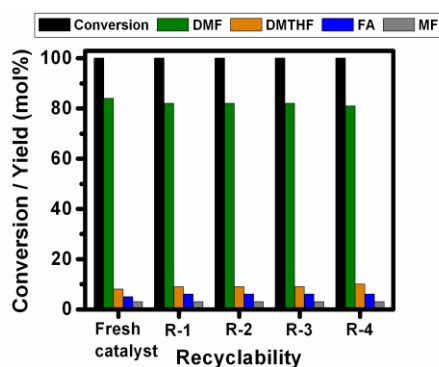
Fig. 4.11 Recyclability study in CTH of HMF over 2wt% Ru-NMC-3 catalyst.

Reaction conditions: molar ratio of HMF to Ru (200); temperature (160 °C); N_2 pressure (20 bar); solvent and hydrogen donor (2-propanol, 25 mL); reaction time (8 h).
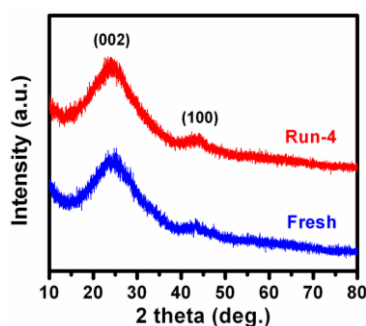
Fig. 4.12 XRD patterns of the fresh and used 2wt% Ru-NMC-3 catalyst.
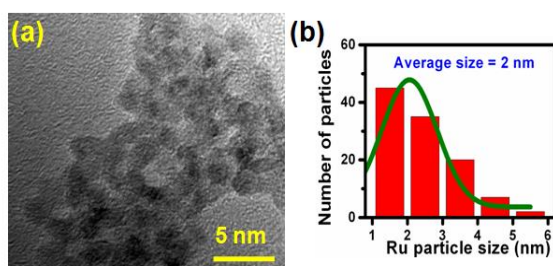
Fig. 4.13 (a) TEM image and (b) the Ru nanoparticles size distribution for reused (after 4 recycles) 2wt% Ru-NMC-3 catalyst.

4.2.2.3. Catalytic activity in CTH of furfural to MF

4.2.2.3.1. Effect of reaction temperature

The effect of reaction temperature on the furfural conversion and product yields was investigated using 2-propanol as a hydrogen donor over 2wt% Ru-NMC-3 catalyst by varying

the temperature in the range of 50-150 °C (Fig. 4.14). The primary product of the transfer hydrogenation of furfural was FA, which is prominent at lower temperatures (80, 100 and 125 °C). In a consecutive step, hydrogenolysis of the –OH group in FA yields MF up to 87 mol% at 140 °C. In parallel to hydrogenation, furfural also undergoes decarbonylation reaction to furan. Furthermore, furan-ring hydrogenated products like 2-methyl tetrahydrofuran (MTHF) and tetrahydrofurfuryl alcohol (THFA) were also observed.
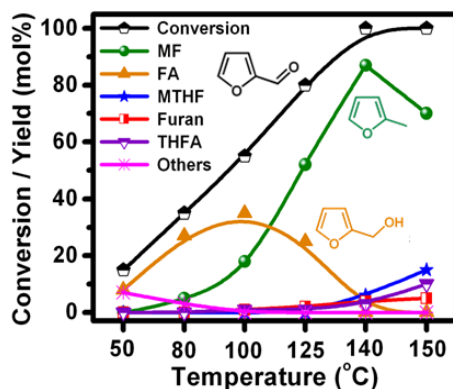
Fig. 4.14 Effect of reaction temperature on furfural conversion and product yields.
Reaction conditions: Furfural (5 mmol); catalyst (2wt% Ru-NMC-3, 25 mg); N_2 pressure (20 bar); solvent and hydrogen donor (2-propanol, 25 mL); reaction time (10 h). Others include ethers.

4.2.2.3.2. Effect of hydrogen donor

The effect of hydrogen donor on CTH reaction of furfural was examined over 2wt% Ru-NMC-3 catalyst at 140 °C (Fig. 4.15). The results clearly suggest that the catalyst activity greatly depends on the nature of hydrogen donor used. The furfural conversion increases from 44 to 100 mol% and follow the reactivity order: methanol < 1-butanol < ethanol < 1-propanol < 2-butanol < 2-propanol. Among the hydrogen donors tested, 2-propanol displayed the highest activity leading to 87 mol% MF yield. These results are in good agreement with the reported results, which suggest that during CTH secondary alcohols have a better tendency to release hydrogen than primary alcohols.[4,9f]
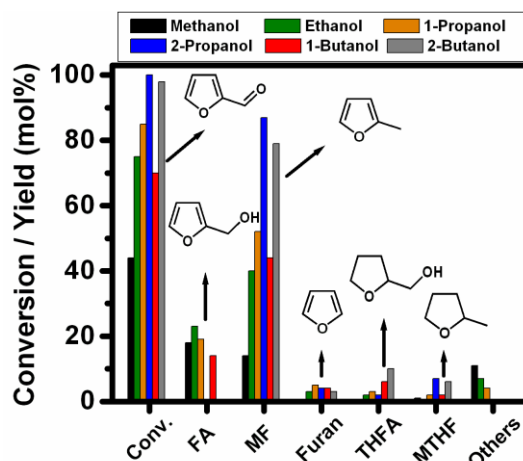
Fig. 4.15 Effect of hydrogen donor on furfural conversion and product yields.
<u>Reaction conditions:</u> Furfural (5 mmol); catalyst (2wt% Ru-NMC-3, 25 mg); N_2 pressure (20 bar); solvent and hydrogen donor (25 mL); reaction time (10 h). Others include ethers.

4.2.3. Conclusions

NMC's with different nitrogen content were synthesized and characterized by various physico-chemical techniques. Catalysts with highly dispersed metal nanoparticles were prepared using NMC's as supports, by ultrasonic-assisted method. The activity and selectivity of different supported metal catalysts were investigated for CTH reaction of biomass-derived HMF and furfural to produce DMF and MF, respectively using alcohols as a hydrogen donor. It was found that during CTH, temperature, hydrogen donor, nitrogen content, type of the metal, basicity of the catalyst and catalyst support play a vital role in the conversion of substrate to give desired product. The CTH activity was improved with increasing nitrogen content and basicity of the catalyst. Under optimized reaction conditions, 2wt% Ru-NMC-3 catalyst gave 84 and 87 mol% yield of DMF and MF, respectively with 2-propanol as the hydrogen donor. The catalyst could be reused four times without much loss in activity. The NMC supported Ru catalysts holds promising potential for the reductive upgradation of biomass-derived compounds to chemicals and fuels through CTH process.

4.3. References

1. (a) G. W. Huber, S. Iborra and A. Corma, *Chem. Rev.,* 2006, **106**, 4044; (b) A. Corma, S. Iborra and A. Velty, *Chem. Rev.,* 2007, **107**, 2411; I J. N. Chheda, G. W. Huber and J. A. Dumesic, *Angew. Chem., Int. Ed.*, 2007, **46**, 7164; (d) K. Shimizu and A. Satsuma, *Energy Environ. Sci.*, 2011, **4**, 3140.

2.   (a) E. L. Kunkes, D. A. Simonetti, R. M. West, J. C. Serrano-Ruiz, C. A. Gärtner and J. A. Dumesic, *Science*, 2008, **322**, 417; (b) A. J. Ragauskas, C. K. Williams, B. H. Davision, G. Britovsek, J. Cairney, C. A. Eckert, W. J. Frederick Jr., J. P. Hallett, D. J. Leak, C. L. Liotta, J. R. Mielenz, R. Murphy, R. Templer and T. Tschaplinski, *Science,* 2006, **311**, 484.

3.   (a) R. Karinen, K. Vilonen and M. Niemela, *ChemSusChem*, 2011, **4**, 1002; b) J. B. Binder, J. J. Blank, A. V. Cefali and R. T. Raines, *ChemSusChem,* 2010, **3**, 1268; c) C. Aellig and I. Hermans, *ChemSusChem,* 2012, **5**, 1737.

4.   D. Scholz, C. Aellig and I. Hermans, *ChemSusChem,* 2014, **7**, 268.

5.   Y. Román-Leshkov, C. J. Barrett, Z. Y. Liu and J. A. Dumesic, *Nature,* 2007, **447**, 982.

6.   C. Wang, H. Xu, R. Daniel, A. Ghafourian, J. M. Herreros, S. Shuai and X. Ma, *Fuel,* 2013, **103**, 200.

7.   (a) J. B. Binder and R. T. Raines, *J. Am. Chem. Soc.,* 2009, **131**, 1979; (b) M. Chidambaram and A. T. Bell, *Green Chem.,* 2010, **12**, 1253; I G.-H. Wang, J. Hilgert, F. H. Richter, F. Wang, H.-J. Bongard, B. Spliethoff, C. Weidenthaler and F. Schuth, *Nat. Mater.* 2014, **13**, 293; (d) J. Zhang, L. Lin and S. Liu, *Energy Fuels,* 2012, **26**, 4560; (e) Y. Zu, P. Yang, J. Wang, X. Liu, J. Ren, G. Lu and Y. Wang, *Appl. Catal. B,* 2014, **146**, 244; (f) L. Hu, X. Tang, J. Xu, Z. Wu, L. Lin and S. Liu, *Ind. Eng. Chem. Res.,* 2014, **53**, 3056; (g) Y. B. Huang, M. Y. Chen, L. Yan, Q. X. Guo and Y. Fu, *ChemSusChem,* 2014, **7**, 1068; (h) S. Nishimura, N. Ikeda and K. Ebitani, *Catal. Today,* 2014, **232**, 89; (i) M. Chatterjee, T. Ishizaka, H. Kawanami, *Green Chem.,* 2014, 16, 1543; (j) A. J. Kumalaputri, G. Bottari, P. M. Erne, H. J. Heeres and K. Barta, *ChemSusChem,* 2014, **7**, 2266; (k) X. Kong, Y. Zhu, H. Zheng, F. Dong, Y. Zhu and Y. W. Li, *RSC Adv.,* 2014, **4**, 60467.

8.   (a) H. Y. Zheng, Y. L. Zhu, Z. Q. Bai, L. Huang, H. W. Xiang and Y. W. Li, *Green Chem.,* 2006, **8**, 107; (b) H. Y. Zheng, Y. L. Zhu, B. T. Teng, Z. Q. Bai, C. H. Zhang, H. W. Xiang and Y. W. Li, *J. Mol. Catal. A,* 2006, **246**, 18.

9.   (a) J. Jae, W. Zheng, R. F. Lobo and D. G. Vlachos, *ChemSusChem,* 2013, **6**, 1158; (b) T. S. Hansen, K. Barta, P. T. Anastas, P. C. Ford and A. Riisager, *Green Chem.,* 2012, **14**, 2457; I S. Morikawa, *Noguchi Kenkyusho Jiho*, 1980, **23**, 39; (d) C. Aellig, F. Jenny, D. Scholz, P. Wolf, I. Giovinazzo, F. Kollhoff and I. Hermans, *Catal. Sci. Technol.,* 2014, **4**, 2326; (e) P. Panagiotopoulou and D. G. Vlachos, *Appl. Catal. A,* 2014, **480**, 17; (f) P. Panagiotopoulou, N. Martin and D. G. Vlachos, *J. Mol. Catal. A,* 2014, **392**, 223.

10. T. Thananatthanachon and T. B. Rauchfuss, *Angew. Chem., Int. Ed.,* 2010, **49**, 6616.

11. (a) T. Thananatthanachon and T. B. Rauchfuss, *Angew. Chem.,* 2010, **122**, 6766; (b) S. De, S. Dutta and B. Saha, *ChemSusChem*, 2012, **5**, 1826.

12. H. Chen, F. Sun, J. Wang, W. Li, W. Qiao, L. Ling and D. Long, *J. Phys. Chem. C,* 2013, **117**, 8318.

13. P. Zhang, Y. Gong, H. Li, Z. Chen and Y. Wang, *Nat. Commun.,* 2013, **4**, 1593.

14. X. Xu, Y. Li, Y. Gong, P. Zhang, H. Li and Y. Wang, *J. Am. Chem. Soc.,* 2012, **134**, 16987.

15. X. Xie, J. Long, J. Xu, L. Chen, Y. Wang, Z. Zhang and X. Wang, *RSC Adv.,* 2012, **2**, 12438.

16. J. J. F. Scholten, A. P. Pijpers and M. L. Hustings, *Catal. Rev. Sci. Eng.,* 1985, **27**, 151.

17. N. M. Bertero, A. F. Trasarti, C. R. Apesteguía and A. J. Marchi, *Appl. Catal. A*, 2011, **394**, 228.

18. (a) M. Chia and J. A. Dumesic, *Chem. Commun.*, 2011, **47**, 12233; (b) J. Song, L. Wu, B. Zhou, H. Zhou, H. Fan, Y. Yang, Q. Meng and B. Han, *Green Chem.*, 2015, **17**, 1626.

19. (a) J. Amadou, K. Chizari, M. Houlle, I. Janowska, O. Ersen, D. Begin and C. Pham-Huu, *Catal. Today,* 2008, **138**, 62; (b) K. Chizari, I. Janowska, M. Houlle, I. Florea, O. Ersen, T. Romero, P. Bernhardt, M. J. Ledoux and C. Pham-Huu, *Appl. Catal. A,* 2010, **380**, 72.

20. (a) M. Fang, N. Machalaba and R. A. Sanchez-Delgado, *Dalton Trans.,* 2011, **40**, 10621; (b) R. A. Sanchez-Delgado, N. Machalaba and N. Ng-a-qui, *Catal. Comm.,* 2007, **8**, 2115.

21. R. A. W. Johnstone, A. H. Wilby and I. D. Entwistle, *Chem. Rev.,* 1985, **85**, 129.

22. Y. B. Huang, Z. Yang, M. Y. Chen, J. J. Dai, Q. X. Guo and Y. Fu, *ChemSusChem,* 2013, **6**, 1348.

23. H. Kobayashi, H. Matsuhashi, T. Komanoya, K. Hara and A. Fukuoka, *Chem. Commun.,* 2011, **47**, 2366.

Chapter 5

Chemoselective hydrogenation of cinnamaldehyde over Pd and Au supported on nitrogen-doped mesoporous carbon

5.1. Introduction

Chemoselective hydrogenation of α,β-unsaturated carbonyl compounds into their corresponding unsaturated alcohols and saturated carbonyls over heterogeneous catalysts has gained increasing attention during the recent years, for both scientific and economic reasons.[1] As a representative α,β-unsaturated aldehyde, cinnamaldehyde (CA) is particularly important because it can be selectively hydrogenated to hydrocinnamaldehyde (HCA) and cinnamyl alcohol (CAL), depending on whether C=C bond is hydrogenated or the C=O bond (Scheme 5.1). HCA and CAL are vital intermediates for the synthesis of many fine chemicals, perfumes and pharmaceuticals.[2] HCA was found to be an important intermediate in the preparation of drugs used for HIV treatment.[2] In view of the industrial importance of the CA hydrogenation products (HCA and CAL), development of efficient catalysts that operate at moderate reaction conditions is highly desirable.
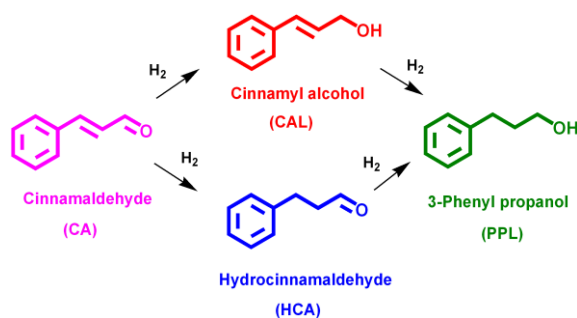
Scheme 5.1 Reaction pathways for hydrogenation of CA.

Carbon materials, which are intensely researched these days have some exceptional features (chemical and thermal stability, high BET surface area, etc.), as a new class of solid supports for a variety of heterogeneous catalysts.[3,4] However, noble metals (e.g., Pd, Pt, Rh and Ru) finely dispersed on carbons easily leach during catalytic processes as a result of weak interaction between carbon surface and the metal particles. Moreover, the catalytic or chemical properties of carbons do not always meet the sharply growing requirements of heterogeneous catalyst supports. Hence, modification of carbon is essential in the majority of cases.[5] Usually, single-walled carbon nanotubes cannot effectively anchor Pd nanoparticles without defects.[6] In order to reinforce the interaction between metal nanoparticles and the support, carbon materials are generally oxidized using HNO_3 to introduce required defects.[7]

Nitrogen-doped carbon materials have attracted worldwide attention due to their outstanding performance in various applications, particularly as catalyst supports[8], material for

supercapacitors[9], for metal-free oxygen reduction reaction[10], hydrogenation reaction[11], etc. Doping with electron-rich nitrogen atoms in the carbon architecture can enhance electrical, chemical and functional properties.[12] Nitrogen-doped carbon materials show several features that are significantly different from their undoped counterparts. The presence of nitrogen atoms in the carbon matrix could also modify the electronic and chemical interactions with the deposited metal nanoparticles, which can inturn modify the overall catalytic activity as well as selectivity.[13] Visualizing these properties, the nitrogen-doped mesoporous carbons (NMC's) were explored as catalyst support for the liquid-phase chemoselective hydrogenation of CA using Pd and Au as active metals.

5.2. Literature on the hydrogenation of cinnamaldehyde

The activity and selectivity of catalysts are very important in CA hydrogenation due to play of complicated reaction mechanisms, including dissociative/non-dissociative and competitive/non-competitive adsorption as well as formation of coke, side reactions, adsorption of solvents, etc (Scheme 5.2).[1c,2a,14] To circumvent these issues, it is necessary to choose suitable catalytic system. The chemoselective hydrogenation of CA to HCA and CAL were studied over various supported metal catalysts. The CA hydrogenation can be categorized into following two parts depending on whether HCA or CAL is formed selectively during the hydrogenation:

   (i) Hydrogenation of CA to HCA
   (ii) Hydrogenation of CA to CAL

5.2.1. Hydrogenation of CA to HCA

Ledoux *et al.* studied selective hydrogenation of CA to HCA over Pd catalyst supported on carbon nanofibers (CNFs).[15a] Conversion of CA was 100% at 98% HCA selectivity, when the reaction was carried out at 80 °C for 30 h. Liu *et al*. reported 91.3% HCA selectivity at 98.6% CA conversion by using Pd catalyst supported on multiwalled carbon nanotubes (MWCNTs) under 40 bar H_2 and 148 bar CO_2 pressure at 60 °C.[15b] Arai *et al.* obtained 87% HCA selectivity and 100% CA conversion using Pd/C catalyst under 40 bar H_2 and 80 bar CO_2 pressure.[15c] Amadou *et al.* achieved 90% HCA selectivity at nearly 100% CA conversion over Pd supported on nitrogen-doped carbon nanotubes at 80 °C in 8 h.[15d] Begin *et al.* used few-layer graphene supported Pd catalyst to obtain 92% HCA selectivity and 85% CA conversion at 80 °C

in 10 h.[15e] Giambastiani *et al.* reported 97% HCA selectivity and 100% CA conversion by using Pd/γ-Al$_2$O$_3$ at 100 °C in 3 h.[15f] Melsheimer *et al.* achieved 100% CA conversion and 75% HCA selectivity over Pd/SiO$_2$ catalyst.[15g] Zhang *et al.* studied CA hydrogenation over SiO$_2$ supported nickel phosphide catalyst and obtained 93% HCA selectivity and 78% CA conversion at 120 °C.[15h] Marchi *et al.* reported 59.5% HCA selectivity with 60% CA conversion by using Cu/SiO$_2$ catalyst at 120 °C in 6 h.[15i]
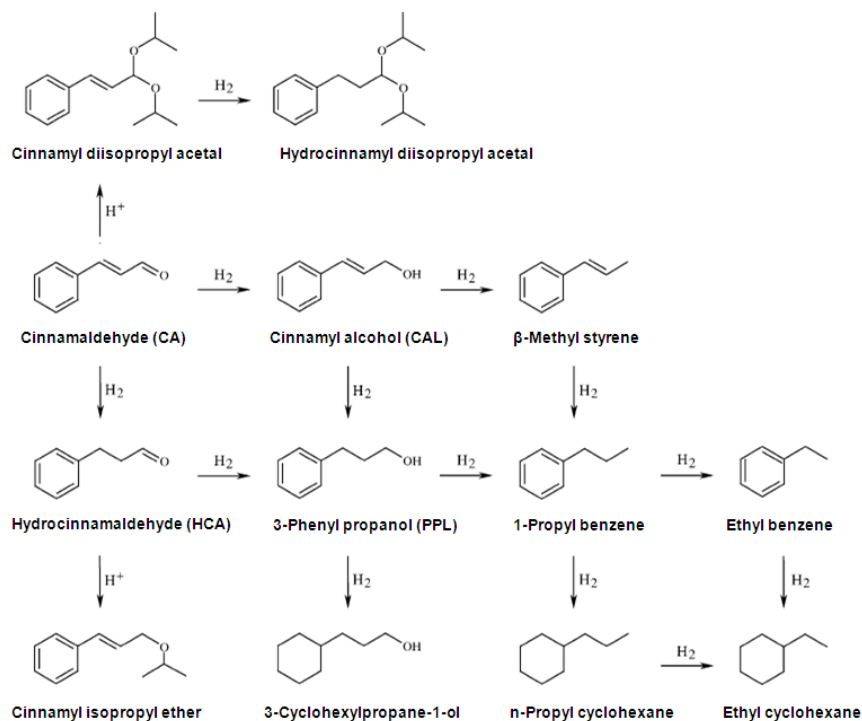
Scheme 5.2 Reaction network for hydrogenation of CA to different products.[2a]

5.2.2. Hydrogenation of CA to CAL

Bitter *et al.* studied the effect of metal particle size on the product selectivity in the CA hydrogenation over Pt and Ru catalysts supported on CNFs.[16a] Over the catalysts with oxygen groups on the CNFs surface, the bigger metal particles (3.5 nm) showed higher selectivity for CAL. Interestingly, when the oxygen groups were removed from the CNFs surface, the smaller metal particles (2 nm) showed higher CAL selectivity. Authors explained this metal particle size effect by a change in the adsorption mode of the CA molecule as a function of the polarity of the catalyst support. Rong *et al.* achieved 69.6% CAL selectivity at 89.6% CA conversion by using reduced graphene oxide supported Pt catalyst.[16b] Huang *et al.* reported a catalyst based on Pt nanoparticles confined inside the cavities of an amino-functionalized Zr-terephthalate metal-

organic framework for the selective hydrogenation of CA.[16c] This gave CA conversion of 98.7% with 91.7% CAL selectivity. Deng *et al.* obtained 82% CAL selectivity at 86% CA conversion over Au nanoparticles supported on ferric hydroxide.[16d] Chen *et al.* could achieve 77.8% CA conversion and 84.8% CAL selectivity by using hydrotalcite supported Au catalyst.[16e] Faria *et al.* used MWCNTs supported Ir catalyst to obtain nearly 70% CAL selectivity at 50% CA conversion.[16f] Song *et al.* reported Cu supported on ordered mesoporous carbon for CA hydrogenation that showed 82% CAL selectivity at 64% CA conversion.[16g] Tan *et al.* obtained 93% CAL selectivity at 100% CA conversion over bimetallic PtFe supported on mesoporous carbon.[16h] Casella *et al.* studied CA hydrogenation over SiO_2 supported bimetallic PtSn catalyst and achieved 80% CAL selectivity at 60% CA conversion.[16i]

Thus, it may be seen that a variety of supported metal catalysts were explored for the hydrogenation of CA to produce HCA or CAL selectively. However, most of the reported results do not provide good HCA/CAL selectivity at high CA conversion and have some disadvantages like high metal content of the catalyst and the need of higher H_2 pressure. Therefore, there is a need to develop efficient catalyst systems which can offer selectively HCA/CAL at moderate reaction temperatures under low H_2 pressure. Hence, this chapter deals with the selective hydrogenation of CA to HCA and CAL using molecular H_2. The results of this chapter are divided into two parts. Part-5A deals with the hydrogenation of CA to HCA over supported Pd catalysts, while part-5B deals with the hydrogenation of CA to CAL over supported Au catalysts.

5.3. Part 5A: Hydrogenation of CA to HCA over supported Pd catalysts

Mesoporous carbon (MC), activated carbon (AC) and NMC supported Pd catalysts were tested for the selective hydrogenation of CA to HCA. Various reaction parameters were optimized with an objective to achieve high CA conversion and HCA selectivity.

5.3.1. Experimental procedures

5.3.1.1. Materials

All the chemicals were reagent grade and used without further purification. Acetonitrile, cyclohexane, toluene, ethanol, 2-propanol, $NaBH_4$, CA (98%), HCA (98%), CAL (98%) and PPL (98%) were procured from Loba chemie, Mumbai. Whereas, $PdCl_2 \cdot 2H_2O$ and AC were purchased from Alfa Aesar.

5.3.1.2. Evaluation of catalysts

All the hydrogenation reactions were carried out using 100 mL parr autoclave (SS316). In a typical experiment, 1 g of CA (7.5 mmol), 25 mL of solvent and the required amount of freshly reduced catalyst was introduced into the reactor vessel. The reactor contents were thoroughly mixed and purged two to three times with H_2. Subsequently, the autoclave is pressurized to the required H_2 pressure and the reaction was conducted at 30 °C under continuous stirring (800 rpm). During the reaction, liquid samples were withdrawn periodically and analyzed by a GC (Agilent 7890A) equipped with a FID having CP Sil 8 CB capillary column (30 m length, 0.25 mm diameter). Product identification was done using authentic standards and by using GC-MS (Shimadzu, GCMS-QP2010 Ultra; HP-5 column; 30 m length, 0.25 mm diameter).

5.3.2. Results and discussion

5.3.2.1. Catalyst characterization

5.3.2.1.1. X-ray diffraction (XRD)

The XRD patterns of NMC, 2wt% Pd-NMC, 2wt% Pd-AC and 2wt% Pd-MC are given in Fig. 5.1. A broad diffraction peak at around 25.2° and a weak reflection around 43.7° were observed for NMC, that correspond to (002) and (100) planes of graphite-type lattice, respectively.[17] The XRD pattern of 2wt% Pd-NMC was similar to that of NMC and does not contain any diffraction peaks related to the metallic Pd, suggesting formation of highly dispersed Pd nanoparticles. The diffraction peaks of Pd in 2wt% Pd-AC were weak. However, sharp diffraction peaks of Pd at 40.1, 46.7, 68.1 and 82.1° were detected in 2wt% Pd-MC, which were assigned to (111), (200), (220) and (311) crystalline planes of metallic Pd, respectively.
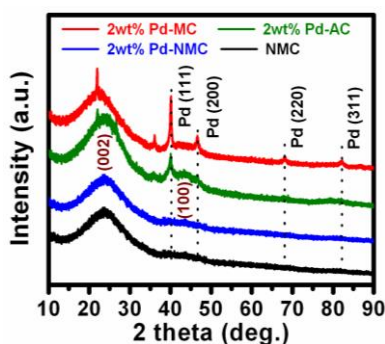
Fig. 5.1 XRD of NMC and supported Pd catalysts.

5.3.2.1.2. N₂-Physisorption

As shown in Fig. 5.2, NMC, 2wt% Pd-NMC and 2wt% Pd-MC samples shows type IV adsorption-desorption isotherms with an H2 hysteresis loop, demonstrating the typical

mesoporous structure of the materials whereas 2wt% Pd-AC exhibits type II adsorption-desorption isotherm, showing the microporous nature of the sample. The detailed pore parameters and physicochemical properties of the various samples are summarized in Table 5.1.
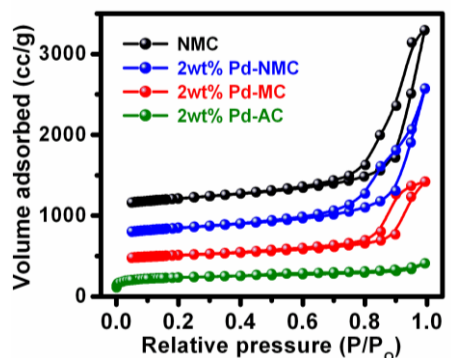
Fig. 5.2 N_2 adsorption-desorption isotherms of NMC and supported Pd catalysts.

Table 5.1 Textural properties and Pd metal characteristics of the catalysts.

Catalyst	Pd content[a] (wt%)	BET surface area (m²/g)	Micropore surface area[b] (m²/g)	Average pore diameter [c] (nm)	Nitrogen content[d] (wt%)	Average Pd particle size[e] (nm)	Pd metal dispersion [f] (%)	Pd metal surface area[g] (m²/g)
NMC	--	844	103	12.4	11.6	--	--	--
2wt% Pd-NMC	2.05	791	85	12.2	11.5	2.4	54.0	4.15
2wt% Pd-MC	1.97	712	116	13.0	0	7.7	16.8	1.29
2wt% Pd-AC	1.94	1020	663	3.8	0	4.6	28.2	2.16

[a] Determined by ICP-OES. [b] Determined by t-plot method. [c] Calculated from desorption branch of N_2 sorption isotherm by BJH method. [d] Determined using elemental analysis. [e] Calculated based on TEM analysis. [f] Estimated using average Pd particle size obtained from TEM analysis and by employing equation described by Isaifan *et al.* in reference 19. [g] Calculated by assuming Pd metal particles in hemispherical shape with the flat side on the support.

5.3.2.1.3. Raman spectroscopy

Raman spectroscopy was used to study the graphitic nature of the carbon (Fig. 5.3). It consists of characteristic D- and G-bands of disordered graphitic carbon materials, situated at 1335 and 1590 cm^{-1}, respectively. The D-band reflects defects in carbons while the G-band indicates the graphitic structure of carbons.[17] The intensity ratios of the D-band to the G-band (I_D/I_G, calculated from integral area of the peaks) are 1.68, 1.75, 2.38 and 2.45 for 2wt% Pd-AC, 2wt% Pd-MC, NMC and 2wt% Pd-NMC, respectively. The higher I_D/I_G ratios of nitrogen containing samples compared to nitrogen-free samples (2wt% Pd-AC and 2wt% Pd-MC),

suggests that the incorporation of nitrogen in carbon frameworks led to more disordered structures.[17]
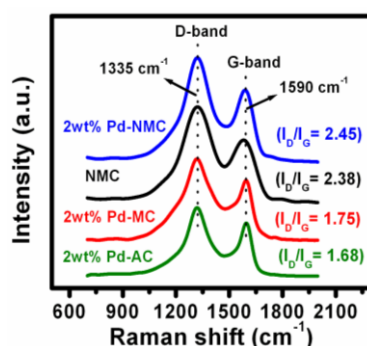
Fig. 5.3 Raman spectra of NMC and supported Pd catalysts.

5.3.2.1.4. Transmission electron microscopy (TEM)

The mesoporous structure of NMC and MC can be further confirmed by TEM observations (Fig. 5.4), which revealed that both samples consists of randomly distributed spherical mesopores with disordered amorphous carbon structure. It can be seen that the Pd nanoparticles with an average size of 2.4 nm were homogeneously distributed throughout the NMC support (Fig. 5.5a,5.5b). On the other hand, Pd nanoparticles were found to be dispersed unevenly and large agglomerated Pd nanoparticles were detected on the surface of MC and AC (Fig. 5.5c, 5.5d, 5.5e, 5.5f). The average particle sizes of Pd nanoparticles in 2wt% Pd-MC and 2wt% Pd-AC were found to be 7.7 and 4.6 nm, respectively. Thus, it can be concluded that the dominant contributor for stabilizing Pd nanoparticles is the nitrogen dopant.[18]
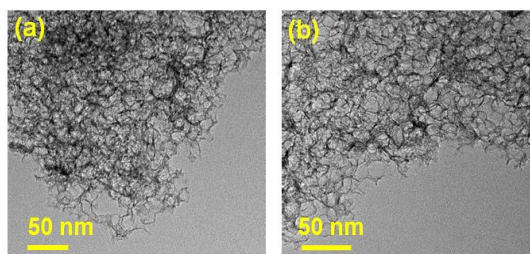
Fig. 5.4 TEM image of the (a) MC and (b) NMC.
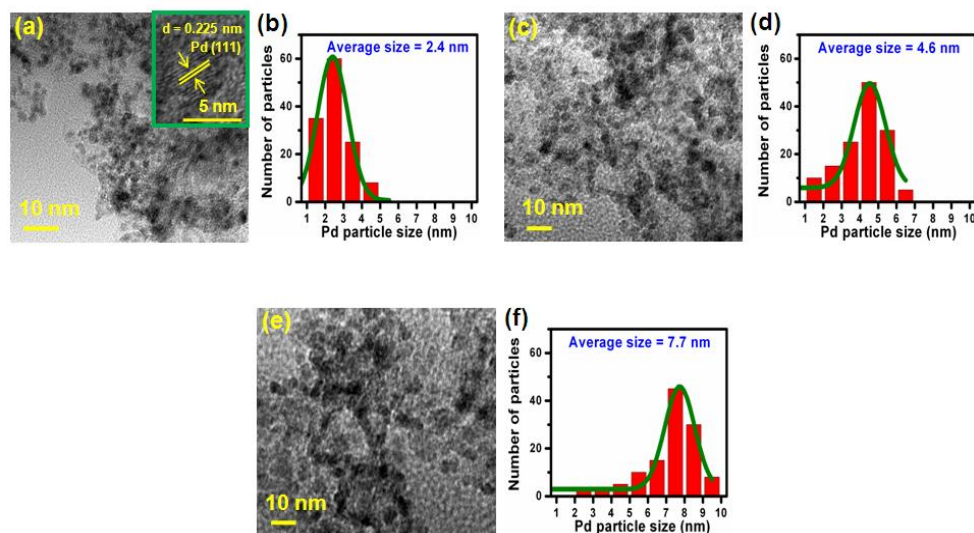
Fig. 5.5 TEM images and the Pd nanoparticle size distribution of 2wt% Pd-NMC (5.5a and 5.5b), 2wt% Pd-AC (5.5c and 5.5d) and 2wt% Pd-MC (5.5e and 5.5f), respectively.

5.3.2.1.5. Pd dispersion and metal surface area

The average particle size of Pd nanoparticles (based on TEM analysis) in 2wt% Pd-NMC, 2wt% Pd-AC and 2wt% Pd-MC catalysts were used to calculate dispersion (%) of Pd assuming spherical shape of particles and using the formula described by Isaifan *et al.*[19] The Pd dispersion values were: 2wt% Pd-NMC, 54%; 2wt% Pd-MC, 16.8% and 2wt% Pd-AC, 28.2% (Table 5.1). The high dispersion (54%) of Pd on NMC confirms the homogeneous distribution of Pd nanoparticles over the support. Pd metal surface area was calculated by assuming that the Pd nanoparticles are hemispherical in shape with the flat side on the support. These values for 2wt% Pd-NMC, 2wt% Pd-MC and 2wt% Pd-AC catalysts were calculated as 4.15, 1.29 and 2.16 m^2/g, respectively (Table 5.1).

5.3.2.1.6. X-ray photoelectron spectroscopy (XPS)

In XPS studies of NMC, carbon, oxygen and nitrogen peaks were observed while only carbon and oxygen peaks were seen for MC (Fig. 5.6a). The nitrogen 1s spectra of NMC (Fig. 5.6b) are curve-fitted into three peaks with the binding energies of 398.2, 400.4 and 401.8 eV that correspond to pyridinic N (N1), pyrrolic N (N2) and graphitic N (N3), respectively.[17] The Pd 3d XPS spectra of 2wt% Pd-MC (Fig. 5.6c) and 2wt% Pd-NMC (Fig. 5.6d) consist of two peaks corresponding to Pd 3d$_{5/2}$ and Pd 3d$_{3/2}$. The peaks around 336.1 and 341.2 eV were assigned to metallic Pd (Pd$°$), corresponding to Pd$°$ 3d$_{5/2}$ and Pd$°$ 3d$_{3/2}$, respectively.[8,11] Whereas, the peaks at 337.8 and 342.7 eV are attributed the Pd in the +2 oxidation state (PdO),

related to Pd^{2+} $3d_{5/2}$ and Pd^{2+} $3d_{3/2}$, respectively.[8,11] According to XPS data, the Pd° percentage in 2wt% Pd-NMC and 2wt% Pd-MC were 86 and 65%, respectively. These results clearly show that the incorporation of nitrogen in the carbon texture resulted in increased proportions of metallic Pd.[8,11]
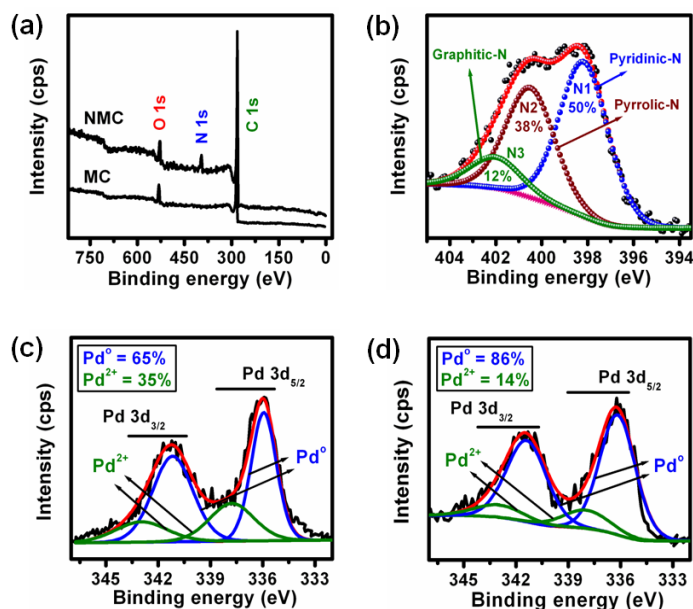
Fig. 5.6 (a) XPS scan of MC and NMC, (b) High resolution XPS spectra of N 1s in NMC, (c) XPS spectra of Pd 3d in 2wt% Pd-MC and (d) XPS spectra of Pd 3d in 2wt% Pd-NMC.

5.3.2.2. Catalytic activity in hydrogenation of CA to HCA

5.3.2.2.1. Effect of solvent

Solvent plays a very important role in heterogeneous catalytic hydrogenation and it can possibly even alter the distribution of the products.[20] Hydrogenation of CA was carried out in polar–aprotic (acetonitrile), protic (ethanol and 2-propanol), non-polar (cyclohexane and toluene) and water solvents. Table 5.2 represents the CA conversions and products selectivity's over 2wt% Pd-NMC catalyst at 30 °C. The chemical and physical properties of the solvents used (solvent polarity and H_2 solubility) are also given in Table 5.2. Under the reaction conditions investigated, mainly HCA and 3-phenyl propanol (PPL) products were observed. The CA conversion was found to be relatively higher in ethanol and 2-propanol compared to other solvents. The lower CA conversion observed in cyclohexane and toluene might be due to the poor solubility of reactant molecules in these solvents (entry 2 and 3, Table 5.2). It is interesting to note that HCA selectivity was in the range of 81.2 to 93% in all the solvents. When 2-propanol

was employed as solvent; relatively higher catalytic activity was observed. The conversion of CA was 100% within 3 h of reaction to give 93% HCA selectivity at a TOF value of 987 h^{-1} (entry 5, Table 5.2). Although, 2-propanol is known as a hydrogen transfer reagent, the results suggest that the effect of transfer hydrogenation was nil under the studied reaction conditions (entry 6, Table 5.2). In case of water as solvent, low reactivity (TOF = 229 h^{-1}) with 23.2% CA conversion and 81.2% HCA selectivity was seen (entry 7, Table 5.2). The inferior catalytic activity in water solvent may be due to the poor solubility of H_2 in water (Table 5.2).[21] In this particular case, probably H_2 solubility along with solvent polarity play key role in the elevation of catalytic activity. In view of higher apparent activity and superior HCA selectivity (93%), 2-propanol was chosen as the solvent for further investigations.

Table 5.2 Hydrogenation of CA in different solvents over 2wt% Pd-NMC.[a]

Entry	Solvent	Solvent polarity index	H_2 solubility[b] (mmol/L)	Conv. (%)	Products selectivity (%)			TOF[d] (h^{-1})
					HCA	PPL	Others[c]	
1	Acetonitrile	5.8	--	71.2	88.3	11.7	0	702
2	Cyclohexane	0.2	3.72	43.5	91.1	8.9	0	429
3	Toluene	2.4	2.75	57.3	87.5	12.5	0	565
4	Ethanol	5.2	3.43	89.7	83.0	12.2	4.8	885
5	2-Propanol	3.9	3.9	100	93.0	4.9	2.1	987
6[e]	2-Propanol	3.9	3.9	--	--	--	--	--
7	Water	9.0	0.81	23.2	81.2	18.8	0	229

[a] <u>Reaction conditions:</u> CA (7.5 mmol); catalyst (2wt% Pd-NMC, 25 mg); solvent (25 mL); H_2 pressure (5 bar); reaction time (3 h); temperature (30 °C). [b] H_2 solubility in various solvents, taken from reference 21. [c] Other products include acetal and ethers. [d] TOF = turnover frequency (moles of CA converted per mole of surface Pd per unit hour). [e] Reaction in the absence of H_2.

5.3.2.2.2. Comparison of various supported Pd catalysts

To study the effect of the support, 2wt% Pd-NMC catalyst was compared with other catalysts including 2wt% Pd-MC and 2wt% Pd-AC under identical reaction conditions (30 °C and 5 bar H_2 pressure). These results are given in the Fig. 5.7. Among the different catalysts, 2wt% Pd-NMC exhibited relatively better hydrogenation activity affording 93% HCA selectivity with 100% CA conversion within 3 h. The HCA selectivity for MC and NMC-based catalysts

were almost stable at 66 and 93%, respectively. However, HCA selectivity for AC-based catalyst was decreased from 53 to 44% with increasing CA conversion. MC-supported Pd nanoparticles were not effective for this reaction, as HCA selectivity was low combined with poor CA conversion. The reasons for this may arise from the uneven distribution and relatively large size of Pd nanoparticles (7.7 nm). Similarly, 2wt% Pd-AC catalyst gave low HCA selectivity, in spite of having high surface area (1020 m^2/g, Table 5.1) and PPL was obtained in significant quantities. The high microporosity of AC (> 60% of total surface area, Table 5.1) might hinder the diffusion of the reactant molecules and may not favour desorption of partially hydrogenated products.[15a] Hence, hydrogenation reaction proceeds more slowly with low HCA selectivity. The presence of acidic sites on AC could also modify the hydrogenation pathway leading to the loss in selectivity.[15a] The enhanced catalytic activity and better C=C hydrogenation selectivity observed on N-doped Pd catalyst could be attributed to several factors: (1) small particle size of Pd nanoparticles (2.4 nm) as a result of metal-support interaction between Pd and NMC support, (2) higher Pd metal surface area (4.15 m^2/g, Table 5.1), (3) activation of Pd nanoparticles by nitrogen present in the support,[15d] which in turn may modify the adsorption mode of the reactant and selectivity of the products,[22,23] and (4) mesoporosity of NMC support that facilities diffusion of reactant and hydrogenated products.
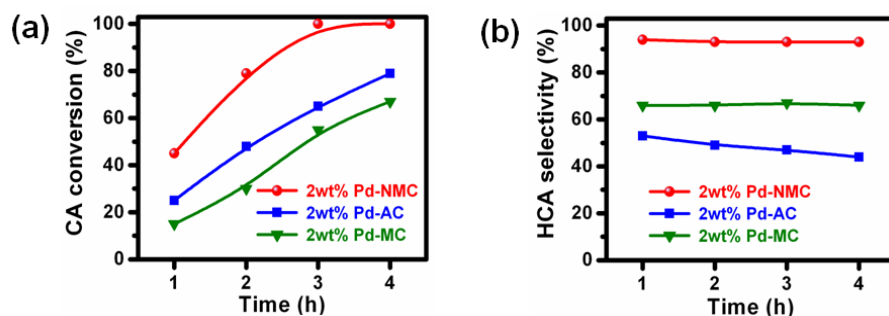
Fig. 5.7 (a) CA conversion and (b) HCA selectivity as a function of reaction time over different Pd catalysts. Reaction conditions: CA (7.5 mmol); catalyst (25 mg); solvent (2-propanol, 25 mL); H_2 pressure (5 bar); temperature (30 °C).

The experiments were also conducted on 2wt% Pd-NMC and 2wt% Pd-AC catalysts using equimolar mixture of HCA and CAL, which are C=C and C=O hydrogenated products of CA, respectively (Fig. 5.8). The HCA did not undergo further hydrogenation to PPL on both the catalysts under the reaction conditions employed (30 °C and 5 bar H_2 pressure), which indicates that the re-adsorption of the HCA molecule through the C=O bond did not occur on the Pd

nanoparticles irrespective of the nature of support. However, CAL was converted to PPL in considerable quantities on both the catalysts. The results in Fig. 5.7 and Fig. 5.8 clearly suggest that on 2wt% Pd-AC, the CA adsorbed in such a way that almost simultaneous hydrogenation of the C=C and C=O bonds takes place whereas on the 2wt% Pd-NMC catalyst the C=C hydrogenated product (HCA) was rapidly desorbed from the active sites. These are very important results, since it point outs that all PPL obtained in CA hydrogenation under the reaction conditions does actually come via the formation of CAL as an intermediate. Similar observations were made by Mahmoud *et al.*[2b] in HCA hydrogenation over Pd/SiO$_2$ catalyst. This catalyst was unable to form PPL from HCA in significant quantities at normal temperature. However, the hydrogenation of CAL to PPL proceeds nearly 30 times faster than the hydrogenation of CA to CAL.
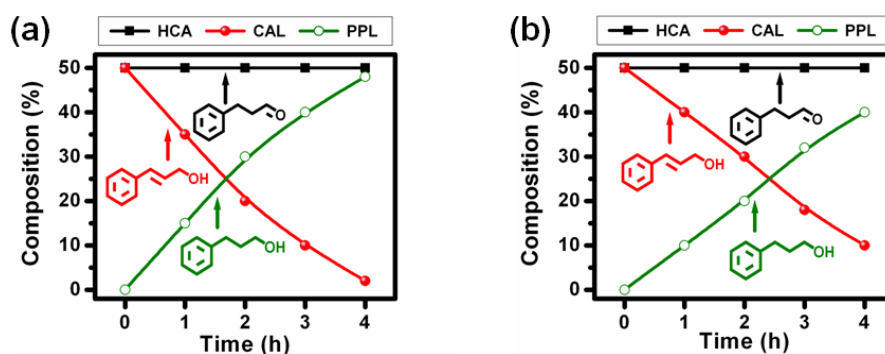
Fig. 5.8 Hydrogenation of HCA and CAL over (a) 2wt% Pd-NMC and (b) 2wt% Pd-AC catalyst as a function of reaction time.
Reaction conditions: HCA (4 mmol); CAL (4 mmol); catalyst (25 mg); solvent (2-propanol, 25 mL); H$_2$ pressure (5 bar); temperature (30 °C).

5.3.2.2.3. Effect of H$_2$ pressure

The influence of H$_2$ pressure on the CA hydrogenation was studied by varying it in the range of 1-5 bar over 2wt% Pd-NMC at 30 °C (Fig. 5.9). The CA conversion was improved from 40 to 100% as the H$_2$ pressure increased from 1 to 5 bar. But, the HCA selectivity was not altered much and remained nearly same at 93%. Hence, 5 bar H$_2$ pressure was found to be optimum to attain 100% CA conversion and 93% HCA selectivity within 3 h. At 1 bar H$_2$ pressure similar activity can be achieved after longer reaction time (9 h).
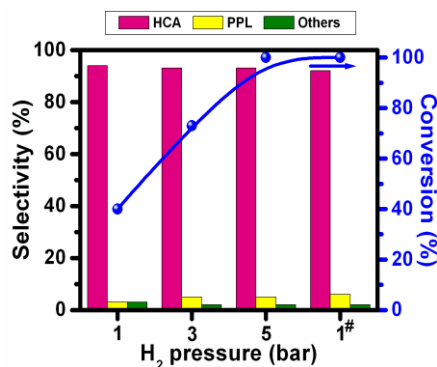
Fig. 5.9 Effect of H$_2$ pressure on CA hydrogenation and product selectivity's.
Reaction conditions: CA (7.5 mmol); catalyst (2wt% Pd-NMC, 25 mg); solvent (2-propanol, 25 mL); temperature (30 °C); time (3 h, # 9 h).

5.3.2.2.4. The possible reaction mechanism

There has been a relationship between metal d-band width and the product selectivity in the hydrogenation of α,β unsaturated carbonyl compounds.[2a,24] The Huckel calculations suggest that the narrower the metal d-band width, larger the interaction of the metal surface with the conjugated C=C bond compared to the C=O bond.[25] The width of the metal d-band increases in the following order: Pd < Pt < Ir ≈ Os.[25] Therefore, the chemisorption of C=C bond is more favorable over the Pd metal catalysts. DFT calculations have revealed that the maleic anhydride interacts with the Pd (111) surface through the C=C bond.[26] Over 2wt% Pd-NMC catalyst, the C=C bond in CA molecule may get adsorbed almost parallel to the Pd metal surface as a result of small size of Pd nanoparticles (2.4 nm). Presumably, the close interaction between C=C bond and Pd metal surface may lead to higher catalytic performance. Scheme 5.3 demonstrates the proposed step sequence in the chemoselective hydrogenation of CA. In the first step, the CA interacts with the Pd surface through the C=C bond and H$_2$ molecule is dissociated from the electronically promoted Pd (due to nitrogen in the carbon texture). Subsequently, the selective hydrogenation of C=C bond takes place by the attack of the activated hydrogen species. Because of the mesoporous channels in the NMC support, the formed saturated carbonyl (HCA) rapidly leaves the surface of the catalyst and replaced by a new reactant molecule (CA). Thus, further hydrogenation of HCA to saturated alcohol (PPL) is avoided.
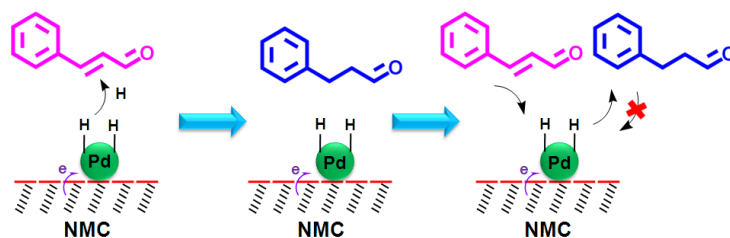
Scheme 5.3 Possible reaction mechanism of selective hydrogenation of CA over 2wt% Pd-NMC.

5.3.2.2.5. Recyclability study

The recyclability of 2wt% Pd-NMC catalyst was evaluated by repeating the reaction with the same catalyst without any regeneration or activation (Fig. 5.10). To our delight, 2wt% Pd-NMC was active even after six recycles without any significant drop in CA conversion and HCA selectivity, which is a prerequisite for practical applications. In order to gain more insight into catalytic activity, XRD and TEM analysis of used catalysts was carried out. XRD results revealed that the catalyst was not subjected to any changes during the reusability experiments (Fig. 5.11). The TEM image of the 2wt% Pd-NMC after 6 recycles exhibited an average Pd nanoparticles size of 2.6 nm (Fig. 5.12), which is almost similar to that of the fresh catalyst (Fig. 5.5a and 5.5b). These results demonstrate excellent stability of the catalyst. The product mixture after each recycle was analyzed for the presence of Pd due to leaching. No such leaching of Pd was observed, indicating strong interaction between the Pd nanoparticles and NMC support. In addition, the amount of Pd in the catalyst was almost same that of the starting catalyst even after six recycles.
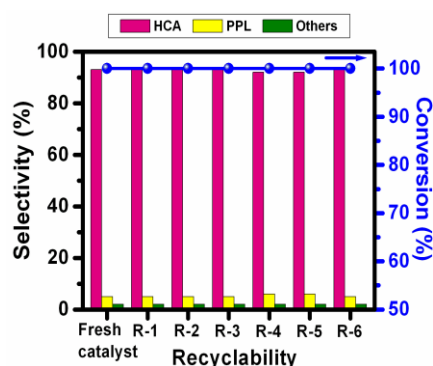
Fig. 5.10 Recyclability study of 2wt% Pd-NMC catalyst in the CA hydrogenation.
Reaction conditions: molar ratio of CA to Pd (1600); solvent (2-propanol, 25 mL); H_2 pressure (5 bar); reaction time (3 h); temperature (30 °C). Other products include acetal and ethers.
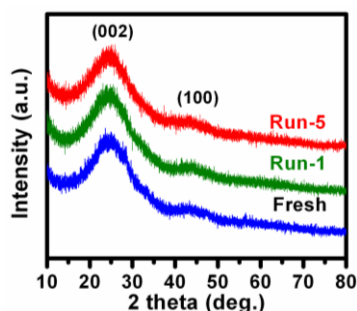
Fig. 5.11 XRD patterns of the fresh and used 2wt% Pd-NMC catalyst.
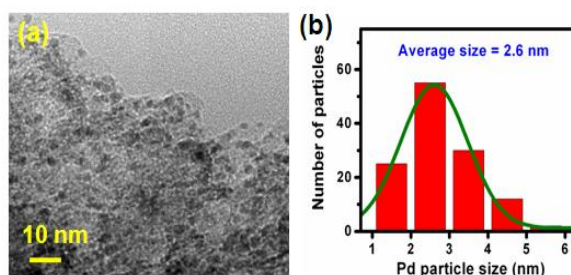
Fig. 5.12 (a) TEM image and (b) the Pd nanoparticles size distribution of re-used (after 6 recycles) 2wt% Pd-NMC catalyst.

5.3.3. Conclusions

Chemoselective liquid-phase hydrogenation of CA was investigated over Pd supported on NMC, MC and AC catalysts. Catalyst 2wt% Pd-NMC shows an excellent catalytic activity and high HCA selectivity (93%) under mild reaction conditions (30 °C, 5 bar H_2). It can be reused for 6 times without any loss in activity and selectivity. This excellent performance originates from the mesoporous network and introduction of nitrogen atoms. The mesoporous structure of NMC support inhibits the limitation of mass transfer of the reactant molecules to the active sites and promotes the free diffusion of the hydrogenated products. The incorporation of nitrogen atoms in the carbon framework not only leads to a very stable and homogeneous dispersion of Pd nanoparticles but also to possible electronic and morphologic modifications of the active phase. This synthesis approach (by incorporation of heteroatoms in the catalyst support) may lead to the design of many powerful catalysts, which can be used for the production of numerous fine chemicals.

5.4. Part 5B: Hydrogenation of CA to CAL over supported Au catalysts

Au catalysts supported on NMC, MC and metal oxides (Al_2O_3, MgO and TiO_2) were tested for the selective hydrogenation of CA to CAL. Various process parameters that influence this reaction were optimized with an aim to increase the CA conversion and CAL selectivity.

5.4.1. Experimental procedures

5.4.1.1. Materials

All the chemicals were reagent grade and used without further purification. Acetonitrile, cyclohexane, toluene, chloroform, methanol, ethanol, 1-propanol, 2-propanol, $NaBH_4$, Al_2O_3, MgO and TiO_2, CA (98%), HCA (98%), CAL (98%) and PPL (98%) were procured from Loba chemie, Mumbai, while $HAuCl_4 \cdot 3H_2O$ was purchased from Alfa Aesar.

5.4.1.2. Evaluation of catalysts

All the hydrogenation reactions were carried out in 100 mL parr autoclave (SS316). In a typical experiment, 1 g of CA (7.5 mmol), 25 mL of solvent and the required amount of the freshly reduced catalyst was introduced into the reactor vessel. The reactor contents were mixed thoroughly and purged two to three times with H_2 before pressurizing the vessel to the required level. The reaction was carried out at desired temperature under continuous stirring (800 rpm). Liquid samples withdrawn periodically during the reaction were analyzed by GC (Agilent 7890A) equipped with FID and CP Sil 8 CB capillary column (30 m length, 0.25 mm diameter). Product identification was done using authentic standards and with the help of GC-MS (Shimadzu, GCMS-QP2010 Ultra; HP-5 column; 30 m length, 0.25 mm diameter).

5.4.2. Results and discussion

5.4.2.1. Catalyst characterization

5.4.2.1.1. X-ray diffraction (XRD)

The XRD patterns of NMC and supported Au catalysts prepared by different methods are shown in Fig. 5.13. A broad diffraction peak at around 25.2° (2θ) and a weak reflection around 43.7° (2θ) were observed for NMC, which are assigned to (002) and (100) planes of graphite-type lattice, respectively.[17] The XRD pattern of 1wt% Au-NMC-SI and 1wt% Au-NMC-DP catalysts were similar to that of NMC and does not contain any diffraction peaks corresponding to the metallic Au, suggesting formation of highly dispersed Au nanoparticles. However, for

1wt% Au-NMC-IW catalyst, weak diffraction peaks at 2θ values of 38.2 and 44.5° were seen that were assigned to (111) and (200) crystalline planes of metallic Au, respectively.
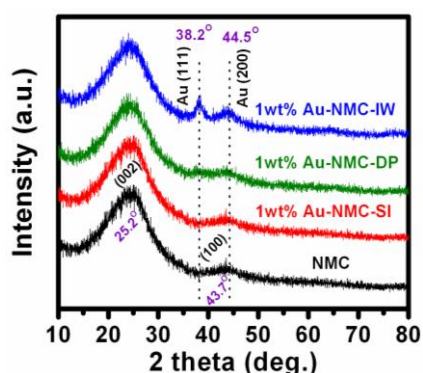
Fig. 5.13 XRD patterns of NMC and supported Au catalysts prepared by different methods.

5.4.2.1.2. N₂-Physisorption

The BET surface areas of NMC and supported Au catalysts are given in Table 5.3. The surface areas of NMC, 1wt% Au-NMC-IW, 1wt% Au-NMC-DP, 1wt% Au-NMC-SI, 1wt% Au-MC-SI, 1wt% Au-Al₂O₃, 1wt% Au-MgO and 1wt% Au-TiO₂ were 844, 785, 769, 757, 690, 190, 82 and 32 m²/g, respectively.

Table 5.3 Physico-chemical characteristics of supported Au catalysts.					
Catalyst	Au content[a] (wt%)	BET surface area (m²/g)	Nitrogen content[b] (wt%)	Average Au particle size[c] (nm)	Au metal dispersion[d] (%)	Au metal surface area[e] (m²/g)
NMC	--	844	11.6	--	--	--
1wt% Au-NMC-IW	0.96	785	11.5	4.2	30.0	0.74
1wt% Au-NMC-DP	0.89	769	11.3	2.3	54.8	1.34
1wt% Au-NMC-SI	0.94	757	11.3	1.6	78.8	1.94
1wt% Au-MC-SI	0.92	690	0	3.4	37.1	0.91
1wt% Au-Al₂O₃	0.97	190	0	--	--	--
1wt% Au-MgO	0.91	82	0	5.5	22.9	0.56
1wt% Au-TiO₂	0.90	32	0	--	--	--

[a] Determined by ICP-OES. [b] Calculated by elemental analysis. [c] Calculated based on TEM analysis. [d] Estimated on the basis of average Au particle size calculated from TEM analysis and using equation described by Isaifan *et al.* in reference 19. [e] Calculated by assuming Au metal particles in hemispherical shape with flat side on the support.

5.4.2.1.3. Transmission electron microscopy (TEM)

The Au nanoparticles sizes as well as their distribution on various supported Au catalysts were investigated by TEM (Fig. 5.14). The Au nanoparticles were dispersed unevenly and larger

in size on the surface of MgO with an average particle size of 5.5 nm (Fig. 5.14a,5.14b). In contrast, Au nanoparticles were dispersed homogeneously over NMC support with an average particle size of 4.2, 2.3 and 1.6 nm for 1wt% Au-NMC-IW, 1wt% Au-NMC-DP and 1wt% Au-NMC-SI catalysts, respectively (Fig. 5.14c,5.14d,5.14e,5.14f,5.14g,5.14h). It is pertinent to note that sol-immobilization technique has a beneficial effect in the preparation of highly dispersed Au nanoparticles (1.6 nm size) compared to incipient-wetness and deposition-precipitation methods.
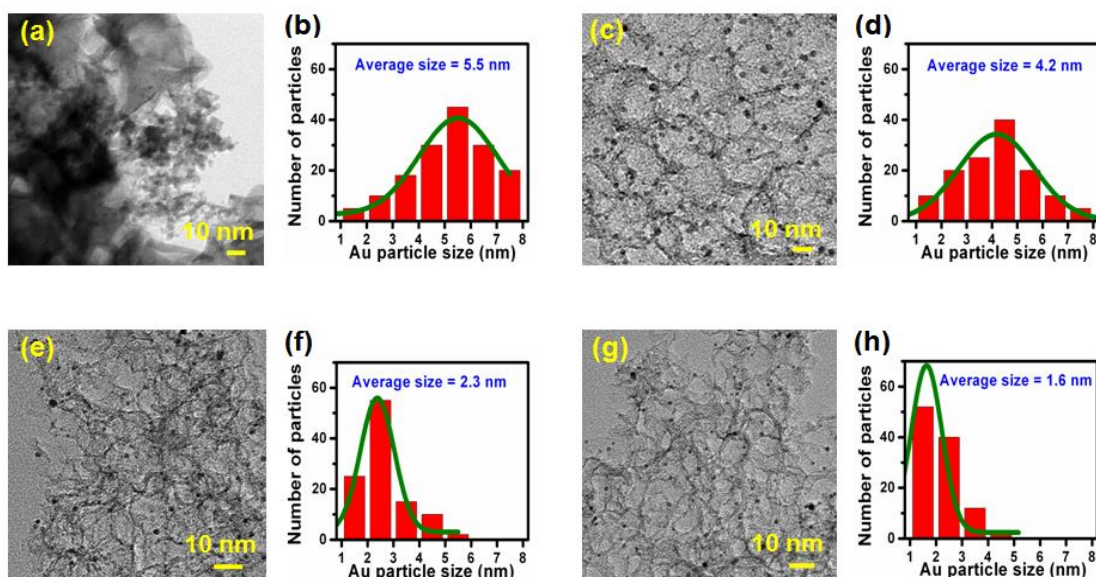
Fig. 5.14 TEM images and the Au nanoparticle size distribution for 1wt% Au-MgO (5.14a and 5.14b), 1wt% Au-NMC-IW (5.14c and 5.14d), 1wt% Au-NMC-DP (5.14e and 5.14f) and 1wt% Au-NMC-SI (5.14g and 5.14h), respectively.

5.4.2.1.4. Au dispersion and metal surface area

The average particle size of Au nanoparticles (based on TEM analysis) in 1wt% Au-MgO, 1wt% Au-NMC-IW, 1wt% Au-NMC-DP, 1wt% Au-NMC-SI and 1wt% Au-MC-SI catalysts were used to calculate % Au dispersion assuming spherical shape of particles and by employing the formula described by Isaifan *et al.*[19] The Au dispersion values were: 1wt% Au-MgO, 22.9%; 1wt% Au-NMC-IW, 30%; 1wt% Au-NMC-DP, 54.8%; 1wt% Au-NMC-SI, 78.8% and 1wt% Au-MC-SI, 37.1% (Table 5.3). Au metal surface area was calculated by assuming that the Au nanoparticles are hemispherical in shape with the flat side on the support. These values for 1wt% Au-MgO, 1wt% Au-NMC-IW, 1wt% Au-NMC-DP, 1wt% Au-NMC-SI and 1wt% Au-MC-SI catalysts were calculated as 0.56, 0.74, 1.34, 1.94 and 0.91 m^2/g, respectively (Table 5.3).

Thus, catalyst prepared by sol-immobilization technique shows the highest value of Au dispersion (78.8%) and high Au metal surface area (1.94 m^2/g).

5.4.2.2. Catalytic activity in hydrogenation of CA to CAL

5.4.2.2.1. Effect of solvent

The nature of solvent was found to have profound influence on CA conversion and CAL selectivity (Table 5.4). Hydrogenation of CA was carried out in non-polar (toluene and cyclohexane), polar–aprotic (acetonitrile and chloroform) and protic (methanol, ethanol, 1-propanol and 2-propanol) solvents. Table 5.4 presents CA conversion and products selectivity's over 1wt% Au-NMC-SI catalyst at 120 °C along with solvent polarity. Under the reaction conditions investigated, HCA, CAL and PPL were major products in the hydrogenation of CA. A small fraction of high molecular weight condensation products (others) were also observed. The conversion of CA in cyclohexane and toluene was low (entry 1 and 2, Table 5.4), which might be due to poor solubility of CA in these solvents.[27] Moreover, non-selective hydrogenation of C=C and C=O bonds takes place in toluene, cyclohexane, chloroform and acetonitrile solvents (entries 1-4, Table 5.4).[27]

Table 5.4 Hydrogenation of CA in different solvents over 1wt% Au-NMC-SI.[a]

Entry	Solvent	Solvent polarity index	CA conv. (%)	Products selectivity (%)			
				CAL	HCA	PPL	Others[b]
1	Cyclohexane	0.2	15.6	17	52	24	7
2	Toluene	2.4	31.4	24	48	13	15
3	Chloroform	4.1	42.5	20	45	22	13
4	Acetonitrile	5.8	55.5	28	39	23	10
5	Methanol	5.1	100	63	10	6	21
6	Ethanol	5.2	96.5	71	8	9	12
7	1-Propanol	4.0	91.6	69	8	13	10
8	2-Propanol	3.9	94.2	78	9	11	2
9[c]	2-Propanol	3.9	12.3	0	0	0	100

[a] Reaction conditions: CA (7.5 mmol); catalyst (1wt% Au-NMC-SI, 25 mg); solvent (25 mL); H$_2$ pressure (20 bar); reaction time (10 h); temperature (120 °C). [b] Others include acetal, ethers and high molecular weight condensation products. [c] In the absence of H$_2$.

CA conversion was found to be relatively high in alcohol solvents than in other solvents. The formation of undesired products (others including acetals and ethers) was negligible (2%) in 2-propanol but was significant (10-21%) in other alcohols (compare entries 5-8 in Table 5.4). This shows that etherification reaction favoured in lower alcohols (methanol, ethanol and 1-propanol).[27] It was quite interesting to note that mainly CAL was formed in 2-propanol solvent with 78% selectivity at 94.2% CA conversion (entry 8, Table 5.4). Although, 2-propanol is known as a hydrogen transfer reagent, the results shows that the effect of transfer hydrogenation was nil under the given reaction conditions (entry 9, Table 5.4). Hence, 2-propanol was chosen as the solvent of choice for further studies.

5.4.2.2.2. Comparison of various supported Au catalysts

To study the effect of catalyst preparation method, 1wt% Au-NMC-SI catalyst was compared with 1wt% Au-NMC-IW and 1wt% Au-NMC-DP catalysts under similar reaction conditions in CA hydrogenation (Table 5.5). Catalyst 1wt% Au-NMC-SI exhibited relatively better activity giving 78% CAL selectivity at 94.2% CA conversion (entries 1-3, Table 5.5). The variation in catalytic activity and CAL selectivity may be attributed to the differences in Au nanoparticle size of the catalysts since the nitrogen-content in these catalysts is nearly same (Table 5.3). Generally, supported Au catalysts show lower hydrogenation activity compared to other noble metals (Ru, Pt and Pd) due to completely filled d-orbitals of the former.[2a] However, catalytic activity of Au catalysts can be substantially improved by decreasing the size of Au clusters and by the electronic modification of Au and supported material.[28] The superior activity of small Au nanoparticles originates from the shape and the position of its d band. The adsorbate bonding strength and hence catalytic activity is highly dependent on the position of d band with respect to Fermi level.[28] When the d states are close to the Fermi level, the interaction is expected to be strongest.[28,29] For small Au nanoclusters, the d band lies closer to Fermi level compared to bulk Au.[30] Consequently, small Au nanoparticles can form bonds with reactants[31], whereas bulk Au cannot.[32] Hence, small Au clusters are indispensable to achieve higher activity. Moreover, the significant increase in the C=O hydrogenation rate with decreasing Au nanoparticles size compared to C=C hydrogenation rate, can be explained by the increase in the number of d electrons with decreasing Au nanoparticles size.[31] Additionally, Au nanoparticles are electronically rich due to transfer of electron density from nitrogen atoms.[18] The higher electron density on Au nanoparticles affects the binding energies. Au nanoparticles

with higher electron density can facilitate back bonding interaction with π^*_{CO} and thereby enhance the CAL selectivity during hydrogenation of CA.[1b,25] Furthermore, the basicity of NMC support (0.41 mmol/g) will also help for the adsorption of CA molecule via C=O group and thus, improve catalytic activity and CAL selectivity.

The catalyst performance of 1wt% Au-NMC-SI was also compared with nitrogen-free carbon (MC) and metal oxide (Al_2O_3, MgO and TiO_2) supported Au catalysts (Table 5.5). Catalyst 1wt% Au-MC-SI exhibited poor catalytic activity leading to 38.5% CA conversion and only 19% CAL selectivity (entry 4, Table 5.5). Similarly, metal oxide supported Au catalysts also showed lower catalytic activity and CAL selectivity (entries 5-7, Table 5.5). Therefore, small Au nanoparticles and basic catalyst supports are necessary to achieve higher CA hydrogenation activity and good CAL selectivity.

Table 5.5 Comparison of various supported Au catalysts for CA hydrogenation.[a]

Entry	Catalyst	CA conv. (%)	Products selectivity (%)				TOF[c] (h^{-1})
			CAL	HCA	PPL	Others[b]	
1	1wt% Au-NMC-IW	59.0	43	39	9	9	348
2	1wt% Au-NMC-DP	81.2	63	22	9	6	479
3	1wt% Au-NMC-SI	94.2	78	9	11	2	556
4	1wt% Au-MC-SI	38.5	19	50	20	11	227
5	1wt% Au-Al_2O_3	33.4	14	66	8	12	197
6	1wt% Au-MgO	45.6	22	53	16	9	269
7	1wt% Au-TiO_2	31.5	12	63	13	12	186

[a] Reaction conditions: molar ratio of CA to Au (5910); solvent (2-propanol, 25 mL); H_2 pressure (20 bar); temperature (120 °C); reaction time (10 h). [b] Others include acetal, ethers and high molecular weight condensation products. [c] TOF = turnover frequency (moles of CA converted per mole of Au per hour).

5.4.2.2.3. Effect of reaction time

In order to elucidate the CA hydrogenation process over 1wt% Au-NMC-SI catalyst, the product concentrations versus reaction time were monitored at 120 °C and the results are given in Fig. 5.15. It can be seen that the CA conversion increased almost linearly with time and the selectivity for CAL remains nearly at 78% up to 10 h. However, with further increase in reaction time from 10 to 14 h, the CA conversion enhanced from 94.2 to 100%, but the CAL selectivity

decreased to 50% and the PPL was dominant (43%). It is very important to note that considerable amount of CAL sequentially converted into PPL on further hydrogenation of C=C bond after CA was completely consumed. These results clearly suggest that CAL adsorbed weakly on the Au metal surface than CA.[28]
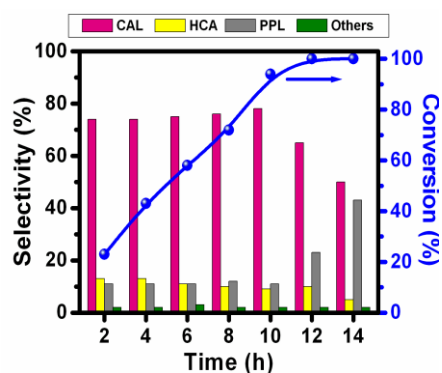
Fig. 5.15 Effect of reaction time on the catalytic performance of 1wt% Au-NMC-SI.
Reaction conditions: CA (7.5 mmol); catalyst (25 mg); temperature (120 °C); solvent (2-propanol, 25 mL); H_2 pressure (20 bar).

5.4.2.2.4. Effect of reaction temperature

Effect of reaction temperature on CA conversion and product selectivity's was studied over 1wt% Au-NMC-SI catalyst and the results are given in Fig. 5.16. Increasing the reaction temperature from 50 to 120 °C influenced the CA conversion and the CAL selectivity to change from 17 to 94.2% and 64 to 78%, respectively after 10 h of reaction time. At higher temperatures (130 °C) similar activity can be achieved in a shorter duration (6 h). The experimental results indicate that the increasing temperature boosts the CA hydrogenation rate as well as CAL selectivity.[15b]
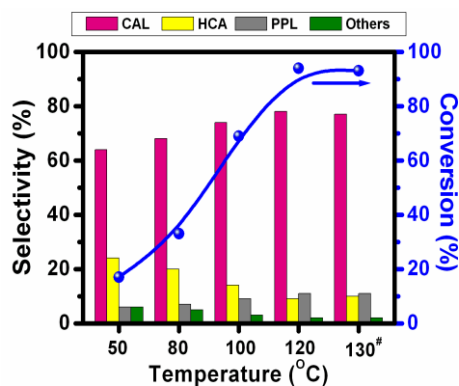
Fig. 5.16 Effect of reaction temperature on the catalytic performance of 1wt% Au-NMC-SI.
Reaction conditions: CA (7.5 mmol); catalyst (25 mg); solvent (2-propanol, 25 mL); H_2 pressure (20 bar); reaction time (10 h, # 6 h).

5.4.2.2.5. Effect of H₂ pressure

Influence of H_2 pressure on the CA conversion and selectivity of products was examined by varying the pressure in the range of 5-25 bar over 1wt% Au-NMC-SI catalyst (Fig. 5.17). The CA conversion increased from 27 to 94.2% as the H_2 pressure enhanced from 5 to 20 bar and the CAL selectivity slightly improved from 72 to 78%. However, at higher H_2 pressure (25 bar), CAL selectivity decreases to 68% with 100% CA conversion. Thus, 20 bar H_2 pressure was found to be optimum to achieve good CAL selectivity (78%).
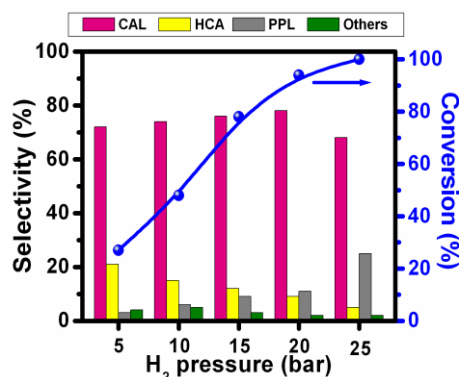
Fig. 5.17 Effect of H_2 pressure on the catalytic performance of 1wt% Au-NMC-SI.
Reaction conditions: CA (7.5 mmol); catalyst (25 mg); temperature (120 °C); solvent (2-propanol, 25 mL); reaction time (10 h).

5.4.2.2.6. Recyclability study

The recyclability study of 1wt% Au-NMC-SI catalyst in CA hydrogenation was carried out by repeating the reaction with the same catalyst (Fig. 5.18). The results in Fig. 5.18 clearly show that the catalytic performance remains nearly same even after being reused for five times. These results indicate good stability of the catalyst.
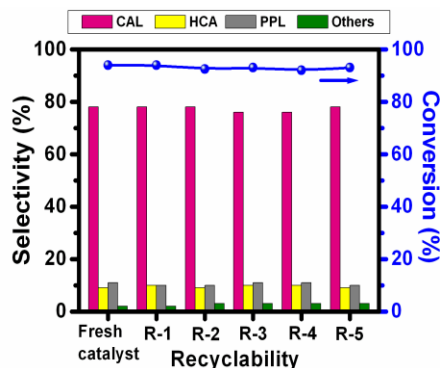
**Fig. 5.18** Recyclability study of 1wt% Au-NMC-SI catalyst in CA hydrogenation.
Reaction conditions: molar ratio of CA to Au (5910); solvent (2-propanol, 25 mL); H_2 pressure (20 bar); temperature (120 °C); reaction time (10 h).

5.4.3. Conclusions

Highly dispersed Au nanoparticles with an average particle size of 1.6 nm were successfully dispersed on NMC support by sol-immobilization technique. The chemoselective hydrogenation of CA was used as a model reaction to evaluate the catalytic activity of various supported Au catalysts. Among the catalysts tested, 1wt% Au-NMC-SI exhibited superior hydrogenation activity affording 78% CAL selectivity at 94.2% CA conversion. Small Au nanoparticles are essential for elevated catalytic activity and good CAL selectivity, because of their higher number of d electrons, which favors the selective hydrogenation of C=O bond in CA. The higher electron density on Au nanoparticles due to transfer of electrons from nitrogen atoms can facilitate back bonding interaction with π^{*}_{CO} and thus enhance the hydrogenation rate of C=O bond. Apart from electronic structure of Au nanoparticles, the basicity of NMC support is also assisting the adsorption of CA through C=O group and thereby improving the catalytic activity and CAL selectivity. Thus, the selectivity of product can be tuned by changing the size of Au nanoparticles as well as by electronic modification of metallic surface and the catalyst support.
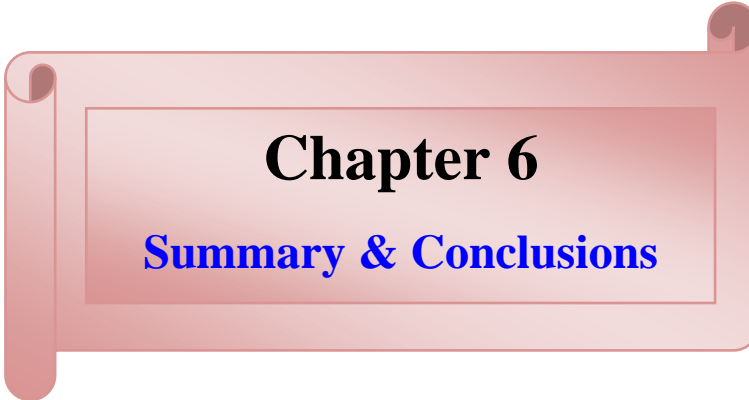
5.5. References

1. (a) M. Boudart, *Nature,* 1994**, 372**, 320; (b) P. Gallezot and D. Richard, *Catal. Rev. Sci. Eng.,*1998, **40**, 81; (c) P. Claus, *Top Catal,* 1998, **5**, 51; (d) U. K. Singh and M. A. Vannice, *Appl. Catal A,* 2001, **213**, 1.

2. (a) P. Maki-Arvela, J. Hajek, T. Salmi and D. Y. Murzin, *Appl. Catal. A,* 2005, **292**, 1; (b) S. Mahmoud, A. Hammoudeh, S. Gharaibeh and J. Melsheimer, *J. Mol. Catal. A,* 2002, **178**, 161.

3. J. Zhu, A. Holmen and D. Chen, *ChemCatChem,* 2013, **5**, 378.

4. (a) M. Antonietti and K. Mullen, *Adv. Mater.,* 2010, **22**, 787; (b) Y. Wan, H. Wang, Q. Zhao, M. Klingstedt, O. Terasaki and D. Zhao, *J. Am. Chem. Soc.,* 2009, **131**, 4541; (c) Y. Hao, G.-P. Hao, D.-C. Guo, C.-Z. Guo, W.-C. Li, M.-R. Li and A.-H. Lu, *ChemCatChem,* 2012, **4**, 1595.

5. (a) R. J. White, R. Luque, V. L. Budarin, J. H. Clark and D. J. Macquarrie, *Chem. Soc. Rev.,* 2009, **38**, 481; (b) F. Clippel, M. Dusselier, R. Van Rompaey, P. Vanelderen, J.

Dijkmans, E. Makshina, L. Giebeler, S. Oswald, G. V. Baron, J. F. M. Denayer, P. P. Pescarmona, P. A. Jacobs and B. F. Sels, *J. Am. Chem. Soc.,* 2012, **134**, 10089.

6. S. Crossley, J. Faria, M. Shen and D. E. Resasco, *Science,* 2010, **327**, 68.

7. V. Z. Radkevich, T. L. Senko, K. Wilson, L. M. Grishenko, A. N. Zaderko and V. Y. Diyuk, *Appl. Catal. A* 2008, **335**, 241.

8. Y. Wang, J. Yao, H. Li, D. Su and M. Antonietti, *J. Am. Chem. Soc.,* 2011, **133**, 2362.

9. L. Zhao, L.-Z. Fan, M.-Q. Zhou, H. Guan, S. Qiao, M. Antonietti and M.-M. Titirici, *Adv. Mater.,* 2010, **22**, 5202.

10. K. P. Gong, F. Du, Z. H. Xia, M. Durstock and L. M. Dai, *Science,* 2009, **323**, 760.

11. X. Xu, Y. Li, Y. Gong, P. Zhang, H. Li and Y. Wang, *J. Am. Chem. Soc.,* 2012, **134**, 16987.

12. (a) W. Yang, T. P. Fellinger and M. Antonietti, *J. Am. Chem. Soc.,* 2011, **133**, 206; (b) P. F. Fulvio, J. S. Lee, R. T. Mayes, X. Q. Wang, S. M. Mahurin and S. Dai, *Phys. Chem. Chem. Phys.,* 2011, **13**, 13486.

13. K. Chizari, I. Janowska, M. Houlle, I. Florea, O. Ersen, T. Romero, P. Bernhardt, M. J. Ledoux and C. Pham-Huu, *Appl. Catal. A,* 2010, **380**, 72.

14. T. Vergunst, F. Kapteijn and J. A. Moulijn, *Catal. Today,* 2001, **66**, 381.

15. (a) C. Pham-Huu, N. Keller, G. Ehret, L. J. Charbonniere, R. Ziessel and M. J. Ledoux, *J. Mol. Catal. A,* 2001, **170**, 155; (b) B. H. Zhao, J. G. Chen, X. Liu, Z. W. Liu, Z. Hao, J. Xiao and Z. T. Liu, *Ind. Eng. Chem. Res.*, 2012, **51**, 11112; (c) F. Zhao, Y. Ikushima, M. Chatterjee, M. Shirai and M. Arai, *Green Chem.,* 2003, **5**, 76; (d) J. Amadou, K. Chizari, M. Houlle, I. Janowska, O. Ersen, D. Begin and C. Pham-Huu, *Catal. Today,* 2008, **138**, 62; (e) T. Truong-Huu, K. Chizari, I. Janowska, M. S. Moldovan, O. Ersen, L. D. Nguyen, M. J. Ledoux, C. Pham-Huu and D. Begin, *Catal. Today,* 2012, **189**, 77; (f) A. M. R. Galletti, C. Antonetti, A. M. Venezia and G. Giambastiani, *Appl. Catal. A,* 2010, **386**, 124; (g) S. Mahmoud, A. Hammoudeh, S. Gharaibeh and J. Melsheimer, *J. Mol. Catal. A,* 2002, **178**, 161; (h) H. Wang, Y. Shu, M. Zheng and T. Zhang, *Catal. Lett.,* 2008, **124**, 219; (i) A. J. Marchi, D. A. Gordo, A. F. Trasarti and C. R. Apesteguía, *Appl. Catal. A*, 2003, **249**, 53.

16. (a) A. J. Plomp, H. Vuori, A. O. I. Krause, K. P. de Jong and J. H. Bitter, *Appl. Catal. A,* 2008, **351**, 9; (b) Z. Sun, Z. Rong, Y. Wang, Y. Xia, W. Du and Y. Wang, *RSC Adv.*, 2014, **4**, 1874; (c) Z. Guo, C. Xiao, R. V. Maligal-Ganesh, L. Zhou, T. W. Goh, X. Li, D. Tesfagaber, A. Thiel and W. Huang, *ACS Catal.,* 2014, **4**, 1340; (d) L. Liu, B. Qiao, Y. Ma,

J. Zhang and Y. Deng, *Dalton Trans.*, 2008, 2542; (e) K. J. You, C. T. Chang, B. J. Liaw, C. T. Huang and Y. Z. Chen, *Appl. Catal. A,* 2009, **361**, 65; (f) B. F. Machado, H. T. Gomes, P. Serp, P. Kalck and J. L. Faria, *ChemCatChem*, 2010, **2**, 190; (g) Z. Liu, Y. Yang, J. Mi, X. Tan and Y. Song, *Catal. Commun.,* 2012, **21**, 58; (h) Z. Liu, X. Tan, J. Li and C. Lv, *New J. Chem.,* 2013, **37**, 1350; (i) A. B. Merlo, B. F. Machado, V. Vetere, J. L. Faria and M. L. Casella, *Appl. Catal. A*, 2010, **383**, 43.

17. H. Chen, F. Sun, J. Wang, W. Li, W. Qiao, L. Ling and D. Long, *J. Phys. Chem. C,* 2013, **117**, 8318.

18. X. Xie, J. Long, J. Xu, L. Chen, Y. Wang, Z. Zhang and X. Wang, *RSC Adv.,* 2012, **2**, 12438.

19. R. J. Isaifan, H. A. E. Dole, E. Obeid, L. Lizarrag, P. Vernoux and E. A. Baranova, *Electrochem. Solid-State Lett.,* 2012, **15** (3) E14-E17.

20. (a) R. J. Hou, T. F. Wang and X. C. Lan, *Ind. Eng. Chem. Res.,* 2013, **52**, 13305; (b) S. Mukherjee and M. A. Vannice, *J. Catal.,* 2006, **243**, 108.

21. (a) Z. Wei, Y. Gong, T. Xiong, P. Zhang, H. Li and Y. Wang, *Catal. Sci. Technol,* 2015, **5**, 397; (b) M. M. Wang, L. He, Y. M. Liu, Y. Cao, H. Y. He and K. N. Fan, *Green Chem.*, 2011, **13**, 602; (c) S. Fujiwara, N. Takanashi, R. Nishiyabu and Y. Kubo, *Green Chem.*, 2014, **16**, 3230.

22. R. Schlogl, Surface composition and structure of active carbon, in: F. Schuth, K. S. W. Sing, J. Weitkamp (Eds.), Handbook of Porous Solids, Wiley–VCH, 2002, pp. 1863–1900.

23. C. Pham-Huu, N. Keller, G. Ehret and M. J. Ledoux, *J. Catal.,* 2001, **200**, 400.

24. Y. A. Ryndin, C. C. Santini, D. Prat and J. M. Basset, *J. Catal.,* 2000, **190,** 364

25. F. Delbecq and P. Sautet, *J. Catal.,* 1995, **152**, 217.

26. V. Pallassana, M. Neurock and G. W. Coulston, *J. Phys. Chem. B,* 1999, **103**, 8973.

27. J. Shi, R. Nie, P. Chen and Z. Hou, *Catal. Commun.,* 2013, **41**, 101.

28. E. Bus, R. Prins and J. A. van Bokhoven, *Catal. Commun.,* 2007, **8**, 1397.

29. B. Hammer and J. K. Nørskov, *Nature,* 1995, **376**, 238.

30. (a) N. Lopez and J. K. Nørskov, *Surf. Sci.* 2002, **515**, 175; (b) P. K. Jain, *Struct. Chem.* 2005, **16**, 421.

31. J. T. Miller, A. J. Kropf, Y. Zha, J. R. Regalbuto, L. Delannoy, C. Louis, E. Bus and J. A. van Bokhoven, *J. Catal.,* 2006, **240**, 222.

32.   G. C. Bond and D. T. Thompson, *Catal. Rev.,* 1999, **41**, 319.

Chapter 6

Summary & Conclusions

6.1. Summary and Conclusions

The present thesis reports reductive upgradation of biomass-derived feedstocks and hydrogenation of cinnamaldehyde (CA) employing various novel supported metal catalysts. The thesis is divided into 6 chapters which include a chapter on summary of the work carried out for this dissertation and the conclusions arrived at the end of the work.

Chapter 1 gives a brief introduction to the significance of biomass-derived feedstocks for the synthesis of fuels and chemicals. Prime importance is given to the hydrogenolysis of biomass-derived furfural and 5-hydroxymethylfurfural (HMF) to 2-methylfuran (MF) and 2,5-dimethylfuran (DMF), respectively. Hydrogenation of furfural to furfuryl alcohol (FA) is also discussed. The significance and properties of furfural, HMF, MF, DMF and FA is also described in this introduction. In addition, this chapter also includes an introduction to the selective hydrogenation of CA, a representative of α,β-unsaturated carbonyl compounds. The industrial importance of cinnamyl alcohol (CAL) and hydrocinnamaldehyde (HCA), which are produced on hydrogenation of CA is highlighted. It also describes a variety of catalyst supports that are used in this study, such as hydrotalcites, zeolites, carbon materials and nitrogen-doped carbons. Finally, the objectives of the thesis are outlined briefly.

Chapter 2 describes the catalyst preparation methods and experimental techniques used for their characterization. The catalysts prepared were Ru-doped hydrotalcites and NaY zeolite supported Ru, Pt, Pd, Rh, Au, Ni and Cu catalysts. In addition, nitrogen-doped mesoporous carbons (NMC's) with different N-contents were synthesized and were used as supports for Ru, Pt, Pd, Rh, Au, Ni and Cu metals. They were characterized by using various physico-chemical techniques including XRD, N_2 sorption, H_2 chemisorption, SEM, TEM, Raman spectroscopy, XPS, TPD of NH_3 and CO_2, TPR in H_2, ICP-OES, *etc*. Theory and experimental procedures employed to use each of these techniques have been outlined in this chapter.

Chapter 3 starts with detailed literature review on the conversion of HMF to DMF, followed by the present work on reductive upgradation of biomass-derived components. This reaction is carried out on two types of supported Ru catalysts using molecular H_2. Hence, the chapter is divided into two parts, i.e., part 3A and 3B. Part 3A deals with the investigations related to Ru-doped hydrotalcite catalysts for hydrogenolysis of HMF to DMF. Characterization of Ru-doped hydrotalcite catalysts was carried out using XRD, SEM and TEM, to study their

structure and morphology before and after Ru incorporation. The results of N_2 sorption, H_2 chemisorption, TPR and XPS are also discussed in detail. The catalytic activity in HMF hydrogenolysis and optimization of reaction conditions is also given in this part. Part 3B deals with the hydrogenolysis of HMF to DMF and hydrogenation of furfural to FA using NaY zeolite supported metal catalysts. It discusses the characterization results of the catalysts using XRD, N_2 sorption, H_2 chemisorption, SEM, TEM, NH_3-TPD, TPR, XPS, *etc*. The experimental results for the preparation of DMF and FA are also given.

The characterization studies show that highly dispersed Ru can be obtained on calcination of hydrotalcite-like precursors, which were synthesized through co-precipitation. A catalyst containing only 0.56 wt% Ru yielded 58 mol% of DMF, showing that smaller Ru crystallites are needed for higher DMF yield, as consecutive ring hydrogenation is suppressed. Higher DMF yields were obtained when 2-propanol was used as the solvent, as a result of hydrogen transfer from 2-propanol to HMF. This catalyst was recyclable without any noticeable loss in activity.

Among various transition metal exchanged NaY zeolite catalysts, Ru-NaY showed relatively higher activity and gave 78 mol% DMF yield in very short duration (1 h). DMF yields were correlated with dispersion of Ru metal and its crystallite size. This catalyst also exhibited excellent recyclability. Based on the results, a plausible reaction pathway for the DMF from HMF was proposed. The results show that DMF is formed through hydrogenolysis of –OH groups in 2,5-bis(hydroxymethyl)furan (BHMF) followed by 5-methyl furfuryl alcohol (MFA). Catalyst Ru-NaY also gave 86 mol% FA yield during furfural hydrogenation, showing the multiple use of the Ru-NaY catalyst.

Chapter 4 described the characterization results of NMC's with different N-contents, nitrogen-free mesoporous carbon (MC) and supported metal catalysts using XRD, N_2 sorption, XPS, Raman spectroscopy, TEM, CO_2-TPD, *etc*. The catalytic activity in transfer hydrogenolysis of HMF and furfural is also described in detail.

Catalytic transfer hydrogenolysis of furfural to MF and HMF to DMF was carried out over metal supported on NMC's. It was found that during hydrogenolysis reaction, temperature, hydrogen donor, nitrogen content, size of the Ru nanoparticles and the catalyst support play vital role in the conversion of substrate to give desired product. Transfer hydrogenolysis activity was enhanced with increasing nitrogen content of the catalyst. Under optimized reaction conditions, 2wt% Ru-NMC catalyst with 11.6 wt% nitrogen content gave 84 and 87 mol% yield of DMF and

MF on hydrogenation of HMF and furfural, respectively, with 2-propanol as the hydrogen donor. This catalyst was recyclable and its excellent performance was attributed to the high Ru dispersion and stabilization of Ru nanoparticles by the nitrogen present in the support. The characterization results were correlated with the catalytic performance at the end of the chapter.

Chapter 5 begins with detailed literature review on the hydrogenation of CA to HCA and CAL. Later it discusses the selective hydrogenation of CA to HCA and CAL over supported metal catalysts using molecular H_2. This chapter is divided into two parts. Part 5A deals with hydrogenation of CA to HCA. It discusses characterization results of supported Pd catalysts using XRD, N_2 sorption, XPS, TEM, Raman spectroscopy, *etc*. The catalytic activity in selective hydrogenation of CA to HCA is also discussed in this part. Part 5B deals with selective hydrogenation of CA to CAL using NMC and metal oxide supported Au catalysts. The characterization of Au catalysts was carried out using various physico-chemical techniques. It also describes the catalytic activity of these catalysts in the conversion of CA to CAL.

Catalyst with 2wt% Pd on NMC showed outstanding activity and high HCA selectivity (93%) under mild reaction conditions (30 °C, 1 bar H_2). The observed high catalytic activity and better C=C hydrogenation selectivity were attributed to nano particle size of Pd, as a result of peculiar metal-support interaction between Pd and NMC. The high activity was also attributed to mesoporosity that facilies easier diffusion of reactants and hydrogenated products. The 2wt% Pd-NMC catalyst was recyclable without any loss in activity and HCA selectivity.

Part 5B deals with discussion on highly dispersed Au on NMC, which was prepared by sol-immobilization technique. Among the supported Au catalysts tested, 1wt% Au-NMC catalyst displayed superior hydrogenation activity and good CAL selectivity (78%). The presence of small Au nanoparticles are essential for achieving higher activity, because of their higher number of d electrons, which favors the selective hydrogenation of C=O bond in CA. Further, the basicity of NMC support also facilitates the adsorption of CA through their C=O group that leads to improved catalytic activity and CAL selectivity. The catalytic performance of 1wt% Au-NMC remains same in recyclability study.

It is necessary at the end of all chapters in a thesis to sum up the research investigations carried out for the benefit of the reader. Thus, **chapter 6** summarizes the conclusions reached based on the experimental results during these studies. Firstly it describes the content of each

chapter in detail with glimpses of results at the end. This section also offers some suggestions for future research work in the given areas.

6.2. Suggestions for future research

The objective of the present investigations is to utilize biomass-derived compounds for the preparation of chemicals and fuels via hydrogenation and hydrogenolysis pathways, which in turn can lead to significant contributions towards the sustainable approach for the production of chemicals and fuels from renewable feedstocks. It also includes the synthesis of industrially important fine chemicals by selective hydrogenation of CA, a representative of α,β-unsaturated carbonyl compounds. By and large, these investigations unravel factors influencing the catalytic activity of supported metal catalysts in hydrogenation/hydrogenolysis reactions.

Hydrogen is mostly used in the reductive upgradation of biomass-derived compounds. However, it is desirable to minimize the use of external H_2 required for biofuel production, due to reasons of logistics and safety. In this thesis, we have reported an alternative process route for the hydrogenolysis of HMF to DMF and furfural to MF by catalytic transfer hydrogenation (CTH), in which hydrogen donor is used as a hydrogen source, instead of molecular H_2. Various alcohols (methanol, ethanol, 1-propanol, 2-propanol, 1-butanol and 2-butanol) were used as a hydrogen donor as well as reaction medium. For CTH process, Ru nanoparticles supported on NMC were found to be excellent catalysts for the utilization of biomass-derived HMF and furfural to obtain biofuels. Therefore, NMC supported metal catalysts can be exploited for reductive transformation of different biomass derivatives to chemicals and fuels via CTH process using preferably secondary alcohols as a hydrogen donor. For example, conversion of glucose to sorbitol, xylose to xylitol, cellulose to sugar alcohols, levulinic acid to γ-valerolactone, glycerol to 1,2-propanediol can be investigated through CTH process. Moreover, NMC supported metal catalysts can also be employed for aqueous phase reforming to produce H_2 from biomass-derived feedstocks such as glycerol, glucose, cellulose, starch, *etc*. Further, NMC supported metal (Ru, Pt and Au) catalysts can be used for the selective hydrogenation of varieties of α,β-unsaturated carbonyl compounds to prepare numerous fine chemicals.

PUBLICATIONS

1. Renewable fuels from biomass-derived compounds: Ru-containing hydrotalcites as catalysts for conversion of HMF to 2,5-dimethylfuran.

    Atul S. Nagpure, Ashok Kumar Venugopal, Nishita Lucas, M. Manikandan, Raja Thirumalaiswamy and Satyanarayana Chilukuri
    Catalysis Science & Technology, (2015), 5, 1463-1472.

2. Efficient preparation of liquid fuel 2,5-dimethylfuran from biomass derived HMF over Ru-NaY catalyst.

    Atul S. Nagpure, Nishita Lucas and Satyanarayana Chilukuri
    ACS Sustainable Chemistry & Engineering, (2015), 3, 2909-2916.

3. Dehydration of fructose to 5-hydroxymethylfurfural over ordered AlSBA-15 catalysts.

    Nishita Lucas, Ganesh Kokate, **Atul S. Nagpure** and Satyanarayana Chilukuri
    Microporous & Mesoporous Materials, (2013), 181, 38–46.

4. Novel catalysts for valorization of biomass to value-added chemicals and fuels.

    Nishita Lucas, Narasimha Rao Kanna, **Atul S. Nagpure**, Ganesh Kokate and Satyanarayana Chilukuri
    Journal of Chemical Sciences, (2014), 126, 403-413.

5. Promotional effect of Fe on the performance of supported Cu catalyst for ambient pressure hydrogenation of furfural.

    M. Manikandan, Ashok Kumar Venugopal, **Atul S. Nagpure**, Satyanarayana Chilukuri and Raja Thirumalaiswamy
    RSC Advances, (2016), 6, 3888-3898.

6. Catalytic transfer hydrogenation of biomass-derived furanic compounds to fuels over nitrogen-doped mesoporous carbon supported metal catalysts.

    Atul S. Nagpure and Satyanarayana Chilukuri
    (Communicated to ChemSusChem)

7. Chemoselective hydrogenation of cinnamaldehyde to hydrocinnamaldehyde over nitrogen-doped mesoporous carbon supported Pd catalyst.

   Atul S. Nagpure and Satyanarayana Chilukuri
   (Communicated to RSC Advances)

8. Production of renewable gasoline additive 2,5-dimethylfuran from HMF over Mg-OMS-1 supported Ru catalyst.

   Atul S. Nagpure and Satyanarayana Chilukuri
   (to be communicated)

9. Admirable catalytic activity of Cu nanoparticles supported on HY zeolite for efficient preparation of γ-valerolactone from levulinic acid.

   Atul S. Nagpure and Satyanarayana Chilukuri
   (Manuscript under preparation)

PATENT APPLICATIONS

1. An improved process for the preparation of 2,5-dimethylfuran and furfuryl alcohol over supported Ru catalysts.

   Satyanarayana Chilukuri, **Atul S. Nagpure** and Nishita Lucas
   WO 2015111078 A1 (2013-NCL-0120, 2014-NF-0004, 0183/DEL/2014)

2. Biomass derivatives to fuels over metals supported on nitrogen doped mesoporous carbon.

   Satyanarayana Chilukuri and **Atul S. Nagpure**
   (2015-NCL-0064, 2015-NF-0220, 2833/DEL/2015)